UNIVERSITY OF
LIVERPOOL

Department of Engineering

PhD Thesis

Engineered Micro to Nano Scale Surface Structures with the Potential to Influence Stem Cell Interactions

Thesis submitted in accordance with the requirements of the University of Liverpool for the degree of Doctor of Philosophy

By

Craig J. Williams

Laser Group
Department of Engineering
The University of Liverpool
Brownlow Hill
Liverpool
UK
L69 3GH

Declaration

I hereby declare that all of the work contained within this dissertation has not been submitted for any other qualification.

Signed: Dated:

Publications

- Williams, C.J., Edwardson, S.P., Croft, J., Sharp, M., French, P., Ansari, I.A., Perrie, W., Cheng, J., Dearden, G., Watkins, K.G. 2008. Production Of Micro And Nano Scale Features On Polymer Surfaces With SPM Based Lithography And Ultra Short Pulsed Lasers. ICALEO® 2007 Congress Proceedings, Laser Nanoprocessing Conference. Paper N103
- Dima, A., Gagliardi, M., Dun, L., Perrie, W., Williams, C.J., Rendina, I., Dearden, G., Watkins, K.G. 2009. Nano-Silicon Sol-Gel Film Refraction Index Modulation with Femtosecond Laser. Solid State Phenomena. 154, 101-106.
- Dima, A., Dima, M., Watkins, K.G., Dearden, G., Dun, L., Williams, C.J., Casalino, M., Gagliardi, M., Rendina, I., Della Corte F.G. 2009. Switching devices in sol–gel hybrid thin film technology. Thin Solid Films. 517, 4658–4662
- Dima, A., Della Corte, F.G., Williams, C.J., Watkins, K.G., Dearden, G., O'Hare, N., Casalino, M., Rendina, I., Dima, M. 2008. Silicon nano-particles in SiO2 sol–gel film for nano-crystal memory device applications. Microelectronics Journal. 39, 768–770
- Semaltianos, N.G., Perrie, W., Vishnyakov, V., Murray, R., Williams, C.J., Edwardson, S.P., Dearden, G., French, P., Sharp, M., Logothetidis, S., Watkins, K.G. 2008. Nanoparticle formation by the debris produced by femtosecond laser ablation of silicon in ambient air. Materials Letters. 62, 2165–2170.
- Semaltianos, N.G., Perrie, W., Sharp, M., Williams, C.J., Edwardson, S.P., Dearden, G., Watkins, K.G. 2007. Nano-Particle Generation By Femto Second Laser Ablation. CALEO® 2007 Congress Proceedings, Nanomanufacturing Conference. Paper N405, 114-118

- Edwardson, S.P., Perrie, W., Williams, C.J., Sharp, M., Dearden, G., Wang, Z.B., Whitehead, D., Crouse, P., Lui, Z., Li, L., Watkins, K.G. 2007. Micro And Nano Manipulation For Engineering Manufacture. Laser Assisted Net Shape Engingeering 5. LANE 2007, 1167-1176
- Mullett, J.D., Dodd, R., Williams, C.J., Triantos, G., Dearden, G., Shenton, A.T., Watkins, K.G., Carroll, S.D., Scarisbrick, A.D., Keen, S. 2007. The influence of beam energy, mode and focal length on the control of laser ignition in an internal combustion engine. J. Phys. D: Appl. Phys. 40, 4730–4739
- Edwards, K., Edwardson, S.P., Carey, C., Williams, C.J., Dearden, G., Watkins, K.G. 2007. Laser Peen Forming For 2d Shaping And Micro Adjustment. ICALEO® 2007 Congress Proceedings, Laser Microprocessing Conference. Paper M605, 156-165
- Edwards, K., Edwardson, S.P., Carey, C., Williams, C.J., Dearden, G., Watkins, K.G. 2007. Laser Peen Forming For 2d Shaping And Adjustment Of Metallic Components. Laser Assisted Net Shape Engineering 5. LANE 2007, 569-580
- Carey, C., Cantwell, W.J., Dearden, G., Edwards, K.R., Edwardson, S.P., Mullett, J.D., Williams, C.J., Watkins, K.G. 2007. laser Assisted Net Shape Engineering 5. LANE 2007, 673-686

Abstract

The work presented in this thesis explores and discusses the design, development and investigates of the use of micro to nano scale engineered surface structures and how these structures affect the development of human embryonic stem (HuES) cells when they are seeded onto these structures.

HuES cells are of great interest to the field of regenerative medicine. It is hoped that the use of HuES cells can lead to treatments for many degenerative diseases, such as Parkinson's disease, Alzheimer's disease and Diabetes. It is also speculated the use of HuES cells could lead to the ability to repair damage to organs and body tissue including the heart and spinal column. HuES cells are unique in the body, they are able to differentiate into nearly any of the over 200 different cells in the human body. They are also self renewing, able to replicate themselves almost indefinably. One of the major obstacles to the use of HuES cells as a therapeutic treatment is the inability to control and select how the cells differentiate. Currently HuES cells are instructed to differentiate using specific growth factors. These often contain elements derived from animals, so making the method unsuitable for use. Recent advances in micromachining has allowed for studies to be carried out looking at the link between cells and surface topography. Using this it is hypothesised that surface topography can be used to control HuES cell differentiation, removing the need for growth factors.

Several micro, nano and multi scale surface topographies have been produced using laser and lithography techniques. Unique surface feature have been produced directly on glass and polymers, or on stainless steel and then moulded in a polymer. These samples have then been used to observe ho HuES cell react to those surface features.

HuES cells have been observed undergoing differentiation as a direct result of the multi scale surface features. These results suggest that a nanopattern capable of inhibiting HuES spreading has been identified. Which, when used in microscale patterns, can control cellular properties.

Acknowledgements

The time it has taken to research and write this thesis has been enthralling, exiting and satisfying time in my life, I am greatly thankful for the opportunity to undertake this research, without the following people, however, it would not have been possible.

I must first thank my supervisors Prof. Ken Watkins and Dr Geoff Dearden for giving me the opportunity to work in their group and for providing support and guidance throughout the project. Working in the Laser Group has been a fantastic experience and is made so by the people who work there. Thanks goes to Dr Stuart Edwardson who was there to offer advice and help whenever it was needed. A thanks goes to Joe Croft, Leigh Mellor, Jian Cheng, Dun Lu, Olivier Allegre and Jack Mullet for their help and expertise in the setup and workings of laser systems and particularly for their friendship. Also to Taku Sato, John Griffiths, Paul Fitzsimons and Rob Dodd who made up the rest of the 'Laser Grazers'. For his technical help and expertise, I express my gratitude to Andy Snaylam for his help in cutting, polishing and building a range of equipment and samples that have been essential to my work.

Extra thanks go to Dr Kenny Edwards and Dr. Chris Carry for office cricket, 5-aside football, garden barbeques, pub crawls and generally making the group a great place to work and the office a great place to be.

To the past and present staff at the LLEC, Dr Martin Sharp, Dr Paul French, Dr Eamonn Fearon, Dr Antonella Dima and Dr Walter Perri, I express my thanks for their help and assistance and making the LLEC an enjoyable place of work for 4 years. Particular thanks goes to Doug Eckford, who was always there for help, assistance and discussions on virtually anything.

I would like to thank Prof. David Edgar and Dr Rachel Williams for giving me the opportunity to work in the world of cell biology and for their time, help and advice. Extra thanks is owed to Dr Deepak Kalaskar and Dr Joni Downs for their efforts, help and assistance in conducting the cell experiments Thanks goes to them all for letting an astrophysicist into their biology lab.

Particular thanks is due to Simon Dixon and Fred Laws from Biomer Technology, who as well as providing considerable time and materials to the project, took a great interest in my work and offered essential advice and expertise.

Finally I would like to thank my family. To my Mum and Dad for their help and support through my, seemingly, never ending student status. To my brother Adam for his support and weekly online gaming sessions. Thanks also to my Gran, Nan, Uncle Phil, Ang, Steve, Mike and Brian for their constant encouragement and regular care packages and the odd round of golf. Not to forget our faithful roughbeard collie, Maxwell, who was always around and didn't complain too much about missing the odd walk.

A special thanks goes to my partner, Claire, for her all her love, friendship, help, support, motivation and encouragement, as well as for generally looking after me.

The Author would like to acknowledge the EPSRC and NWDA for their funding support of this research.

Contents

List of Figures

List of Tables

Notation

Symbols

E	-	Energy	[J]
h	-	Planck's Constant	
v	-	Frequency	[Hz]
d	-	Beam waist diameter	[m]
λ	-	Wavelength	[m]
N	-	F - Number	
θ	-	Angular resolution	
D	-	Aperture diameter	[m]
m	-	Mass	[Kg]
ω	-	Resonant frequency	[Hz]
K_{eff}	-	Effective spring constant	[N/m]
K	-	Spring constant	[N/m]
f	-	Force gradient	[N]

Abbreviations

FN	-	Fibronectin
AFM	-	Atomic Force Microscope
DIC	-	Differential interference Microscopy
LIPSS	-	Laser induced periodic surface structures
SPP	-	Surface plasmon polaritons

Chapter 1

Introduction

1.1 Motivation for Research

Human embryonic stem cells (HuES) cells have, in recent times, been the subject of much debate and controversy. Much of this controversy originates from ethical issues concerned with how HuES are obtained from human embryos and that the benefits of using HuES cells are unproven [1]. Despite this, the opportunities offered by HuES cells to cure the most debilitating of diseases are hard to deny. HuES cells are able to differentiate into any of the cells of the body (pluripotancy) and can propagate indefinitely (self renewal). These two attributes mean that HuES cells have the potential to revolutionise medicine. Medical fields as diverse as biological development, drug research and the emerging area of regenerative medicine, are looking to HuES cells as a solution to many of today's medical problems [2].

The most high profile of these areas is that of regenerative medicine. It is hoped that HuES cells could be used to find cures for a wide range of degenerative diseases from Parkinson's and Alzheimer's disease to heart disease. Other areas of interest, such as spinal cord damage and diabetes, are also possible applications for HuES cell treatments [3].

There are. however, still scientific barriers to the advancement HuES cells as a therapeutic treatment. One of the main problems is the selection and expansion of pure populations of desired cell types [3]. In order to take

advantage of the pluripotant nature of HuES cells a method for making them differentiate into the desired cell type is necessary. At present this is achieved using growth factors [4]. The problem is that these growth factors often contain components of animal origin and are therefore not suitable for use in a therapeutic treatment. A solution is needed that does not rely on these growth factors to promote controlled HuES cell differentiation.

The use of surface topography has been hypothesized as a possible method of controlling cell behaviour and in turn promoting HuES cell differentiation [5]. If surface topography could be used in this way, it would be a further step towards using HuES cells as a therapeutic treatment for regenerative medicine.

1.2 Thesis Aim and Objectives

The primary aim of the work presented is to produce a surface topography that could be used to observe HuES cell behaviour and report on how the HuES cell reacted when grown on those surfaces. The specific objectives of the research were to:

- Design and produce a number of substrates with which to observe HuES cell behaviour. The substrates must be compatible with biology experimental procedures and methods.
- Design and produce substrates that can observe HuES cell behaviour on a range of size scales, from the micro to nano scale.
- Investigate the ability of new processing techniques to produce these substrates and assesd the suitability of these methods for producing the substrates in large enough volumes to be used in cell experiments and observations.
- Observe and report the behaviour of HuES cells when they are seeded onto the produced substrates.
- Specifically observe HuES cell differentiation and assess the effect the substrate surface topography has on the HuES cells.

1.3 Thesis Structure and Overview.

This thesis is divided into six chapters which detail the design and development of producing multi scale surface topographies and report on the observations of HuES cell interaction with these features. It begins with this introductory chapter, outlining the thesis aim and objectives. It is followed by chapter 2, which presents a review of background literature and the current state of the art. Chapter 2 give details of the current understanding of HuES cells, cell attachment and how cells interact with surface topography in vitro. Current methods of producing these surface features are also introduced.

Chapter 3 contains work on producing micro scale surface topography using a femtosecond pulsed laser to drill blind holes on glass substrates. A set of different patterns were produced and HuES cells were seeded onto them and observed. The primary objective was to investigate if it was possible to cause any change in cell behaviour with an engineered surface topography.

The work in Chapter 4 continued the work started in chapter 3. The results from Chapter 3 were used to refine the production of substrates. A different laser system was used to produce surface features faster and over larger areas than the system used in chapter 3. Surface features were produced on stainless steel plates and moulded using a polymer. This produced significantly more samples than the previous technique, meaning more detailed cell observations could be undertaken. Using the substrates it was possible to observe HuES cell differentiation.

Chapter 5 investigated a more novel method for producing surface topographies. An atomic force microscope (AFM) was used to machine surface features at a true <100 nm scale. The AFM was first used to observe the surface topography of glass cover slips coated in fibronectin, a protein involved in cell surface interaction and attachment. The fibronectin was measured and used as a model for a synthetic biomimetic surface

topography which could allow HuES cell observations on nanoscale surface topographies.

Finally a conclusion of the presented research is given in chapter 6, along with recommendations for further and future investigation.

1.4. References

[1] McLaren, A. 2007. A Scientist's View of the Ethicsof Human Embryonic Stem Cell Research. Cell Stem Cell. 1, 23-26.

[2] Edwards, B.E., Gearhart, J.D., Wallach, E.E. 2000. The human pluripotent stem cell: impact on medicine and society. Fertility and Sterility. 74, 1-7.

[3] Gerecht-Nir, S., Itskovitz-Eldor, J. 2004. The promise of human embryonic stem cells. Best Practice & Research Clinical Obstetrics and Gynecology. 18, 843–852

[4] Conley, B.J., Young, J.C., Trounson, A.O., Mollard, R. 2004. Derivation, propagation and differentiation of human embryonic stem cells. The International Journal of Biochemistry & Cell Biology. 36, 555–567.

[5] Bakeine, G.J., Ban, J., Grenci, Pozzato, A., Dal Zilio, S., Prasciolu, M., Businaro, L., Tormen, M., Ruaro, M.E. 2009. Design, fabrication and evaluation of nano scale surface topography as a tool in directing differentiation and organisation of embryonic stem-cell-derived neural precursors. Microelectronic Engineering 86, 1435–1438.

Chapter 2

Literature and State of the Art Review

2.1 Introduction

This chapter documents a current state of the art review looking at the advance of techniques for producing artificial micro and nano scale surface topographies. The review will concentrate on Laser Micro Machining and Atomic Force Microscopy (AFM) Lithography, as these are the techniques used in the work presented later. Also, a state of the art review is included on topography-cell interactions and responses, relevant to the experimental chapters in the thesis. Specifically it will cover the work done, to date, on how cells interact with micro to nano scale surfaces. Detail on human Embryonic Stem (HuES) cells and the unique niche that HuES cells fit into, is also included

2.2 Engineering Nano and Micro Scale Surfaces.

The methods for manufacture of the structured substrates used in this study were laser micro machining and nano lithography using an atomic force microscope. The following sections will focus on the advances made in these techniques which has allowed them to be used to produce nano and micro scale surface topographies.

The advent of advanced micro and nano engineering techniques has led to advances in experimentation with stem cells and stem cell niches in vitro.

Early experiments have used ultra violet photo lithography to create surfaces using masks and patterned resist layers [1]. Other techniques involve the use of ion beam or electron beam lithography, allowing for feature sizes down to ~20nm and ~10nm respectively. In the case of the ion beam lithography, no mask is required [2][3]. These techniques are however slow and expensive. Faster cheaper methods of creating patterned surfaces have been sought out, the most common and flexible are nano imprint lithography and laser deposition and etching [1].

The methods for manufacture of the structured substrates used in this study were laser micro machining and nano lithography using an atomic force microscope. The following sections will focus on the advances made in these techniques which has allowed them to be used to produce nano and micro scale surface topographies.

2.2.1 Laser Micro Machining

laser micro machining (LMM) is separated from laser beam machining (LBM) in that it uses ultra short pulsed lasers which, as opposed to the lasers used in LBM, produce virtually no heat input into the surface being machined. These ultra short lasers have a high beam quality, which allow for high accuracy and the possibility to produce features on the micro and sub micro scale.

2.2.1.1 The Laser: A brief history

In the 19th century James Clark Maxwell developed a general form of equations for electromagnetism, Maxwell's Equations. This work suggested the existence and possible production of transverse electromagnetic waves with a wide range of wavelengths [4]. In 1905 Einstein used the work of Maxwell and Planck's work on Black Body radiation [5], to suggest the existence of photons. Einstein proposed that these photons can exist as either a wave or a particle, wave-particle duality [6]. This solved a fundamental question about the nature of light which started in the 17th century when competing theories by Newton and Huygens stated that light

was either a particle or wave, respectively. The fundamental work done by Einstein and others including Bohr and Compton has led to the establishment of Quantum Theory; this is what describes the fundamentals of how a laser operates.

The laser operates by exploiting a phenomenon conceived by Einstein in 1917 [7]. 'Laser' is an acronym for Light Amplification by Stimulated Emissions of Radiation. It is the concept of stimulated emission of radiation that Einstein proposed was an everyday occurrence in nature. This was confirmed experimentally in 1928 [8]. It was not until 1960 however, that the first laser was demonstrated by Maiman using a ruby crystal [9]. The laser industry has grown and research and development has lead to many different lasers and applications. Lasers are available in a large range of designs and output properties. Laser radiation is monochromatic (meaning that the range of frequencies of the laser beam is very narrow), coherent and highly polarised. With new advances, lasers offer a non contact method of processing and measurement that is often unsurpassed by other methods.

2.2.1.2 The Laser: Basic Design and Operation

The design of lasers is mostly dependant on type, whether the laser source material is solid state or gas. Most direct micromachining lasers (not using photo lithography masks) are solid state in nature. This means they use a doped crystal or other doped optical element (such as an optical fibre) as the laser medium. On the basic level however the design of the laser cavity is the same for all types.

The primary feature of a laser is the laser cavity. This is an optical oscillator comprising at least two mirrors parallel to each other, centred on an optical axis with an active laser medium. One of these mirrors is only partially reflective. The active laser medium is coupled to an energy source. This energy source will provide the pump energy to the system. The pump energy source varies as the design and type of laser

varies. For solid state lasers it is usually a high power halogen flash lamp or bank of diodes set to a precise frequency to correspond with the absorption frequency of the laser medium. For gas lasers an electrical or radio frequency source is used, again tuned to the particular gas used in a particular laser cavity. Figure 2.1 shows a basic schematic of a solid state, doped crystal (where a crystal is doped with a very small amount, typically as little as 1%, optically active ionic material) laser cavity.

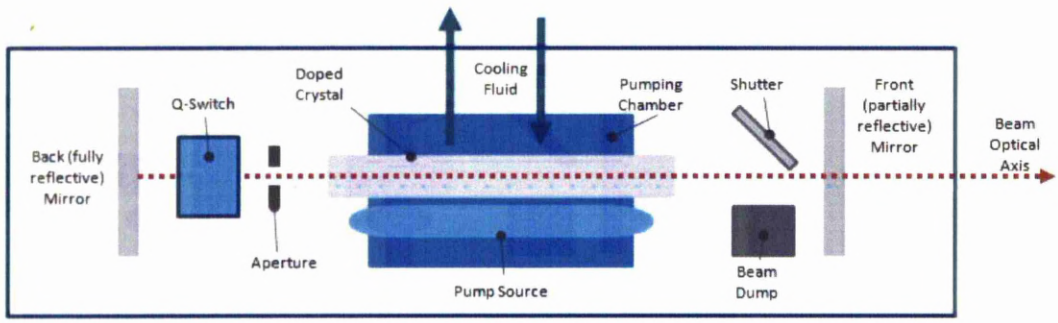

Figure 2.1 Basic schematic representation of a solid state, doped crystal based laser cavity.

The process of creating the laser beam starts with the pump source providing energy to the laser medium. This energy excites the active material in the laser medium (the doped ions in the case of a crystal) and raises them to a higher energy level. When they decay to a lower energy level, a photon is emitted during spontaneous emission. This photon will have a phase and direction. This happens throughout the laser medium. The photons that are in the direction of the optical axis are reflected by the mirrors back into the laser medium, creating an oscillating state. As this occurs the active elements of the media that are in an excited state are perturbed by these photons passing back through the laser medium. This results in a 'stimulated emission' where the photon produced has the same phase, direction, polarisation and frequency as the original photon. This continues as photons continue to oscillate between the mirrors at either end of the cavity,

producing an 'avalanche' of identical photons. This results in light amplification. For stimulated emission to occur, the laser medium must be capable of supporting a 'population inversion'. This is where more of the active part of the laser medium is in the higher/excited energy state than is in the lower energy state. This is to allow for amplification and to avoid absorption by the laser medium. For this to be so, the lifetime of the excited species must be longer than that of the lower energy state. Figure 2.2 shows a simplified energy diagram for a doped crystal based laser, specifically a Nd:YAG laser. The diagram will change depending on the laser medium used.

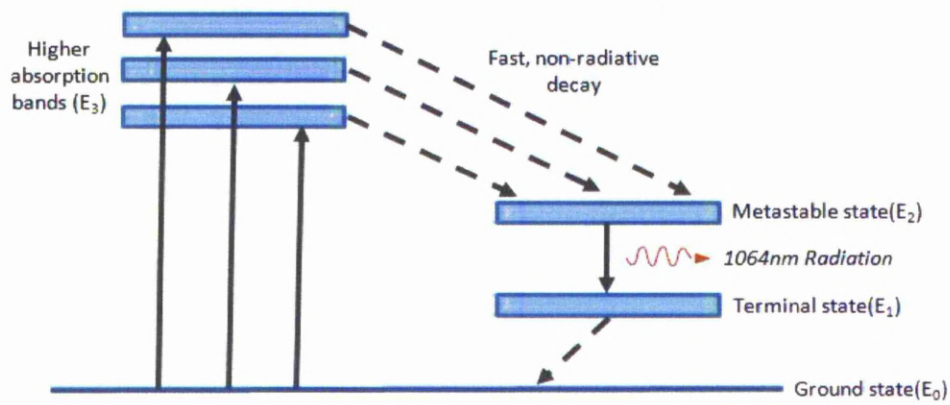

Figure 2.2 Simplified energy level diagram for the pumping of neodymium ions in an Nd:YAG laser cavity

A further component in the cavity to note is the Q-switch (Q standing for Quality). This is particularly important in ultrafast laser systems. The Q-switch can be one of several types; a mechanical 'chopper', a rotating mirror, a saturable absorber, an acousto-optic transducer or an electro-optic transducer. Whatever the form of the Q-switch, its purpose is to spoil the lasing oscillation. If this is done in a controlled way, it can generate pulses of intense power in short pulses. The design of a laser system and the Q-switch is

fundamental to producing lasers capable of emitting ultra short pulses [10][11].

2.2.1.3 Current Laser Micromachining Research and Techniques

It has been said that after the age of steam and then the age of electricity, we are in the age of the photon. Light is used for a wide range of applications from eye surgery to data transfer/telephone technology to materials processing [12]. The property of light to be used in this wide ranging field is the ability to tune and control the form of the light. The energy of a photon (E) is shown in equation (2.1).

$$E = h\nu \quad (2.1)$$

$$\textit{where } h \textit{ is Planks constant and } \nu \textit{ is the frequency}$$

The energy of a photon is dependent on its frequency (wavelength). Light sources of high frequencies result in more energetic photons. Ultra violet, X-Rays and gamma rays have high frequencies and high energy photons. The use of these wavelengths allows for a photolytic process, where the photons have sufficient energy to directly break chemical bonds. Working at these wavelengths is difficult and expensive, requiring complex lasers. If lower frequency light is used, visible and infra red, the photon energy will be lower but if the light is focused it can start a pyrolitic process of heating the material, which if the intensity is high enough can melt a material. This is at the cost of processing capability. The high heat input means that this type of processing is unsuitable for micro machining. The cost and complexity of high energy ultraviolet (Excimer) based lasers and the poor micro scale processing capability of visible an infra red based lasers, has been the limiting factor for laser micro machining. Laser micro machining has only been made a much more viable option with the advent of the ultra short pulsed laser [12]. Depending on the specific process, a wide range of lasers has been used, however. Table 2.1 details the current application fields of micro machining and the lasers generally used for each application.

Field	Laser Type	Application	Material
Microelectronics Packaging	Excimer	Via drilling and interconnect drilling	Plastics, ceramics and silicon
	Solid State (Flash Lamp pumped)	Via drilling and interconnect drilling	Plastics, ceramics, metals and silicon
	Solid State (Diode pumped)	High Volume via drilling	Plastics, metal, inorganic
	Sealed CO_2	Scribing of circuit devices, large panel via drilling	Ceramics, plastics
Semiconductor Manufacturing	Excimer	UV lithography, IC repair, thin films, wafer cleaning.	Resist, plastics, metals, oxides, silicon
	Solid State (lamp and diode pumped)	IC repair, thin films, bulk machining, resistor and capacitor trimming	Plastics, silicon, metals, oxides, thick film
	CO_2	Trimming	Silicon
Data storage devices	Excimer	Wire Stripping, air bearings, read heads, micro via drilling	Plastics, glass, silicon, ceramics
	Solid State (diode pumped)	Disk texturing, servo etching, micro via drilling	Metal, ceramics, plastic
	CO_2	Wire stripping	Plastics
Medical Devices	Excimer	Drilling catheter balloons, angioplasty devices, Micro injection orifice drilling, blood cell slices	Plastics, metals, ceramics, inorganic
	Solid State (lamp and diode pumped)	Stents, diagnostic tools	Metals
	CO_2	Orifice drilling	Plastics
Communication and Computer peripherals	Excimer	Cellular phones, fibre gratings, flat panel annealing, ink jet heads	Plastics, silicon, glass, metals, inorganic
	Solid State (lamp and diode pumped)	Via interconnect coating removal, tape devices	Plastics, metals, oxides, ceramics
	CO_2	Optical circuits	Glass, silicon

Table 2.1 Overview of Laser Micro Machining Applications [11].

Advances in all types of lasers has allowed the field of laser micromachining to grow significantly and as can be seen from table 2.1 are used for specific applications where the individual attributes of each laser type is useful for a particular job. The advances of many types of lasers for a wide range of micromachining has been documented [12]. As this study uses only ultra short lasers, only the advances in this type of laser will be highlighted.

Ultra short pulsed lasers operate using pico ($1x10^{-12}$) and femto ($1x10^{-15}$) second laser pulses. Recent developments have led to an atto (1x10-18) second laser being developed with a 140 nm wavelength [13][14]. Photons delivered in these ultra short pulses can result in multi photon absorption where atoms are affected by several photons simultaneously, giving the same overall effect of being affected by one higher energy photon. If these ultra short pulsed laser beams are directed on a bulk material, the effect can be to strip several electrons from the atoms in the material. This ablates the material in the form of a highly ionised plasma, with very little heat input into the rest of the bulk material. This can be achieved with visible or infra red wavelengths meaning that laser systems can be designed with relatively simple optics [12]. Although ultrafast laser systems usually operate in the visible or infra red, the technology behind creating such ultra short pulses does make them more expensive than standard solid state lasers. Table 2.2 gives a general comparison of solid state lasers and the cost and performance.

Laser type	Solid State (e.g. Nd:YAG)	Q-Switched Solid State	Ultra Short (e.g. Ti:Sapphire)
Pulse Width	1ms	100ns	100fs
Intensity (W/cm^2)	10^8	10^8	10^{15}
Average Power (W)	100-1000	100-1000	1-10
Throughput	High	High	Very Low
Cost	Low	Medium	High
Machine Quality	poor (10s of µm)	Good (µm)	Excellent (sub µm)

Table 2.2 General comparison of solid state lasers and performance [11].

As can be seen from the table, Ultra Short pulsed lasers offer the best processing capability for micromachining but at the cost of throughput and cost.

Presently, most femtosecond lasers are based on titanium:sapphire (Ti:Sapphire), coupled with a chirped pulse amplification technique [15]. Typical commercial systems are available at average powers of 1.5 W and up to 5 kHz repetition rates. They are also capable of producing well below 100 fs pulses, these short pulses are able to produce peak powers of 15 GW. At this short interaction time only the electrons within a material are heated for the interaction duration. Once the laser pulse has stopped, the material experiences the effects of these overheated electrons. Depending on the penetration depth, this can exceed the optical penetration depth of the material. This means that, particularly for low fluences where the diffusion length is smaller than the optical penetration depth, heat diffusion can be strongly suppressed. This allows for high precision at a very low heat influence within the material. This can be on virtually any material due to the high intensity of the laser pulse, allowing for multi-photon effects. The limited average power output of present systems makes them particularly suited to micromachining applications, where the volume of material needed to be removed is small [12].

Applications for ultra short pulsed lasers are numerous from direct use in surgery and the production of medical devices, to grids and gratings, as well as the precision cutting of silicon. An example of this is how ultrashort pulses lasers have opened up new advances in stent production [16]. Coronary stents are used as a minimally invasive treatment as an alternative to bypass operations. New materials such as titanium and bioreabsorbable polymers (which allow for the production of stents which have less complications in use) do not react well to strong thermal loads. Ultra short pulsed lasers are adventitious for producing stents in these materials, Figure 2.3 shows an SEM image of a ultrashort laser produced stent,

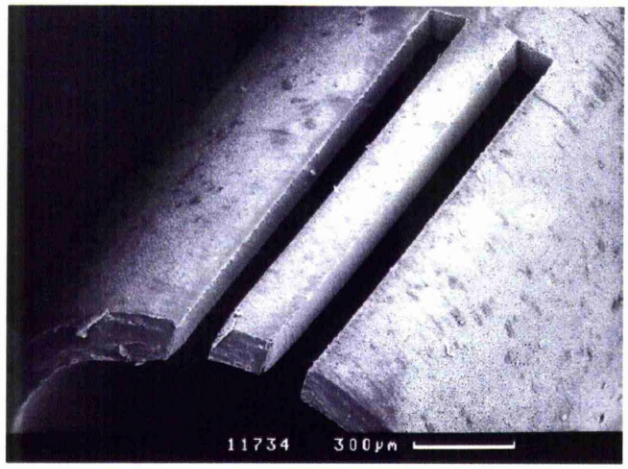

Figure 2.3 Test cuts produced in a PHB (poly-(hydroxybutyrate), which is optically transparent and very heat-sensitive) tube, showing that a micro-machining of this very delicate and heat-sensitive material is possible with minimum thermal load and without the creation of melting [15].

In regards to the cutting of silicon, previously lasers have been unsuitable when cutting high precision structures for the semi conductor industry. This was due to the high heat input which led to thermal melting, deposits and cracks. It has been demonstrated that because thermal and mechanical influences are minimised, ultrashort pulsed laser systems are an ideal tool for cutting thin silicon wafers. Narrow cuts can be performed using a versatile wear free tool [12]. However, there is one problem that can be encountered when using ultrashort pulsed lasers for micro machining. It is that of nano

particle production. Studies have shown that after laser ablation, debris was formed surrounding the craters. This consisted of single crystal Si nano particles with a mean height ranging from ~70 to 500 nm, depending on fluence. While this could be a problem for the semiconductor industry it has been proposed as a method for producing nanoparticles of a controlled size [17]. Figure 2.4 shows an AFM image of debris fields on silicon after processing by a femtosecond laser.

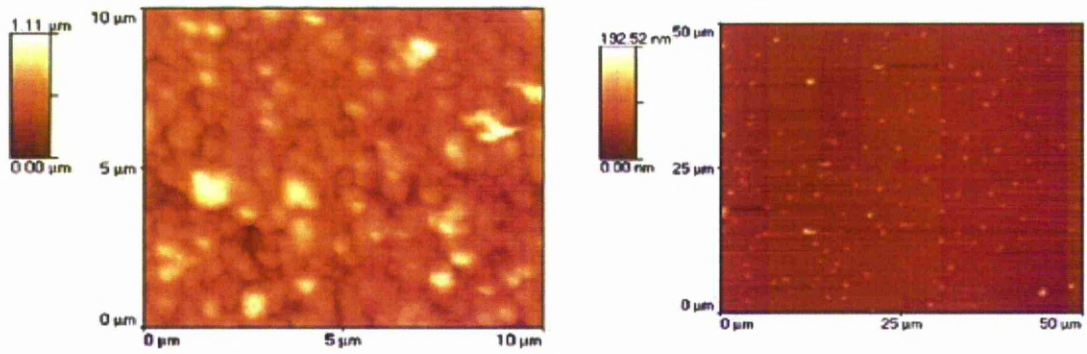

Figure 2.4 AFM images of debris fields surrounding fs laser machined craters on a silicon wafer [16].

There are several other downsides to ultra short pulsed lasers, particularly current generation Ti:Sapphire fs systems. The laser systems are inherently more complex as compared to conventional laser systems, due to the complex optics needed for the chirped amplification system. This can lead to instabilities in the system from changing environmental conditions, such as temperature and vibrations. Ultra short pulsed laser systems, at present, are mainly used for scientific purposes, which necessitates the operation of the laser by highly trained staff. In an industrial operation, such operators are not available. Industrial service requires much easier operation and less maintenance than most of the typical femtosecond lasers can offer. A further drawback is the low average power, provided by commercially available femtosecond lasers. A typical average power is about 1.5W, which limits available pulse energy and repetition rate (typically 4.5 mJ and I kHz). As a result the machining speed is quite low. Recent studies using Spatial

Light Modulators (SLM's) have offered new and novel approaches to increasing throughput however. By Using multiple beams the full power of the laser can be used. The reason for this is the need to work near to the ablation threshold. This means that a large part of the available energy cannot be used without melting tacking place. The SLM technique allows one overpowered main beam to be used as several usefully powered beams [18].

Ultrashort pulsed lasers are presently used for high quality applications, which are not achievable by other means. Due to high capital investment however, low cost applications are not economically viable for this kind of laser. Future laser development, it is predicted, will increase the process speed by increasing repetition rate as well as average output power. By reducing the costs for the laser system as well, economical machining of several applications will be realised [12].

2.2.2 AFM Nano Lithography

The ability to process materials at the nano scale is a very difficult task, particularly for laser systems. With all optical systems lies an inherent factor that limits the resolution, for a microscope or telescope. This limit means that the device has a maximum limit of resolution of the image that they can produce. For a laser system this 'diffraction limit' puts a limit on spot size that a laser can produce and so, a limit on the scale it can machine to. The diffraction limit comes from the fact that when light is focused it does not come together at a point; instead it forms a beam waist at the focal point. Figure 2.5 shows how a Gaussian beam is focused.

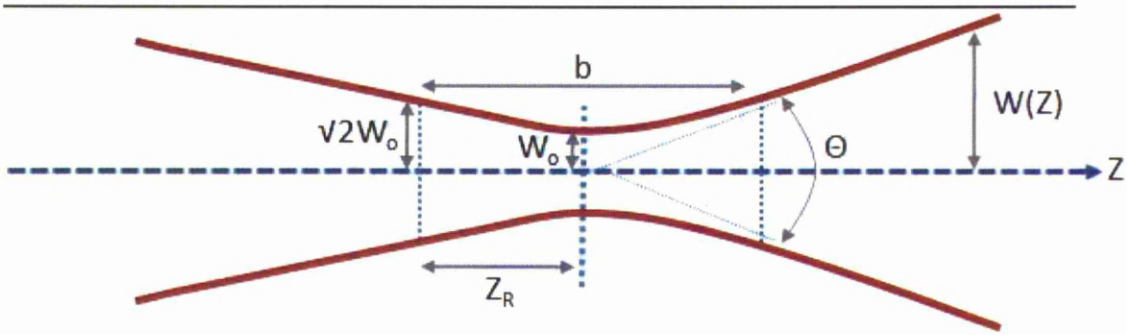

Figure 2.5 Gaussian beam width w(z) as a function of the axial distance z. where; w_0 = beam waist, b = depth of focus, Z_R = Rayleigh range and Θ = total angular divergence

At the beam waist an Airy disc is formed; this is the minimum spot diameter that the laser can form. The radius of this disk (d) is related to the lasers wavelength and is given in equation (2.2). The corresponding angular resolution in space (Θ) is given by equation (2.3).

$$d = 1.22\lambda N \quad (2.2)$$

where λ is the wavelength and N is the f-number (focal length divided by the diameter of the lens)

$$\sin\theta = 1.22\,\frac{\lambda}{D} \quad (2.3)$$

where λ is the wavelength and D is the diameter of the aperture

It is possible to find a way around this problem. One is to use the attributes of a Gaussian beam, that being its shape and energy profile. A Gaussian beam is a beam of electromagnetic radiation whose transverse electric field and intensity (irradiance) distributions are well approximated by Gaussian functions. Which in the case of a laser, the beam is described as operating

on the fundamental transverse mode, or "TEM_{00} mode" of the laser's optical resonator. Figure 2.6 shows a Gaussian beam.

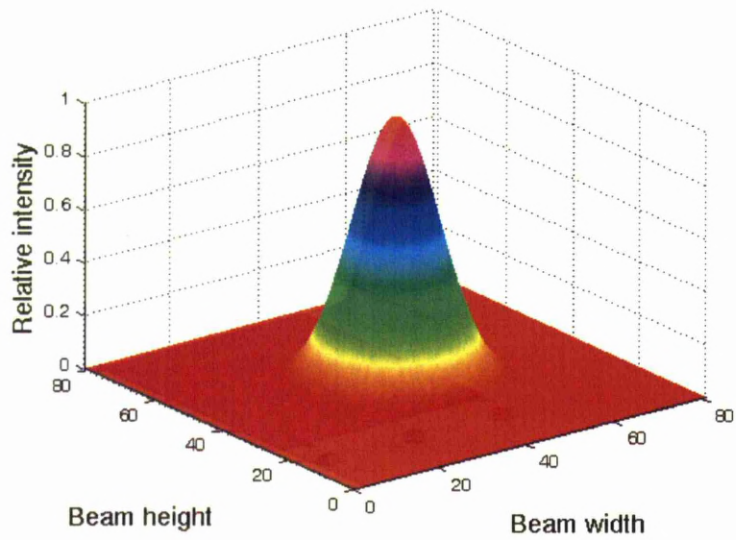

Figure 2.6 Theoretical TEM00 mode Gaussian 3D beam intensity profile [18]

If the energy of a laser beam is controlled so that only the tip of the Gaussian beam is of sufficient energy to process a material (i.e. at the ablation threshold of a material) the effective usable spot size can be decreased. This is known as the sharpened pencil effect [10]. This is more common with standard non micromachining laser processing, The good quality, very near Gaussian beams, of ultrashort pulsed lasers makes this technique possible. However, as such lasers have low average power, it is usable only for materials with low ablation thresholds, such as polymers. Figure 2.7 illustrates the effect of narrowing the spot size of the beam.

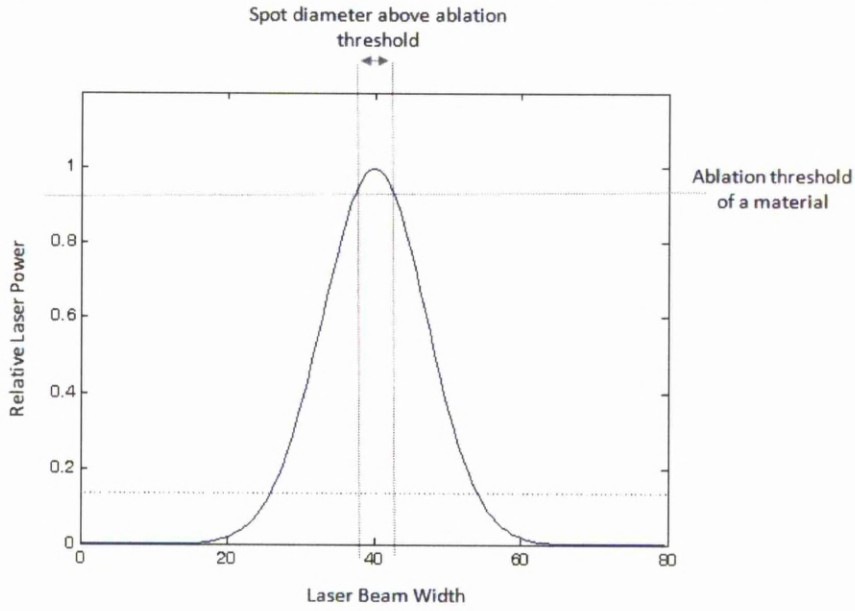

Figure 2.7 The 'sharpened pencil effect' for a Gaussian beam

The other technique is using 'near field' techniques. This is where sub micron to nano scale transparent particles are used to focus the laser beam onto the surface under the particle. This results in a beam smaller than the diffraction limit. To achieve this however requires either a self assembled 'raft' of particles [20] or a complex 'optical tweezers' set up to manipulate the particles to the desired locations under the laser [21]. Both of these techniques require complex optical set up and control of particles to within a few nano meters. In the case of the raft of particles, this is a once only shot as the masking particles are removed after processing with the laser. In the case of the optical tweezers, it must take place in liquid and has limitations on what substrates can be used. The substrate will need to be transparent and very thin due to the very short focal depth needed to achieve the optical trapping.

With optical techniques available but currently in a very early stage of development, another method for producing true nano scale features must be looked for. The atomic force microscope (AFM) allows for such features to be produced.

2.2.2.1 The AFM

Nanotechnology encompasses many processes that are important in the fabrication of integrated circuits, memory devices, display units, biochips and biosensors. One of the key processes in nanofabrication is the creation and construction of functional units in the size regime of less than 100 nm. Two approaches have been used to categorize the generation of nanostructures; the top-down and the bottom up approach. The top-down approach applies various lithographical techniques to create nano scale patterns from a featureless bulk starting material, while the bottom-up route often uses the interactions of molecules and colloidal particles to assemble two- and three-dimensional structures. The conventional techniques for nanofabrication are based on various lithographical methods in the top down approach. Typical examples include photolithography, electron beam lithography, and focused ion beam lithography. They are widely implemented in semiconductor manufacturing. The application of these techniques however, is often limited by their high capital and operating cost, multiple-step processes, and poor accessibility. Several newly developed methods appear to be flexible alternatives for nano scale patterning and fabrication, such as nano-imprint lithography, soft lithography, and AFM nanolithography. These novel methods have the potential to be future low-cost techniques for nano scale pattern formation and replication. Among these newer techniques, AFM nanolithography has shown itself to be a unique tool for materials structuring and patterning with nano meter precision [22].

The AFM was invented in1986 by Binnig, Quate and Gerber [23]. It was designed as a microscope with the ability to resolve objects at the angstrom level. The topographical image of a surface is obtained by recording and regulating the forces felt by a probe as it scans the surface. The AFM can be used to study both insulating and conducting materials, and can be operated in liquid, air or vacuum. The working principle of AFM nanolithography is based on the interaction between the probe and

substrate. The typical radius of curvature of the probe or tip is 10–60 nm, and the tip–substrate separation in close contact condition is <1 nm. When suitable forces are exerted, and/or external fields applied, the probe can induce various physical and chemical processes on the substrate surface. Consequently, localized nanostructures are generated through physical modifications and/or chemical reactions of the surface materials. AFM nanolithography possesses the versatility to pattern a wide range of materials including metals, semiconductors, polymers and biological molecules in different media. Due to its nano scale positioning and imaging capability, AFM nanolithography is uniquely able to create site-specific and localized functional structures. Moreover, the morphological and physical properties of patterns formed can be immediately characterized with AFM by integrating additional measurement modules. This combined fabrication and characterization function in AFM nanolithography allows convenient in situ and in-line pattern creation and characterization [22].

Figure 2.8 shows a basic schematic of how the AFM images a surface. The basic operation of the AFM involves a piezo stage, which moves the sample under the AFM tip and cantilever. The tip sample spacing is controlled using a feedback loop. This is achieved using a laser diode that is directed onto the cantilever via an adjustable mirror. The beam is then directed onto a position sensitive photodiode (PSPD) via another adjustable mirror. The PSPD monitors the movement of the cantilever and uses these data to form an image and control the piezo stage through the feedback loop.

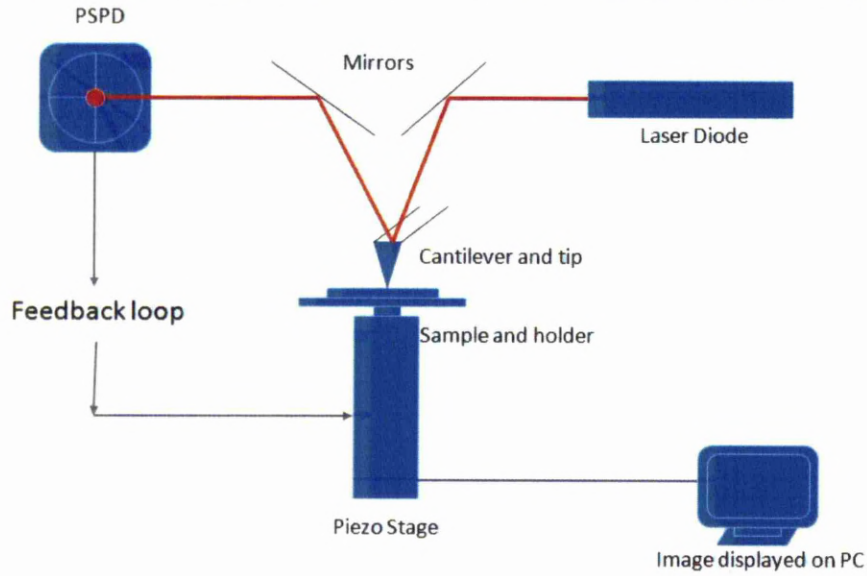

Figure 2.8 Basic schematic of an AFM [23]

An AFM can function using several modes of operation and record many different images of a surface at once. Depending on the mode of operation the AFM can record information about surface friction (Lateral Force Microscopy, LFM), topography, magnetic and electric domain structure (Magnetic and Electro Force Microscopy, MFM and EFM), material hardness and material stiffness. There are three primary modes of operation; Contact mode (CAFM), non-contact mode NC-AFM) and tapping or intermittent contact mode (IC-AFM).

These different imaging modes arise from the two distinct distance regimes that the AFM can operate in. For the contact regime the tip to sample spacing is in the order of a few angstroms. The non-contact regime has a tip to sample spacing of tens to hundreds of angstroms. In the contact regime, the interatomic forces are repulsive, while in the non-contact regime they are attractive, and largely a result of long range Van der Waals interactions. NC-AFM provides a means for measuring sample topography with little or no contact between the tip and the sample. The total force between the tip and the sample in the non-contact regime is very low, generally in the pico Newton range. This low force is advantageous for studying soft or elastic

samples. Because the force between the tip and the sample in the non contact regime is low, it is more difficult to measure than the force in the contact regime, which can be several orders of magnitude greater. In addition, cantilevers used for NC-AFM must be stiffer than those used for contact AFM because soft cantilevers can be pulled into contact with the sample surface. The small force values in the non contact regime and the greater stiffness of the cantilevers used for NC-AFM, are both factors that make the NC-AFM signal small and therefore difficult to measure [22]. This can make operating in NCAFM mode difficult and often time consuming as slower scan speeds must be used to prevent tip snap in, where the cantilever is deflected into the sample and a contact mode regime. Figure 2.9 shows the distance and imaging regimes for an AFM

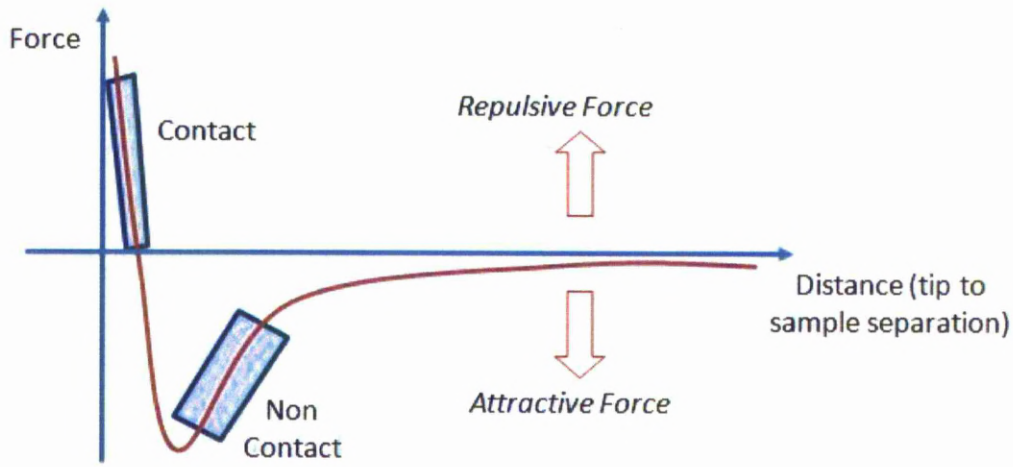

Figure 2.9 Interatomic force vs. distance curve, which illustrates the force between atoms on a cantilever tip and atoms on a sample surface vs. the separation distance between the tip and the sample [23]

In non-contact mode, the system vibrates a stiff cantilever near its resonant frequency (typically from 100 to 400 kHz) with an amplitude of a few tens to hundreds of angstroms. It then detects changes in the resonant frequency or

vibration amplitude as the tip comes near the sample surface. The sensitivity of this detection scheme provides sub-angstrom vertical resolution in the imaged, as with contact AFM. A sample topography is image by controlling the vibrations of the cantilever via the feedback loop of the AFM system. The fundamentals behind this are described as following; The resonant frequency (ω) of the cantilever is described in equation (2.4)

$$\omega = \sqrt{\frac{k_{eff}}{m}} \quad (2.4)$$

where k_{eff} is the Spring constant of the cantilever and m is its mass

Here, the spring constant is written as k_{eff}, the effective spring constant, because the spring constant of the cantilever changes as the cantilever moves into close proximity (within a few hundred angstroms) of the sample surface and inter atomic forces affect its behaviour. Specifically, the spring constant changes when the force between the tip and the sample has a spatial gradient, as it does in the non-contact regime. The effective spring constant k_{eff} is given in equation (2.5).

$$k_{eff} = k - f \quad (2.5)$$

where k is the spring constant of the cantilever and f is the force gradient

The spring constant, k, is the value of the cantilever's spring constant in free space, i.e. it is the value when the cantilever is far from the sample surface. The value of the cantilever's resonant frequency far from the sample surface is referred to as its free-space resonant frequency.

Equations (2.4) and (2.5) show that if the cantilever moves into a tip-to-sample spacing regime where the force gradient is positive and increasing, then the effective spring constant of the cantilever, and therefore its resonant frequency, decreases. Figure 2.9 shows that in the non-contact tip-to-sample spacing regime the force gradient is positive, and it increases

as the tip-to-sample spacing decreases. Thus, when an oscillating cantilever is brought near a sample surface, the force gradient experienced by the cantilever increases, and its resonant frequency decreases. If the resonant frequency of a cantilever shifts then the amplitude of cantilever vibration, at a given frequency, changes. Near a cantilever's resonant frequency this change is large. Figure 2.10 shows a response curve, vibration amplitude vs. frequency, for a cantilever for NC-AFM.

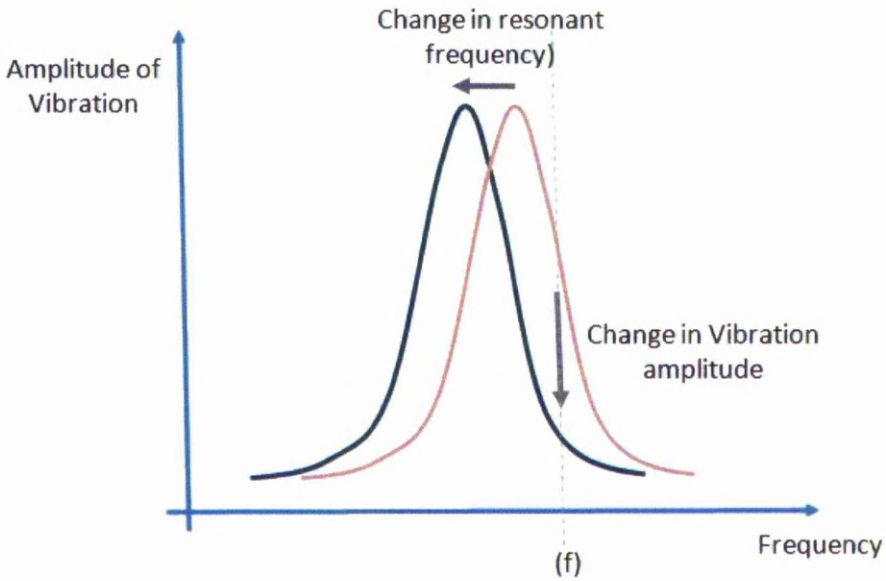

Figure 2.10 Response curve of an AFM cantilever showing vibration amplitude vs. frequency for NC-AFM [23].

If the curve shifts to the left, for example, then there is a change (in this case, a decrease) in the amplitude of cantilever vibration at a given frequency (f). For NC-AFM detection, the cantilever is driven at a fixed frequency near resonance (f in Figure 2.9), and changes in its vibration amplitude are detected. In NC-AFM mode, a drive frequency close to, but greater than, the free-space resonant frequency of the cantilever is selected so that the vibration amplitude decreases significantly as the cantilever is brought closer to the sample surface. These amplitude changes reflect the change in the

force gradient acting on the cantilever, which in turn reflects changes in the tip-to-sample spacing. The feedback loop mechanism operates to maintain a constant cantilever vibration amplitude by adjusting and restoring the tip-to-sample spacing during a scan. As in contact-AFM mode, the amount of scanner z movement necessary to maintain the tip-to-sample spacing (or constant force gradient in the case of NC-AFM) is used to generate an image of topography [24].

To give the best of both worlds, intermittent contact or tapping mode is often used. It allows for the imaging of soft or elastic samples but it is a more stable mode of imaging. The underlying principles for intermittent-contact AFM are the same as those for NC-AFM. The difference is that for IC-AFM the cantilever is driven (forced to vibrate) at a fixed frequency close to, but less than, its free-space resonant frequency. Figure 2.11 shows a response curve, vibration amplitude vs. frequency for a cantilever for NC-AFM.

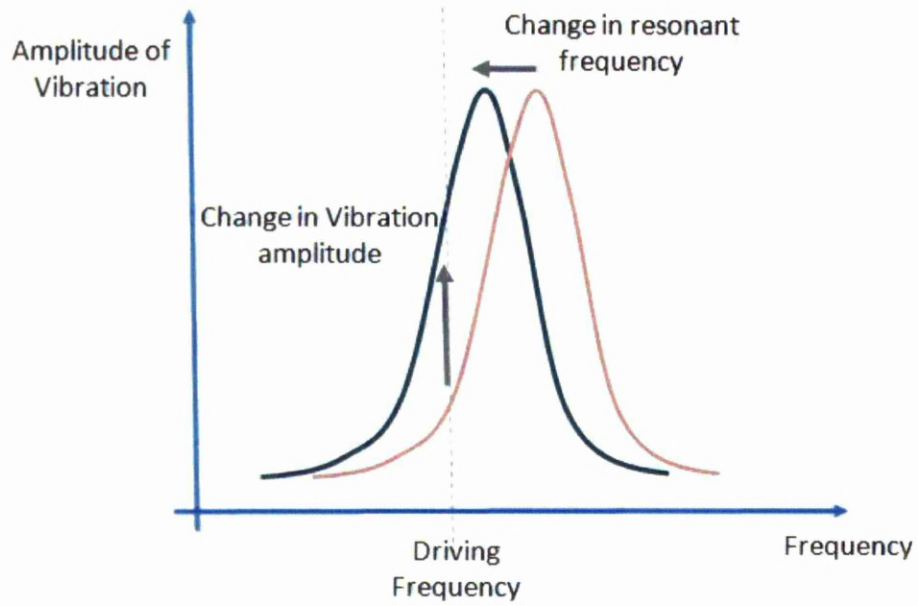

Figure 2.11 Response curve of an AFM cantilever showing vibration amplitude vs. frequency for IC-AFM [23].

Because the drive frequency is just below the free-space resonant frequency, the vibration amplitude of the cantilever increases as the cantilever is brought closer to the sample surface, and intermittent contact is consequently achieved [24]. The imaging is performed in the same manner as for CAFM and NC-AFM.

2.2.2.2 Force Assisted Lithography; Nano Ploughing

Numerous AFM-based lithographic techniques have been developed in the last two decades. Generally, these techniques can be classified into two groups in terms of their operational principles; force-assisted AFM nanolithography and bias-assisted AFM nanolithography. In force-assisted AFM nanolithography, a large force is applied to the tip for pattern fabrication, and the tip–surface interaction is mainly mechanical. Typical methods in this category include mechanical indentation and ploughing, thermo-mechanical writing, nano-manipulation, and dip-pen nanolithography (DPN). During force-assisted nanolithography, forces larger than those used for AFM imaging are loaded onto the tip. The initially featureless surface is then patterned by mechanically scratching, pulling, or pushing the surface atoms and molecules with the probe. In DPN, instead of manipulating the existing molecules on the surfaces, the tip is used as a nano scale pen to directly deposit collections of ink materials onto the substrate to define a functional structure. In bias-assisted AFM nanolithography, the AFM tip is biased to create a localized electric field and the tip acts as a nano scale electrode, for current injection or collection. Under such a high localized field, electrostatic, electrochemical, field emission, dielectric breakdown and explosive gas discharge processes can be initiated to facilitate pattern formation. Depending on the magnitude of tip bias and substrate materials, the application of tip voltage can lead to anodic oxidation electrochemical deposition, electrostatic attraction, and nano scale explosion and shock wave propagation. In anodic oxidation, the tip is negatively biased, and the local field induces the ionic dissociation of a

water meniscus formed between the tip and sample surface. The oxidative OH^- anions migrate along the field and react with the substrates to form oxide structures [22]. As the experiments presented in this study use only force assisted nano ploughing, only this technique will be detailed further.

There are three typical methods used in AFM Nanolithography; Indentation, static ploughing and dynamic ploughing. Indentation is the simplest means of single structure formation in which the tip is immobilized at a specific surface site and a large force is then applied to the tip to indent the surface. In static ploughing, the tip is operated in contact mode, and is scanned with a large load across the surface to define features in the shape of lines, rectangles, and squares. Dynamic ploughing involves scratching the surface with a vibrating tip in tapping mode, and the force of the tip is modulated by adjusting the amplitude of the cantilever oscillations. Since a low force is used to image and modify soft polymers in tapping mode, the pattern irregularities caused by cantilever torsion under high contact forces are minimized in dynamic ploughing. During a dynamic ploughing operation, the cantilever is driven to vibrate near its resonance frequency, and its oscillation amplitude depends on the distance between the tip and sample. Modification of substrate materials is achieved by increasing the modulation amplitude. As the tip approaches the sample surface, structures are created by elastic and plastic deformations of the substrate [22]. A study looking at the different methods for nano ploughing found that dynamic ploughing was the fastest and most practical of the techniques tested [25]. Figure 2.12 shows a basic schematic of how the AFM tip creates structures in a substrate.

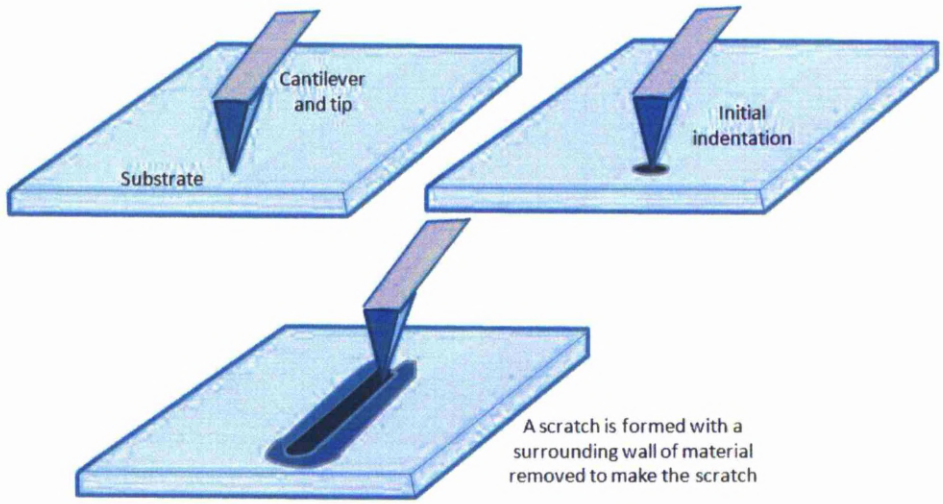

Figure 2.12 Basic schematic for AFM nanolithography

Nano ploughing with the AFM has been performed on several different types of materials. The most common are polymers, due to the soft nature of polymers there has been a strong interest in the patterning of them with the AFM [22]. Work has been done on metal and metal oxides, using diamond tips [25], and in aqueous acid solutions [27], both resulting in sub 100nm structures. Semiconductors have also been successfully patterned with experiments producing 10nm wide patterns on a GaAs surface [28].

AFM nanolithography offers an alternative to other nanofabrication techniques (electron beam lithography, UV photo lithography) but does suffer from one main disadvantage, it is a serial process. The nature of the AFM means only one pattern can be processed at a time. Current methods mean that an initial scan must be completed, processed and imaged for each pattern. To get around this problem arrays of cantilevers have been proposed, allowing for multiple patterns to be processed simultaneously. There have been some successes; a 32x32 cantilever array has been demonstrated for use with thermo-mechanical AFM techniques [29]. Integrating this into current systems however, has yet to be addressed. Further advancement of AFM nanolithography, it is speculated, will rely on

future efforts to understand control and optimise the nanofabrication process [22].

2.3 The Influence of Topography on Cell Response

2.3.1 Cell-Topography interactions

Observations of cell and substrate interactions date back to 1911, a phenomenon known as stereotropism was first documented by Harrison [30] . Embryonic cells were grown on a spider's web and it was noted that the cells would grow along the filaments of the web following the fibres. This was the first noted example of a substrate affecting cell behaviour. The fist link between surface topography and the development of a cell was proposed by Curtis and Varde [31] in 1964. Since then many studies have been conducted using a range of cell, material and topography types [32]. Both nano and micro Scale features have been shown to have an effect on cell. These effects can be categorised into the following types; adhesion, alignment/orientation, morphology, proliferation and differentiation. How the topography influences each of these cell responses is detailed below.

2.3.1.1 Topography and Cell Adhesion

Cells attach to in vitro surfaces via a layer of proteins, this layer is called an extra cellular matrix (ECM) [33]. The composition, type, amount and conformation of this ECM will regulate the secondary phenomena of cellular adherence and protein exchange. The first phase of protein adsorption onto a biomaterial's surface is characterized by the attachment of small rapidly diffusing proteins, This is followed by a progressive replacement by larger proteins with a high affinity to the substrate. Such proteins, with Arginine-Glycine-Aspartic acid (RGD) containing sequences like fibronectin or vitronectin, act as cell receptors and have adhesive properties. The mechanism for this adhesive property is via integrins. Integrins are receptors that can mediate attachment between a cell and the tissues surrounding it

[34]. They bind a cell to the ECM components, such as fibronectin through lock and key sites inside the cell membrane and type specific ligands in the ECM. A schematic diagram of how cells attach to surfaces is shown in Figure 2,13. Figure 2.14 shows a schematic diagram of a cell and the cell adhesion receptors.

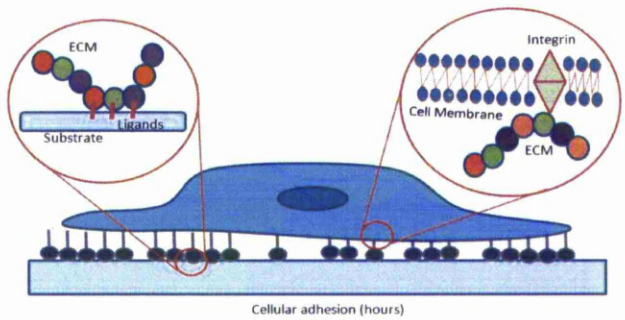

Figure 2.13 Schematic diagram of surface, cell and protein interactions

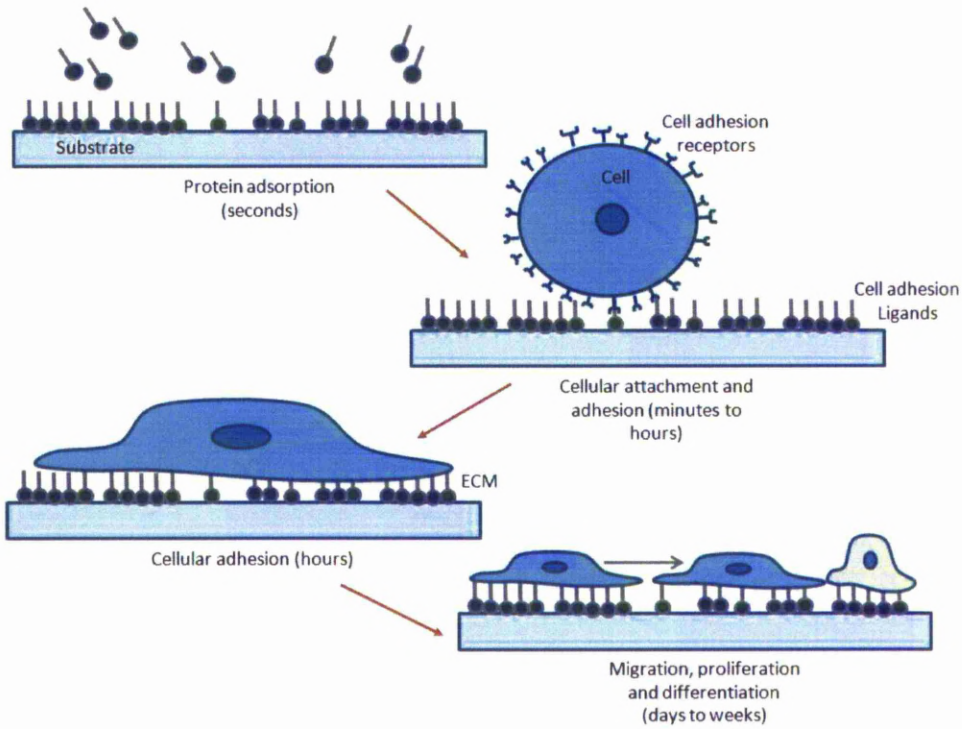

Figure 2.14 Schematic diagram of how a cell attaches to a surface and its effect over time on the cell

The effect of topography on adhesion is unclear. Cell adhesion on micro and nano topographies has been investigated using several different cell types including; human astrocytes on 1µm wide, 250nm deep grooved poly methylmethacrylate (PMMA) [35], Osteoblasts on 4µm wide 5µm deep grooves on polyimide [36], fibroblasts on polycaprolactone (PCL) and PMMA with 35, 75 an 120 nm deep pits [37][38][39] and bladder smooth muscle cells on poly D, L-Lactic acid (PDLA), poly-ether-urethane (PU) and PCL with random 206nm and 370nm features [40]. These studies show improved adhesion, no change in adhesion, reduced adhesion and improved adhesion respectively. The nano and micro scale features have been shown to both improve or reduce adhesion depending on cell type. It is suggested that integrin (cell adhesion receptor) spacing may be a cause of the differences in results [41], where focal adhesions are affected depending on specific nano feature spacing, resulting in increased or decreased cell adhesion.

2.3.1.2 Topography and Cell Alignment, Orientation and Morphology.

A wide range of cells has been shown to respond by aligning to grooved substrates when seeded onto a range of processed materials. In general cells elongate and align in the direction of the grooves, to a greater or lesser extent depending on cell type and on groove depth. Groove width was also a noted factor but to a lesser degree, it has been shown that apart from red blood cells, no other cell type has responded to grooves of greater than 20µm pitch [42]. The range of experiments conducted is shown in table 2.3, this shows the cell type, topography type and size, material type and effect on the cells.

Reference	Cell Type	Material & Feature Type	Feature Width	Feature Height/Depth	Effect on Alignment and Orientation
[43]	Mesenchymal Stem Cells	Grooves on Quartz	1, 4µm	1.1µm	Better alignment in 4µ grooves
[44]	Fibroblasts	Grooves on Silicon dioxide	0.5µm	1µm	Strong Alignment to Groove
[44]	Keratinocytes	Grooves on Silicon dioxide	0.5µm	1µm	No Alignment
[45]	BHK Cells(Baby HamsterKidney)	Grooves on PMMA	2 to 12 µm	0.2 to 1.9µm	Alignment increased with >depth and reduced with >diameter
[35]	Human Astrocytes	Grooves on PMMA	1µm	0.25µm	Strong alignment with features
[36]	Osteoblasts	Groves on Polyimide	4µm	5µm	Strong alignment with features
[46]	Schwann (nerve) Cells	Grooves on PDLA	10µm	3µm	Strong alignment with features
[47]	Rat Astrocytes	Groves on Polystyrene	3µm	20µm	Strong alignment with features
[48]	Fibroblasts	Groves on Polystyrene	20nm to 1µm	5 to 530nm	No Alignment for depths less than 35nm or features less than 100nm in width

Table 2.3 Table showing experiments on micro and nano scale surface topographies with varying cell types detailing changes in cell alignment and orientation

The general trend is that orientation and alignment (in the direction of the groove) increases with increasing feature depth but decreases with groove width [45]. This is with the exception of one study where decreasing groove pitches (from 4 to 0.4μm) appeared to cause epithelial cells to switch, from aligning parallel to the grooves to orientating perpendicular to the grooves, with a decrease in the pitch size [49]. It was noted that this caused a change to the focal adhesion distribution. The trends observed with grooved substrates are not repeated with other micro scale topography 'types' (pits/wells/pillars). However, on the nano scale, it has been reported that fibroblasts can 'feel symmetries' in nano scale pitted substrates [38]. The study concluded that the cells were oriented with the symmetric patterns produced by the pits but no effect was observed when the cells were seeded on a random pattern of the same pits; this was found to be independent of surface chemistry.

The morphology of cells appears to be significantly affected, regardless of cell type, by both micro and nano surface topographies. The resultant change in morphology appears, from the literature, to be related to the type of surface topography. Table 2.4 shows how the different cell type's morphology is affected by surface topography.

From the experiments listed in the above table, grooved features appear to produce elongated cells, bridging narrow deep features or conforming to larger ones. Cells appear to become rounder and smaller on nanometer to ~5μm sized pits/pillar type topography. Again, integrin complexes are looked to for an explanation; the literature points to a direct link between the topography and the cell. The cell membrane, when in contact with the surface topography will undergo mechanical forces which can rearrange the cell attachment sites, so affecting cell morphology [56].

Reference	Cell Type	Material & Feature Type	Feature Width	Feature Height/Depth	Effect on Cell Morphology
[50]	Murine P388D1 macrophage	Grooves on Quartz	0.5 to 25µm	0.5 to 5µm	Cell elongation which is greater for wider grooves
[51]	Human Fibroblasts	Grooves on Epoxy	0.5µm	1µm	Cytoskeleton oriented with grooves
[52]	Rat Bone Cells	Grooves on polystyrene	1 to 10µm	0.5 to 1.5µm	Cells bridge grooves smaller than 5µm width
[36]	Osteoblasts	Grooves on Polyimide	4µm	5µm	Elongation with grooves
[53]	Fibroblasts	Wells on Polycarbonate	7 to 50 µm	0.5 to 2.5 µm	No elongation
[54]	Fibroblasts	Pits in polycaprolactone	80nm	300nm	Cytoskeleton less developed
[55]	Fibroblasts	Pillars on PMMA	100nm	160nm	Smaller and less organised cytoskeleton

Table 2.4 Table showing experiments on micro and nano scale surface topographies with varying cell types detailing changes in cell morphology

2.3.1.3 Topography and Cell Proliferation and Differentiation

Unlike morphology, the effect on topography on cell proliferation appears to be dependant mainly on cell type, However many studies overlook this aspect when looking at cell response. The reason for this may be a lack of systematic studies or the experiments that have been conducted with very robust and prolific cell types [1].

Only a few systematic studies into cell differentiation have been conducted, gene expression has however been shown in some earlier experiments [50][52][56][58]. The most significant study reported that, when human mysenchymal stem cells (huMS) were seeded onto random circular nanostructures, the topography had promoted direct diffentiation of the cells. Of note was that the experiment was conducted in serum free conditions, free of promoter cells in the culture medium [58][59].

2.4 Human Embryonic Stem (HuES) Cells

From the literature it is clear that topography is an important factor in how cells behave and develop, particularly for in vitro experiments. It is also clear that cell type can play a major role in what response a cell has to its underlying surface topography. This study will concentrate on one type of cell, the HuES cell. There is great interest in HuES cells for numerous reasons but few studies have used them in their investigations. The use of HuES cells in therapeutic medicine could offer treatments for many degenerative diseases that today have no cure. The following section will describe the basics of what makes a HuES cell unique and detail the possibilities for them in therapeutic medicine. It will also detail the current level of HuES cell research.

2.4.1 The Human Embryonic Stem Cell

Human embryonic stem cells are pluripotent, unspecialised cells. They are able to differentiate into each of the more than 220 cell types in the adult body. They are able to differentiate both in vitro and in vivo [60]. They are capable of self renewal, propagating themselves indefinably, without differentiating so maintaining their pluripotent state. Under the microscope, they have a large nucleus and prominent nucleoli. In the colonies in which they grow in tissue culture, they have a defined border and the cells are tightly packed within it [61]. Figure 2.15 shows a scanning electron microscope image of an undifferentiated HuES cell.

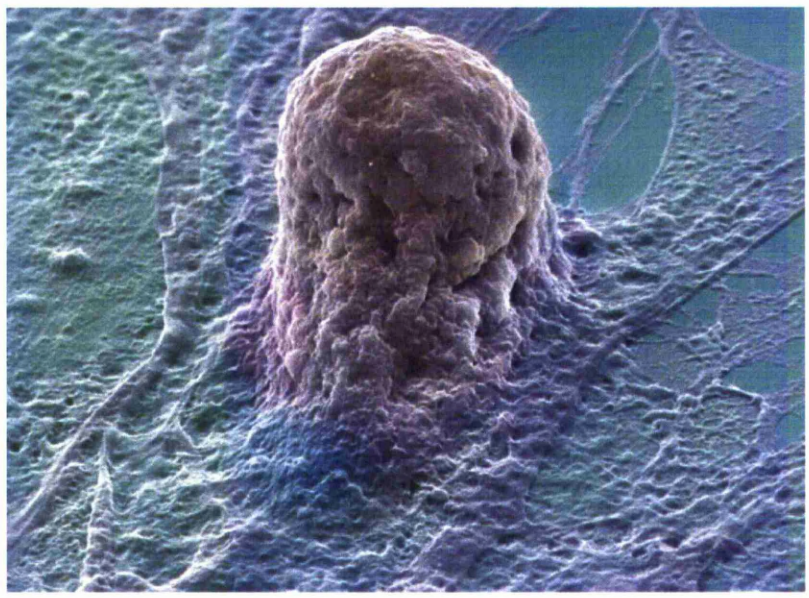

Figure 2.15 Colour-enhanced scanning electron micrograph of a human embryonic stem cell (coloured yellow) growing on a layer of supporting cells (fibroblasts) [62]

HuES cells are harvested from donated embryos at the blastocyst stage [63]. The embryo is composed of the inner cell mass and the trophectoderm. The trophectoderm is committed to forming the outer layer of the placenta, but the inner cell mass retains the ability to form any cell of the body. The embryonic stem cells are derived from this isolated inner cell mass. [64].

The pluripotent cells of the inner cell mass were first identified, using mouse embryos, in the 1980's [65][66]. These newly derived mouse embryonic stem cells (ESC's) were shown to have the capability of plural differentiation and became an attractive tool for understanding early events during the development and renewal of tissues. However, they could not be used for clinical applications so attention focused on human derived stem cells [67]. The first HuES line to be derived was done in 1998 [63] and repeated in 2000 [68]. Since then several more HuES cell lines have been established and new ways of obtaining them have been discovered; donated blastocysts, poor-quality discarded embryos, embryos carrying genetic defects following

preimplantation genetic diagnosis and non-usable aneuploid zygotes. The method for maintaining the HuES cell lines in an undifferentiated state in these early studies required the use of mouse feeder cells. This meant that there was a possibility of contamination of the HuES cells from animal pathogens. The need for an animal free culture systems has therefore been necessary. To date HuES cells have been cultured and maintained in an un-differentiated state using several different types of human cells as a feeder cell layer. These include; foetal and adult muscle and skin, fallopian tube epithelium, glandular endometrium, stromal endometrium, marrow stromal and foreskin cells [67].

A feeder-free layer culture system aimed at facilitating research practices and providing a safer alternative for future clinical applications of HuES cells has been developed using human fibronectin (FN) [69]. This has allowed for a serum and feeder cell free culture medium to be used, standardising investigations into HuES research. How the FN works in this way is a growing area of research.

2.4.2 The potential of HuES cells

The potential of HuES cells comes primarily from the ability to differentiate into all derivatives of the three primary germ layers: ectoderm, endoderm, and mesoderm. Figure 2.16 shows a diagram of the differentiation of human tissue from a fertilised egg.

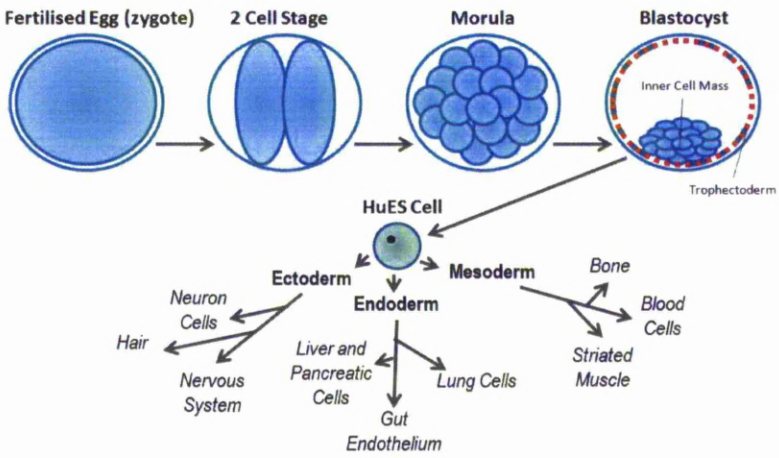

Figure 2.16 Diagram showing the differentiation of human tissue from the fertilised egg.

Many lineages have been derived from HuES cells, these include; neurons, cardiomyocytes, endothelial and smooth muscle cells, hematopoietic cells, osteogenic cells, epidermis, hepatocytes and insulin-producing cells [67]. This ability to culture different human cells in the laboratory has led to great interest for both research and regenerative medicine. Developmental biology is one area of study, providing insight into congenital defects and mechanisms of development embryology, in vitro. The processes behind this, such as tissue differentiation, can be observed and the genes which control them identified. There is also the potential for the use of HuES cells in pharmaceutical research, by observing how new medicines interact with different cell types that differentiate from HuES cells, in a controlled laboratory environment, again in vitro. Models of human disease can be created, and new therapies can be tested, providing additional information and making human trials safer [70]. The area of research that has the most potential to make HuES cells a ground breaking and revolutionising field is if stem cells can be used to generate replacement cells. This could result in new therapies to treat many diseases that impact heavily on human life, such as form cell loss related diseases such as Parkinson's disease, diabetes

and retinal degeneration [63][71][72]. As well as degenerative diseases, there is also potential for HuES cells to be differentiated to provide therapy for cancer patients in need of blood-forming cells in bone marrow, as heart muscle cells after a heart attack, and as nerve cells for spinal injury and other damage or diseases of the central nervous system [70]. The prospect for this is promising, with progress having already been made; differentiated HuES cells have been used to replace human B cells as a therapy for type 1 diabetes [73].

2.4.3 The Stem Cell Niche.

The stem cell niche is an anatomical site that contains a reservoir of multi-potent stem cells. These cells can maintain normal tissue, replenish injured (or aged cell populations) in response to mechanisms that regulate whether they should remain quiescent, undergo self-renewal, or differentiate. The stem cell behaviour is governed by intricate signals that are systemic or presented by the local niche cells [74]. The stem cell niche is described as the microenvironment in which stem cells are found and which interacts with stem cells to regulate stem cell fate. The word 'niche' can be in reference to the in vivo or in vitro stem cell microenvironment. During embryonic development, various niche factors act on embryonic stem cells to alter gene expression and induce their proliferation or differentiation for the development of the foetus. Several factors are important to regulate stem cell characteristics within the niche: cell-cell interactions between stem cells, as well as interactions between stem cells and neighbouring differentiated cells, interactions between stem cells and adhesion molecules, extracellular matrix components, the oxygen tension, growth factors, cytokines, and physiochemical nature of the environment including the pH, ionic strength and metabolites. The stem cells and niche may induce each other during development and reciprocally signal to maintain each other during adulthood. Niches can be thought of as specific anatomic locations that regulate how they participate in tissue generation, maintenance and repair. The niche saves stem cells from depletion, while

protecting the host from over-exuberant stem-cell proliferation. It constitutes a basic unit of tissue physiology, integrating signals that mediate the balanced response of stem cells to the needs of organisms. The interplay between stem cells and their niche creates the dynamic system necessary for sustaining tissues, and for the ultimate design of stem-cell therapeutics. The simple location of stem cells is not sufficient to define a niche. The niche must have both anatomic and functional dimensions [75]

The work presented in this thesis can be thought of as attempting to create an artificial in vitro stem cell niche. As has been indicated in the literature, understanding the different niche conditions in vivo can cause complications in comparing and understanding stem cell behaviours in vitro [74]. Several studies have looked into creating these artificial stem cell niches, with a view to understanding how stem cells respond in vivo. Studies have used gel-like structures containing a hydrated network of glycosaminoglycan chains and protein polymers. Also hydrogels, which are highly hydrated networks of natural alginate and collagen which resemble the natural extra cellular matrix [76] have been studied. Limitations to such materials, including difficulties with reproducible sources of materials, immunogenicity, potential pathogen contamination, and poor control over mechanical properties, have encouraged the development of synthetic biomaterials as cellular substrates [74]. Extensive reviews of these biomaterials have been carried out, looking at surface biocompatibility [77] and bulk properties and surface modifications [78]. The rapidly expanding field of engineering artificial stem cell niches, is anticipated to have a major impact on the biotechnology industry, with further progress in deciphering the complex network of niche signals and in the engineering of artificial microenvironments to control stem cells for numerous applications [74].

2.4 References

[1] Martinez, E., Engel, E., Planell, J,A., Samitier, J. 2009. Effects of artificial micro-and nano-structured surfaces on cell behaviour. Ann Anat. 191, 126—135

[2] Langford, R.N., Petford-Long, A.K., Rommeswinkle, M and Egelkamp, S. 2002. Application of a focused ion beam system to previous termmicronext term and nanoengineering, Mater. Sci. Technol. 18, 743–748

[3] C.R.K. Marrian and D.M. Tennant, Nanofabrication. 2003 J. Vaccum Sci. Technol. A 21, S207–S215

[4] Maxwell J.C. 1864. A Dynamical Theory of the Electromagnetic Field. Philosophical Transactions of the Royal Society of London. 155, 459-512.

[5] Planck M. 1900. On The Theory of the Law of Energy Distribution in the Continuous Spectrum. Annalen der Physik. 1, 99.

[6] Einstein A. 1905. On energy quanta. Annalen der Physik. 17, 132-148

[7] Einstein A. 1917. On the quantum theory of radiation - English Translation, Physikalische Zeitschrift. 18, 121-128.

[8] Ladenburg R. and Kopfermann, H. 1928. Research on the anomalous dispersion of gases - English Translation. Physikalische Zeitschrift. 48, 26-57.

[9] Maiman T.H. 1960. Stimulated optical radiation in ruby. Nature. 187, 493-494.

[10] Steen W.M. 2003. Laser Material Processing. Springer, Third Edition.

[11] Saleh B.E.A. and Teich, M.C. 2007. "Fundamentals of photonics", Wiley, New York, Second Edition

[12] Meijer, J., Du, K., Gillner, A., Hoffmann, D., Kovalenko, V.S., Masuzawa, T., Ostendorf, A., Poprawe. R. and SchulzLaser, W. 2002. Machining by short and ultrashort pulses, state of the art and new opportunities in the age of the photons. CIRP Annals - Manufacturing Technology 51, 531-550.

[13] Hentschel, M., Kienberger, R., Spielmann, C., Reider, G.A., Milosevic, N., Brabec, T., Corkum, P., Heinzmann, U., Drescher, M and Krausz, F. 2001. Attosecond metrology. Nature. 414, 509

[14] Hewett, J. 2002. Time for attosecond consolidation. Optics and Lasers Europe. OLE, 30

[15] Strickland, D and Mourou, G. 1985. Compression of amplified chirped optical pulses, Opt. Comm. 56, 219

[16] Momma, C., U. Knoop, S. Nolte. 1999. Laser cutting of slotted tube coronary stents. State of the art and future developments. Biomedical research. 39-44.

[17] Semaltianos, N.G, Perrie, W., Vishnyakov, V., Murray, R., Williams, C.J., Edwardson, S.P., Dearden, G., French, P., Sharp, M., Logothetidis, S., Watkins, K.G. 2008. Nanoparticle formation by the debris produced by femtosecond laser ablation of silicon in ambient air. Materials Letters. 62, 2165–2170

[18] Kuang, Z., Perrie, W., Leach, J., Sharp, M., Edwardson, S.P., Padgett, M., Dearden, G and Watkins, K.G. 2008. High throughput diffractive multi-beam femtosecond laser processing using a spatial light modulator. Applied Surface Science. 255, 2284–2289

[19] Mullet, J.D. 2009. Laser Induced Ignition Systems for Gasoline Automotive Engines. PhD Thesis, University of Liverpool.

[20] Zhou, Y., Hong, M.H., Fuh, J.Y.H., Lu, L., Lukyanchuk, B.S., Wang, Z.B. 2008. Near-field enhanced femtosecond laser nano-drilling of glass substrate. Journal of Alloys and Compounds 449, 246–249

[21] Mcleod, E. and Arnold, C.B 2009. Array-based optical nanolithography using laser trapped microlenses. Optics Express, 17, 3640-3650

[22] Xie, X.N., Chung, H.J., Sow, C.H., Wee, A.T.S. 2006. Nanoscale materials patterning and engineering by atomic force microscopy nanolithography. Materials Science and Engineering. 54, 1–48

[23] Binnig, G., Quate, C.F, and Gerber, C. 1986. Atomic Force Microscope. Phys. Rev. Lett. 56, 930

[24] Veeco Instruments Inc. 2004. di CP-II User's Guide Part II: Advanced Techniques

[25] Cappella, B. and Sturm, H. 2002. Comparison between dynamic plowing lithography and nanoindentation methods. Journal Of Applied Physics. 91, 506-512

[26] Filho, H.D.F., Maurício, M.H.P., Ponciano, C.R., and Prioli, R. 2004. Metal layer mask patterning by force microscopy lithography. Sci. Eng. B. 112, 194

[27] Kato, Z., Sakairi, M., and Takahashi, H. 2003. Nanopatterning on aluminium surfaces with AFM probe. Surf. Coatings Technol. 169–170, 195-198.

[28] Lü, J., Li, H., An, H., Wang, G., Wang, Y., Li, M., Zhang, Y. and Hu, J. 2004. Positioning Isolation and Biochemical Analysis of Single DNA Molecules Based on Nanomanipulation and Single-Molecule PCR. J. Am. Chem. Soc. 126 (36), 11136–11137

[29] Vettiger, P., Cross, G., Despont, M., Drechsler, U., Dürig, U., Gotsmann, B., Häberle, W., Lantz, M.A., Rothuizen, H.A., Stutz, R. and Binnig, G.K. 2002. IEEE Transactions On Nanotechnology. 1, 39-55

[30] Harrison, R.G.,1911. On the Stereotropism of embryonic cells. Science34,279–281

[31] Curtis, A.S.G., Varde,M., 1964. Control of cell behaviour: topological factors.J.Nat.CancerRes.Inst.33,15–26.

[32] Flemming, R.G., Murphy C.J., Abrams, G.A., Goodman, S.L., Nealey, P.F. 1999. Effects of synthetic micro- and nano-structured surfaces on cell behaviour. Biomaterials 20, 573-588.

[33] Gumbiner, B.M. 1996. Cell Adhesion: The Molecular Basis of Tissue Architecture and Morphogenesis. Cell. 84, 345–357.

[34] Hynes, R.O. 2002. Integrins: Bidirectional, allosteric signaling machines. Cell. 110, 673-687

[35] Baac, H., Lee J-H., Seo, J-M., Park, T.H., Chung, H., Lee, S-D., Kim, S.J. 2004. Submicron-scale topographical control of cell growth using holographic surface relief grating. Materials Science and Engineering. C. 24, 209–212

[36] Charest, J.L., Bryant, L.E., Garcia, A.J., King, W.P. 2004. Hot embossing for micropatterned cell substrates. Biomaterials. 25, 4767–4775

[37] Dalby, M.J, Gadegaard, N., Riehle, M.O., Wilkinson, C. D. W., Curtis, A. S. G. 2004. Investigating filopodia sensing using arrays of defined nano-pits down to 35 nm diameter in size. The International Journal of Biochemistry & Cell Biology. 36, 2005–2015

[38] Curtis, A.S.G., Casey, B., Gallagher, J.O., Pasqui, D., Wood, M.A., Wilkinson, C.D.W. 2001. Substratum nanotopography and the adhesion of biological cells. Are symmetry or regularity of nanotopography important? Biophysical Chemistry. 94, 275–283

[39] Curtis, A. S. G., Gadegaard, N., Dalby, M. J., Riehle, M.O., Wilkinson, C. D. W., and Aitchison, G. 2004. Cells React to Nanoscale Order and Symmetry in Their Surroundings. IEEE Transactions on Nanobioscience. 3, 61-65

[40] Thapa, A., Webster, T.J., Haberstroh, K.M. 2003 Polymers with nano-dimensional surface features enhance bladder smooth muscle cell adhesion. Journal of Biomedical Materials Research Part A. 67A, 1374–1383

[41] Cavalcanti-Adam, E.A., Volberg, T., Micoulet, A., Kessler, H., Geiger B. and Spatz, J.P. 2007. Cell spreading and focal adhesion dynamics are regulated by spacing of integrin ligands. Biophys. J. 92 (8), 2964–2974

[42] Wilkinson, C.D.W., Riehle, M., Wood,M., Gallagher, J. and Curtis A.S.G. 2002. The use of materials patterned on a nano and micro-metric scale in cellular engineering, Mater. Sci. Eng. C 19, 263–269

[43] Wood, A. 1988. Contact guidance on microfabricated substrata: the response of teleost fin mesenchyme cells to repeating topographical patterns, J. Cell Sci. 90, 667–681

[44] Meyle, J., Gutlig, K. and Nisch, W.1995. Variation in contact guidance by human cells on a microstructured surface, J. Biomed. Mater. Res. 29, 81–88

[45] Clark, P. Connolly, P., Curtis, A.S.G., Dow, J.A.T. and Wilkinson, C.D.W. 1990. Topographical control of cell behavior: II. Multiple grooved substrata. Development. 108, 635–644

[46] Miller, C., Shanks, H., Witt, A., Rutkowski, G. and Mallapragada, S. 2001. Oriented Schwann cell growth on micropatterned biodegradable polymer substrates, Biomaterials. 22, 1263–1269

[47] Recknor, J.B., Recknor, J.C., Sakaguchi, D.S. and Mallapragada, S.K. 2004. Oriented astroglial cell growth on micropatterned polystyrene substrates, Biomaterials. 25, 2753–2767

[48] Loesberg, W.A., te Riet, J., van Delft, F.C.M.J.M., Schön, P., Figuredor, C.G., Speller, S., van Loon, J.J.W.A., Walboomers, X.F. and Jansen, J.A. 2007. The threshold at which substrate nanogroove dimensions may influence fibroblast alignment and adhesion. Biomaterials. 28, 3944–3951

[49] Teixeira, A.I., McKie, G.A., Foley, J.D., Bertics, P.J., Nealey, P.F. and Murphy, C.J. 2006. The previous termeffectnext term of environmental factors on the response of human corneal epithelial cells to nanoscale substrate topography. Biomaterials. 27, 3945–3954

[50] Wojciak-Stothard, B. Madeja, Z., Korohoda, W. Curtis, A. and Wilkinson, C. 1995. Activation of macrophage-like cells by multiple grooved substrata. Topographical control of cell behavior, Cell Biol. Int. 19, 485–490

[51] Meyle, J., Wolburg, H., and Recum, A.F. 1993. Surface micromorphology and cellular interactions, J. Biomater. Appl. 7, 362–374

[52] Matsuzaka, K., Walboomers, X.F., Yoshinari, M., Inoue, T. and Jansen, J.A. 2003. The attachment and growth behavior of osteoblast-like cells on microtextured surfaces, Biomaterials. 24, 2711–2719

[53] Hunt, J.A., Williams, R.L., Tavakoli, S.M. and Riches, S.T. 1995. Laser surface modification of polymers to improve biocompatibility. J. Mater. Sci. Mater. Med. 6, 813–817.

[54] Gallagher, J.O., McGhee, K.F., Wilkinson, C.D.W. and Riehle, M.O. 2002. Interaction of animal cells with ordered nanotopography. IEE Trans. Nanobiosci. 1, 24–2

[55] Dalby, M.J., Riehle, M.O., Sutherland, D.S., Agheli, H. and Curtis, A.S.G. 2004. Changes in fibroblast morphology in response to nanocolumns produced by colloidal lithography. Biomaterials. 25, 5415–5422

[56] Andersson, A.S., Bäckhed, F., Euler, A., Richter-Dahlfors, A., Sutherland, D. and Kasemo, B. 2003. Nanoscale features influence epithelial cell morphology and cytokine production. Biomaterials. 24, 3427–3436

[57] Dalby, M.J., Riehle, M.O., Yarwood, S.J., Wilkinson, C.D.W. and Curtis, A.S.G. 2003. Nucleus alignment and cell signaling in fibroblasts: response to a microgrooved topography, Exp. Cell Res. 284, 274–282

[58] Dalby, M.J., McCloy, D., Robertson, M., Agheli, H., Sutherland, D., Affrossman, S. and Oreffo, R.O.C. 2006. Osteoprogenitor response to semi-ordered and random nanotopographies, Biomaterials. 27, 2980–2987

[59] Dalby, M.J., Gadegaard, N., Tare, R., Andar, A., Riehle, M.O., Herzyk, P., Wilkinson, C.D.W. and Oreffo, R.O.C. 2007. The control of human mesenchymal cell differentiation using nanoscale symmetry and disorder, Nat. Mater. 6, 997–1003

[60] Amit, M., Carpenter, M.K., Inokuma, M.S., Chiu, C-P., Harris, C.P., Waknitz, M.A., Itskovitz-Eldor, J. and Thomson, J.A. 2000. Clonally Derived Human Embryonic Stem Cell Lines Maintain Pluripotency and Proliferative Potential for Prolonged Periods of Culture. Developmental Biology. 227, 271-278

[61] Bodnar, M., Meneses, J., Rodriguez, R. T., Firpo, M. T. 2004. Propagation and Maintenance of Undifferentiated Human Embryonic Stem Cells. Stem Cells and Development. 13, 243-253

[62] Colour-enhanced scanning electron micrograph by Annie Cavanagh and Dave McCarthy. Stem cells were grown by Jessica Cooke at King's College London.B0006219. Biomedical Image Awards 2006.

[63] Thomson, J. Itsokovitz-Eldor, J., Shapiro, S. S., Waknitz, M. A., Swiergiel, J. J., Marshall, V. S., Jones, J. M. 1998. Embryonic stem cell lines derived from human blastocysts. Science. 282, 1145-1147

[64] Thomson, J.A. and Odorico, J.S. 2000. Human embryonic stem cell and embryonic germ cell lines. Trends in Biotechnology. 18, 53-57

[65] Evans, M.J. and Kaufman, M.H. 1981. Establishment in culture of pluripotential cells from mouse embryos, Nature. 292,154–156

[66] Martin, G.R. 1981. Isolation of a pluripotent cell line from early mouse embryos cultured in medium conditioned by teratocarcinoma stem cells. Proceedings of the National Academy of Sciences of the USA. 78, 7634–7638

[67] Gerecht-Nir, S. and Itskovitz-Eldor, J. 2004. The promise of human embryonic stem cells. Best Practice & Research Clinical Obstetrics & Gynaecology. 18, 843-852

[68] Reubinoff, B.E., Pera, M.F. and Fong, C. 2000. Embryonic stem cell lines from human blastocysts: somatic differentiation in vitro. Nature Biotechnology. 18, 399–404

[69] Amit, M., Shariki, C., Margulets, V. and Itskovitz-Eldor, J. 2004. Feeder layer and serum-free culture of human embryonic stem cells. Biology of Reproduction. 70, 837–845

[70] He, Q., Li, J., Bettiol, E., Jaconi, M. E. 2003. Embryonic Stem Cells: New possible therapy for degenerative diseases that affect elderly people. The Journals of Gerontology Series A; Biological Sciences and Medical Sciences 58, M279-M287

[71] Enzmann, V., Yolcu, E., Kaplan, H. J., Ildstad, S. T. 2009. Stem cells as tools in regenerative therapy for retinal degeneration. Archives of Ophthalmlogy. 127, 563-571.

[72] Guo, T., & Hebrok, M. 2009. Stem cells to pancreatic B-Cells: New sources for Diabetes cell therapy. Endocrine Reviews. 30, 214-227.

[73] Assady, S., Maor, G., Amit, M., Itskovitz-Eldor, J., Skorecki, K. L., and Tzukerman, M. (2001) Insulin Production by human embryonic stem cells. Diabetes. 50, 1691-1697

[74] Vazin, T and Schaffer, D.V. 2010. Engineering strategies to emulate the stem cell niche. Trends in Biotechnology. 28, 117-124.

[75] Scadden, D.T. 2006. The stem-cell niche as an entity of action. Nature. 441, 1075-1079

[76] Dawson, E., Mapili, G., Erickson, K., Taqvi, S., Roy, K. 2008. Biomaterials for stem cell differentiation, Adv. Drug Deliv. Rev. 60, 215–228

[77] Vadgama, P. 2005. Surface biocompatibility. Annu. Rep. Prog. Chem., Sect. C, 2005, 101, 14–52

[78] Roach, P., Eglin, D., Rohde, K., Perry, C.C. 2007. Modern biomaterials: a review—bulk properties and implications of surface modifications. J Mater Sci: Mater Med. 18, 1263–1277

Chapter 3

Laser Produced Micro Scale Features on Transparent Substrates

3.1 Introduction

The work presented in this chapter involves the use of an Ultra Short Pulse Laser to process the surface of transparent substrates. Experiments focused on attempting to create micro scale surface features on the substrates, with a view to using the processed substrates for cell experiments involving growth and spreading observations.

As the substrates were to be used with living cells, it was desirable to have a substrate that is easy to use in a biological setting. Transparent substrates that allow for standard phase contrast microscopy were selected so standard cell protocols could be used in the cell biology observations. Using an ultrashort pulsed laser system would provide such a technique, allowing for the production of micro sized features, having sufficient energy to couple into a transparent substrate.

A set of samples were produced that were to be used with cell biology experiments. These experiments were designed to show the possibility for cells to be affected by an artificial, engineered topography.

3.1.1 Effect of Topography on Cells

Recent advances in the ability to produce surface features down to the nano level has meant many studies have now taken place to show how different cell types react to different surfaces. Table 3.1 shows some of the studies conducted to date on cell behaviour when grown on substrates with different surface topographies [1]

Feature type	Material	Width*/ diameter	Depth/height	Pitch	Cell type	Effects on orientation and adhesion
Grooves	Quartz	0.5, 5, 10, 25 μm	0.5, 5 μm	1:1	Murine P388D1 macrophage	Orientation
Grooves	Quartz	1, 4 μm	1.1 μm	1:1	Mesenchymal stem cells	Alignment better in the widest grooves
Grooves	Silicon dioxide	0.5 μm	1 μm	1:1	Fibroblasts	Strong alignment
Grooves	Silicon dioxide	0.5 μm	1 μm	1:1	Keratinocytes	No alignment
Grooves	PMMA	2, 3, 6, 12 μm	0.2, 0.5, 1.1, 1.9 μm	1:1	BHK cells	Alignment increased with d. and decreased with w.
Grooves	Photo-responsive PMMA	1 μm	250 nm	1:1	Human astrocytes (HAs)	Improved adhesion, strong alignment
Grooves	PS	1–10 μm	0.5–1.5 μm	N/D	Rat bone cells	Large grooves: focal adhesions all over the surface. Narrow grooves: only on the edges
Grooves	Polyimide	4 μm	5 μm	34 μm	Osteoblasts	Strong alignment, no changes in adhesion
Grooves	PDLA	10 μm	3 μm	20 μm	Schwann cells (nerve cells)	Strong alignment
Grooves	PS	10 μm	3 μm	20 μm	Rat astrocytes	Less adhesion, strong alignment
Grooves	PS	20–1000 nm	5–530 nm	1:1	Fibroblasts	No alignment for depths < 35 nm or widths < 100 nm
Grooves	Silicon	330–2100 nm	600 nm	400–4000 nm	Human corneal epithelial cells	Perpendicular alignment for 400–800 nm pitch. Parallel for 1600–4000 nm
Steps	PMMA	1–18 μm	N/D	N/D	BHK	Alignment at steps
Wells	PC	7, 25, 50 μm	0.5, 1.5, 2.5 μm	1:1	Fibroblasts	No orientation
Pits	PCL	150 nm	80 nm	300 nm	Fibroblasts	Less focal contacts and vinculin pattern
Pits	PCL, PMMA	35, 75 and 120 nm	N/D	100, (200, 300 nm	Fibroblasts	Reduced adhesion, orientation and distinction of symmetries
Random	PLGA, PU, PCL	206, 370 nm	N/D	N/D	Bladder smooth muscle cells	Enhanced adhesion

Abbreviation list: N/D: non-determined; PMMA: poly(methylmethacrylate); PDMS: poly-dimethyl siloxane; PC: polycarbonate; PS: polystyrene; PLLA: poly(L-lactide acid); PET: poly(ethylene terephthalate); PBrS: poly(4-bromostyrene); PCL: polycaprolactone; PDLA: poly(D,L-lactic acid); PLGA: polylactic-co-glycolic-acid; PU: poly-ether-urethane.
*The width parameter refers to the groove width.

Table 3.1 Summary of the effects of micro and nano structured surfaces on cell orientation and adhesion [1]

As can be seen from the table many cell types and surface topographies have been tested, with many different observations made. The work in this chapter concentrates on producing a simple micro scale surface topography with which to observe how one cell type reacts to the surface. Human embryonic stem cells (HuES) are of great interest for their possible applications in therapeutic medicine and tissue engineering and have the

possibility to revolutionise the field [2]. Few studies have looked into using HuES cells with topography experiments, often due to complications arising from ethical issues, around the use of the cells in research and medicine [3] [4].

3.2 Materials and Methods

3.2.1 Substrates

13 mm Borosilicate glass cover slips were obtained from VWR International (Lutterworth, UK) and were used throughout the experiments detailed in this chapter. These were either processed directly or were coated using a complex multi-component acrylic based polymer whose composition can be discretely modified to alter surface properties (The polymer supplied by Biomer Technology Ltd, Runcorn; Liverpool, UK). This polymer was applied to the cover slips by spin coating at 500 rpm for 45 seconds on the glass cover slips using a single wafer spin processor (WS-400B-6NPP-Lite) from Laurell Technologies Corporation. The glass cover slips were then placed on a hot plate at 100°C for 5 minutes and later cured in an oven at 100°C for 45 minutes. The timings for the spin process was found by experimentation over several days. Over spinning (due to too high a spin speed or spin time) would lead to a cloudy and uneven surface which resembled a porous surface when viewed under the AFM. Figure 3.1 shows a 2D AFM image of (a) a glass cover slip coated with the polymer at too high a spin speed (2000 rpm) and (b) a glass cover slip processed at a 500 rpm.

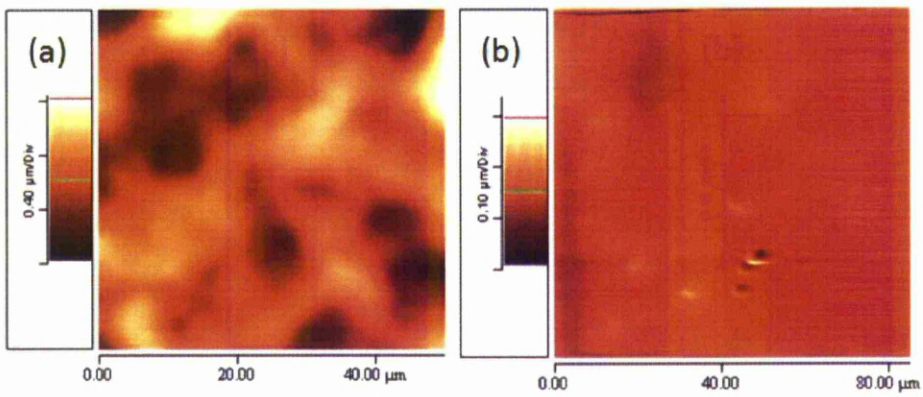

Figureure 3.1 AFM image showing glass cover slips coated with polymer (a) 2000 rpm (b) 500 rpm

3.2.2 Laser System

A Clarke-MXR 2010 system, which delivers maximum pulse energy Ep ≈ 1 mJ at 1 kHz repetition rate, 775 nm fundamental wavelength (λ), 180 femtosecond pulse duration, was used in conjunction with a scanning galvanometer and Aerotec 5-axis stage.

The laser uses a mode locked, diode pumped erbium doped ring fibre laser at 1550 nm whose output is frequency doubled to 775 nm to seed a Ti–sapphire regenerative amplifier. The beam intensity spatial profile is near Gaussian with a measured 3D Gaussian fit parameter of 0.87 (Spyricon LBA300 with Pulnix TM745E CCD camera). The beam is slightly elliptical, 4.8 mm×5.2 mm and shows some residual astigmatism, probably due to cavity design incorporating a Brewster cut Ti–sapphire crystal in the regenerative amplifier. The enclosure temperature is stabilised at 20 °C using a small dedicated chiller (VWR Scientific Products) which also keeps the Ti–sapphire crystal temperature stable. Output pulse stability is typically ±1%. Pre-pulse and post-pulse amplitudes were minimised and measured to be <0.2 and 1.7%, respectively (Coherent power meter/Molectron pyroelectric detector) [5].

The laser processing was controlled using the SAMlight software package. The incident laser power was controlled using a pair of half wave plates to attenuate the beam. Inline power measurement was done using the above power meter. Figure 3.2 shows the experimental laser set up. Figure 3.3 shows a photograph of (a) the laser and (b) the scanning galvanometer, on site at the Lairdside Laser Engineering Centre (LLEC), Birkenhead.

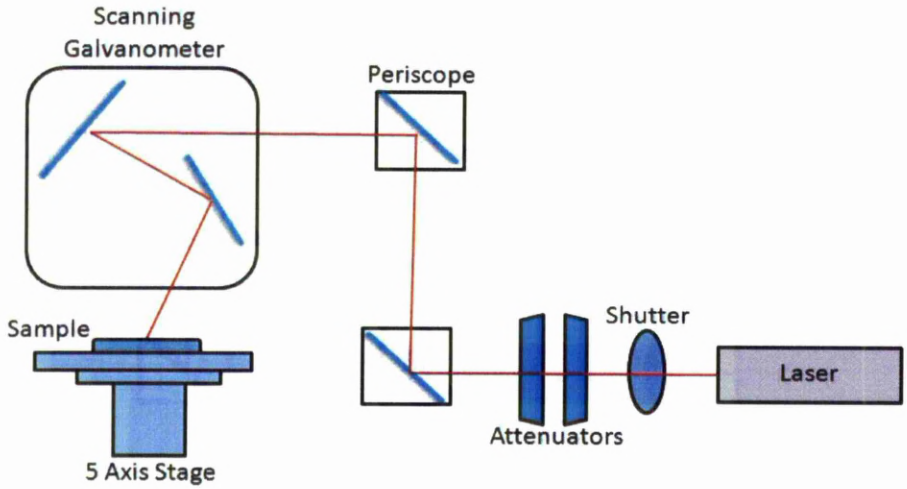

Figure 3.2 Experimental laser setup for micro processing experiments

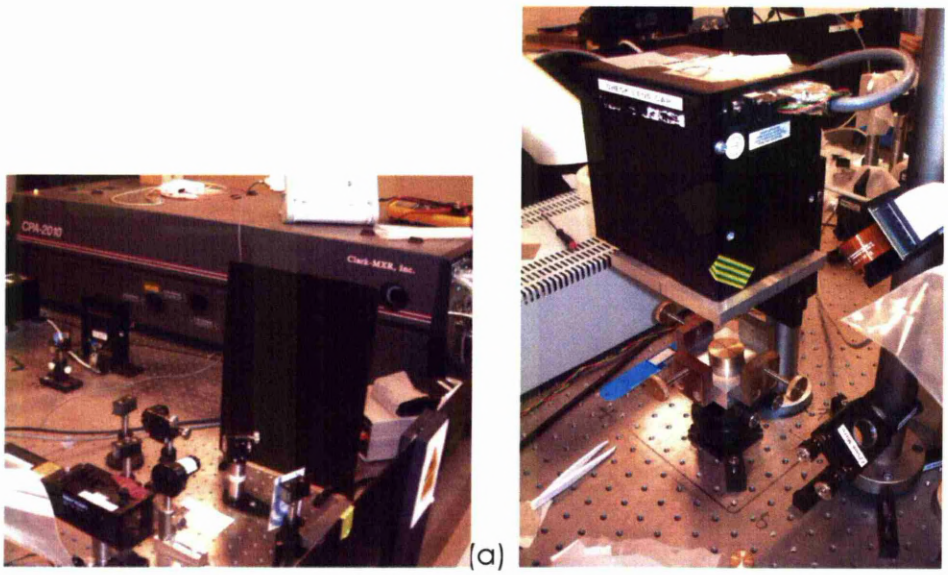

Figure 3.3 Photograph of the Clark femtosecond a) laser head and b) scanning galvanometer used to machine the substrates.

3.2.3 Laser Parameters

Preliminary tests were conducted using the polymer coated glass cover slips. A grid of 40x40 drill events was set up using the SAMlight software. Initial samples were produced at 2.5, 5 and 10 µJ using 50, 50 and 25 pulses respectively. It was found that 10µJ of laser energy and 25 pulses per drill event produced the best results on the polymer coated cover slips.

Using these parameters a set of samples was produced, changing the number of drill events and the distance between them. The patterns were produced on both polymer coated and bare glass cover slips. The patterns produced are detailed in table 3.2.

Hole Spacing (µm)	Number of Drilled Holes(Grid size)	Process Time (s)	Process Energy (µJ)	Number of Laser Pulses per hole
30	40,000 (200x200)	1000	10	25
40	22,500 (150x150)	580	10	25
60	10,000 (100x100)	300	10	25
90	4,900 (70x70)	150	10	25
120	3,025 (55x55)	90	10	25

Table 3.2 - Process parameters, time and pattern overview for processed glass and polymer samples

The samples were produced in batches of 45, 9 of each pattern. This was to allow for the multiple repeats needed for the cell biology observations.

The machined samples were imaged using an optical microscope fitted with Nikon objectives and CCD camera. A Veeco WYCO white light interferometer was also used to ascertain data on the depth of the holes

3.2.4 Growing Cells on the processed substrates

The laser processed samples were taken to the Department Cellular and Molecular Physiology at the University of Liverpool, the experiments being conducted by Dr Joan Downes. Both the polymer and bare glass samples were first coated in fibronectin (FN), this allows for a more rapid cell attachment when using lower seeding densities of cells [6]. The FN was coated and HuES cells seeded on the samples using a standard protocol detailed below.

HuES7 cells (obtained from Harvard University, HuES cells facility, Melton laboratory, MA, USA) were cultured in feeder/ serum free conditions on FN coated surfaces as described before [4]. Cell culture media used throughout this study was composed of 50:50 F12 :DMEM (Lonza) supplemented with 2mM L-glutamine, 1% NEAA, 0.1 mM β-marcatoethanol, 0.1% bovine serum albumin (BSA), serum free supplements N2 (1x), and B27 (1x), human recombinant growth factors i.e., activin A (10ng/ml), Neurotrophin-4 (4ng/ml) and FGF2 (40ng/ml). The cells were cultured on 24 well tissue culture plates pre-coated with a fibronectin coating concentration of 10ug/ml (500ul/well), which was then incubated at 37°C for 1 hour. Cells were maintained in these conditions by subsequent passage after 3-4 days of culture using trypsin. [7].

Cell attachment was checked after 1 hour under a Nikon light microscope and photographs were taken at 24 hours on a Leica inverted microscope at 10X and 40X magnification.

3.3 Results

3.3.1 Laser machining of the Substrates

The laser was successful in producing distinct micro scale features on both the polymer coated and plain glass cover slip. A microscope image of the machined samples is shown in Figure 3.4. A WYCO image used to ascertain the depth of the features is shown in Figure 3.5

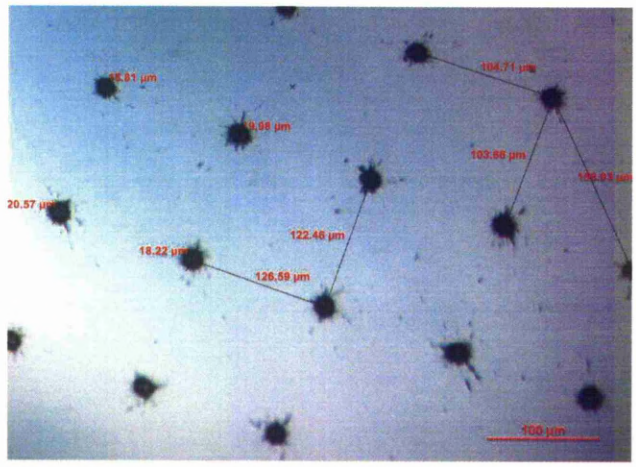

Figure 3.4 Microscope image of the machined micro scale features on glass cover slips

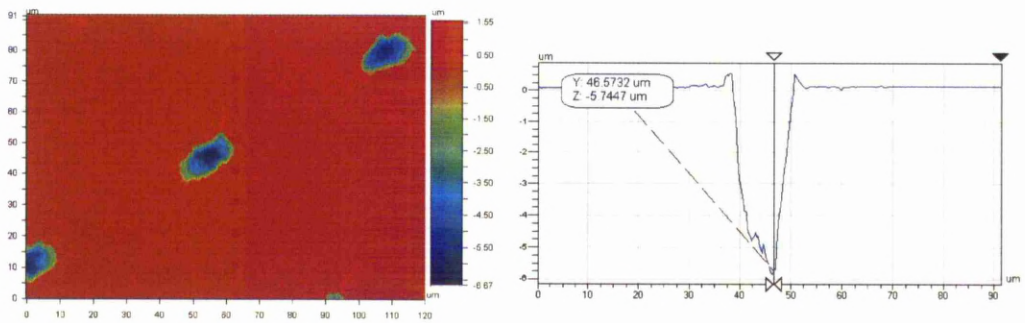

Figure 3.5 WYCO image and depth plot for determining the depth of the machined features on a glass cover slip

Figure 3.5 shows a WYCO image for a typical laser machined hole on the glass substrates, the drilled features are between 18 and 22μm in diameter and slightly elliptical in shape. WYCO depth measurement indicates the depth to be ~6μm. Further measurements are needed to determine the average depth of the drilled holes. Both figure 3.5 and 3.4 show a build up of debris around the machined features.

Although the samples were transparent when viewed under the microscope, a small amount of debris was noticed on the back of the samples. The samples were placed on a brass mount in order to correctly position the samples in the focal plane of the laser beam. This mount appeared to be ablated during the laser processing and so coated the back of the glass cover slips. To avoid the risk of contamination the laser machined cover slips were placed in 24 well plates and incubated in 500μm of cell media for a week at 37.5°C. The cell media was replaced with fresh media every two days to remove the adsorbed debris. Figure 3.6 shows a photograph of the laser processed sample indicating the build up of debris on the back of the glass cover slips. The amount (indicated by the dark area of glass where the machining has taken place) of debris increased with the increase in the number of holes drilled into the substrates.

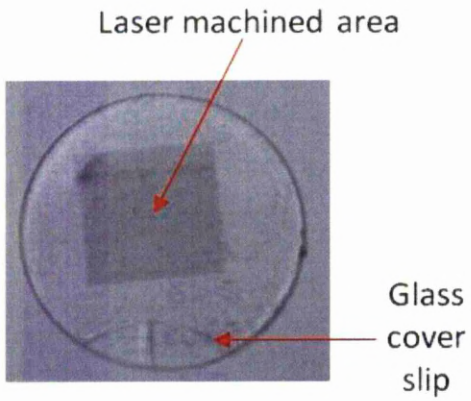

Figure 3.6 Photograph showing the build up of debris (darker area) on the back of laser machined glass cover slips

3.3.2 Cell Observations

Both the plain glass and polymer coated glass samples were prepared for the cell observations. However due to non-ideal conditions when preparing the polymer coatings (possible contamination from the spin coater, hot plate or oven) the polymer proved unstable (the polymer turned opaque) when introduced to the media used in the HuES cell preparation. Due to this, it was not possible to observe the HuES on the polymer samples. Experiments were therefore conducted on the plain glass machined cover slips only. The plain glass cover slips were imaged using phase contrast microscopy and the cells observed. The images are shown in Figure 3.7 to Figure 3.1

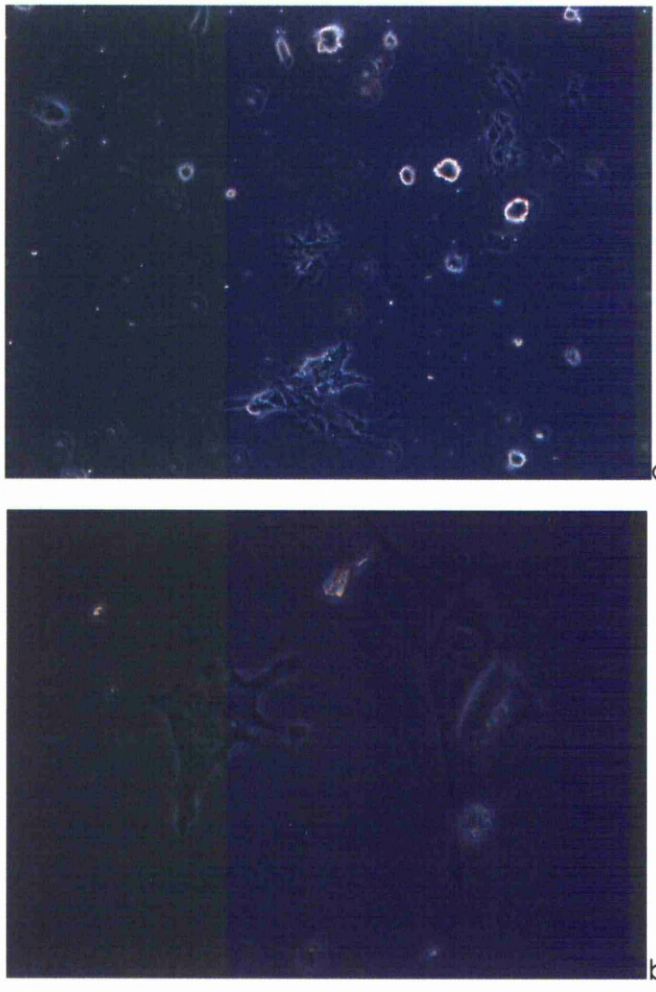

Figure 3.7 Phase contrast microscopy image of HuES cells grown on control plain glass cover slip a) x10 b) x40 magnification

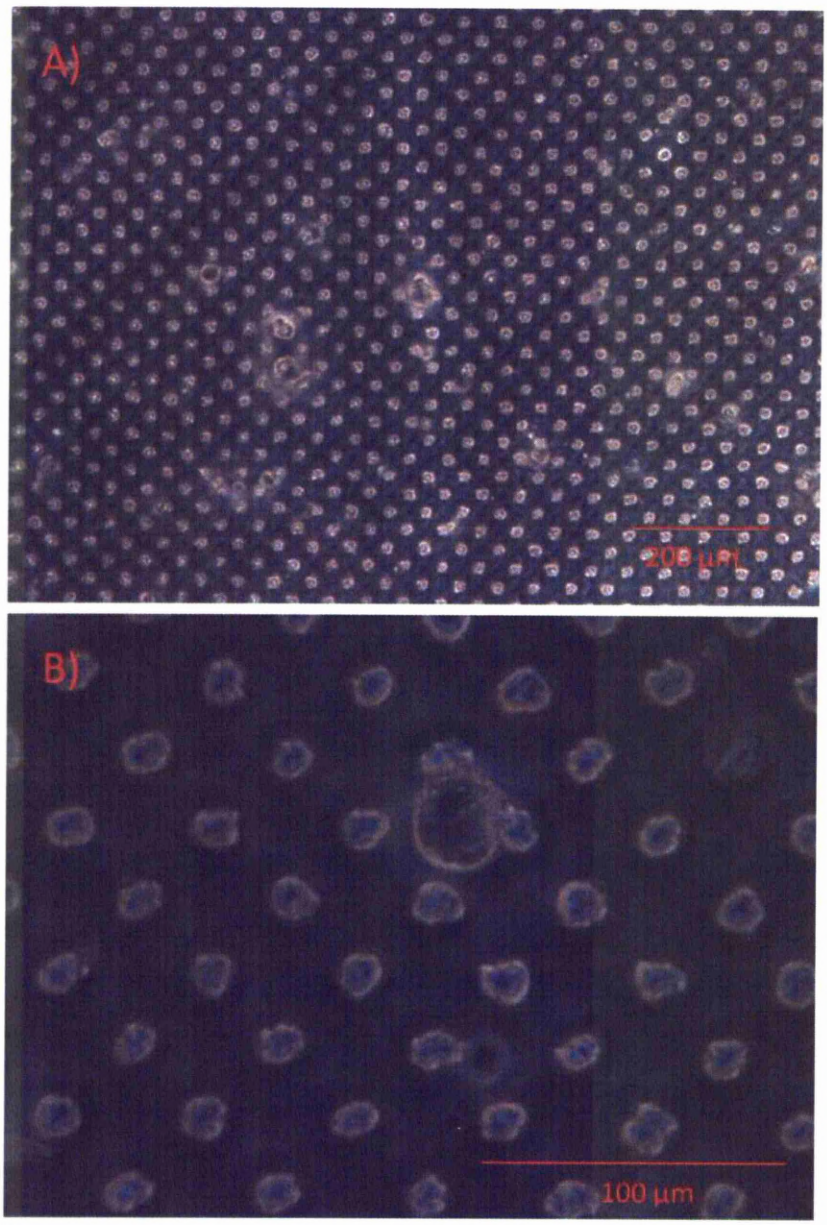

Figure 3.8 Phase contrast microscopy image of HuES cells grown on plain glass cover slip, 40x 40 drill grid laser features a) x10 b) x40 magnification

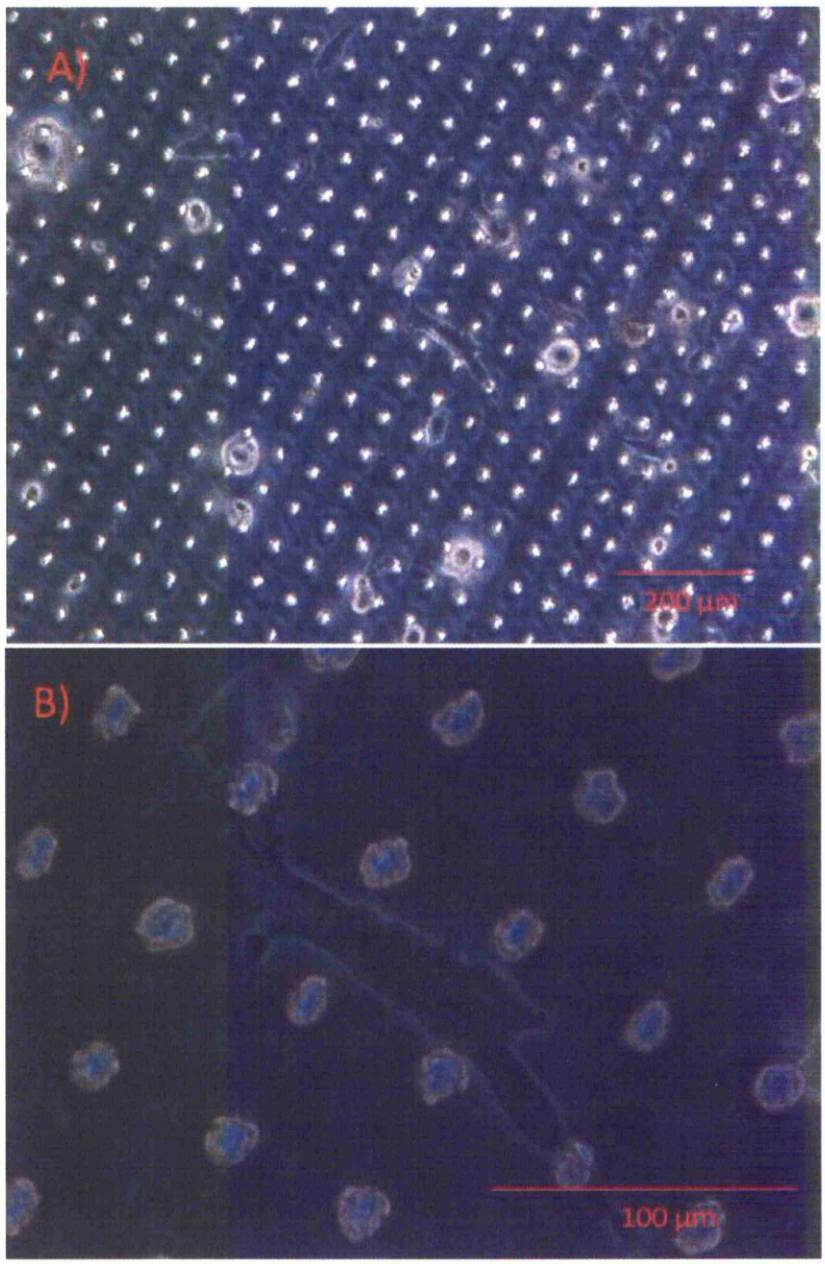

Figure 3.9 Phase contrast microscopy image of HuES cells grown on plain glass cover slip, 60x 60 drill grid laser features a) x10 b) x40 magnification

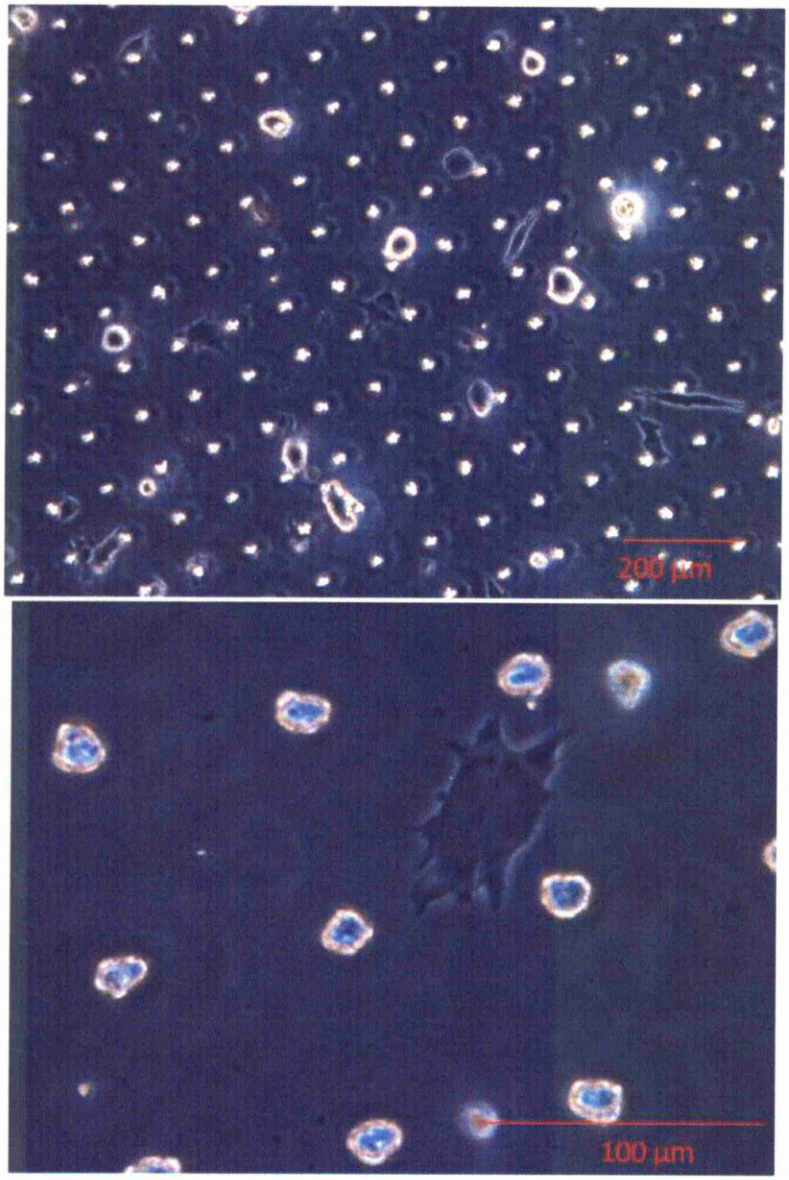

Figure 3.10 Phase contrast microscopy image of HuES cells grown on plain glass cover slip, 90x 90 drill grid laser features a) x10 b) x40 magnification

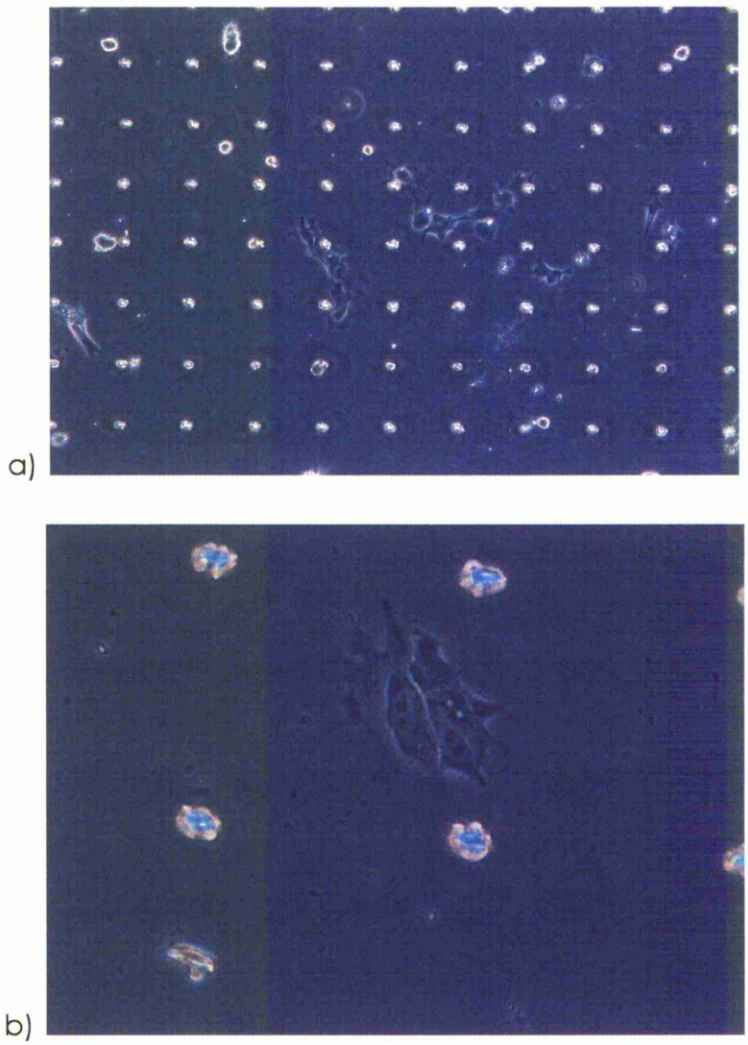

Figure 3.11 Phase contrast microscopy image of HuES cells grown on plain glass cover slip, 120x 120 drill grid laser features a) x10 b) x40 magnification

The images of the HuES cells on the laser processed samples show a difference from the control (unpatterned) sample. Interestingly, each pattern appears to have a different effect on the cells. Starting with the 30 μm spaced wells, due to the dense nature of the pattern no cells could be observed on the substrate. It is assumed that the HuES cells could not attach to the sample and so no cells were observed. Without more detailed microscopy, SEM for example, this cannot be confirmed. The 40 μm spaced wells show the first HuES cells that attach to the patterned substrates. The cells in figure 3.8 can be seen to be sitting in between the wells. The cells are smaller than HuES cells on the control sample after the same time period. Fewer cells are observed when comparing to the control sample. The 60 μm spaced wells shown in figure 3.9 show similar positions in between the wells and a similar size constriction compared to the control. Some cells however have elongated into a spindle shape, again in-between the wells. Cells observed on the 90 μm spaced wells, in figure 3.10, start to look like the cells seeded onto the control sample. The cells are again sited in-between the wells with some cells exhibiting the spindle like morphology as observed in figure 3.9. Finally the HuES cells observed in figure 3.11 appear for the first time to have developed into small colonies, as would be normal for HuES cells on a control, non-patterned substrate [9]. Cells appear to sit on the areas in-between the wells and appear to have a normal shape.

3.4 Discussion

The aim of the work in this chapter was to determine if a laser machined surface topography could be produced on a substrate suitable for cell biology experiments and if that topography could affect the growth of HuES cells

Literature searches indicate that few studies have looked into this type of topography. A few have looked at wells and where they have the change in well spacing has also involved a change in well diameter. The topography

presented here by comparison can test the change in feature spacing while keeping the features a constant size, so reducing variables.

3.4.1 Capability of femto second laser machining method

The femto second laser was able to produce micro scale features in both the glass and polymer samples, the latter being discarded due to contamination in production. The spin coater, hot plate and oven were all used for multiple experiments. Despite cleaning the hot plate and spin coater before use contamination could have still entered the polymer at this stage. The oven however is difficult to clean and is the most likely source of contamination to the polymer. The polymer provided by Biomer Technology Ltd. is complex and unless processed in clean conditions and problems can occur if the samples are contaminated. The opaque appearance observed when the polymer coated cover slips were placed in cell media occurred at different times with different batches. This is perhaps an indication of different levels of contamination entering the samples with the different batches produced, giving further evidence to the samples being contaminated at production. To test the polymer coated samples further, the spin coater would need to be cleaned and transported to Biomer Technology. The samples would then be cured in the clean oven which usually handle the polymer. The plain glass samples were robust and consistent, there being no difference in processing or handling in the cell experiments, as there was no need to coat or alter the cover slips in any way, prior to laser processing.

The laser was capable of producing arrays of fairly consistent features. However, the features were slightly elliptical. This was probably due to the inherent astigmatism in the laser system; this will cause the beam to be slightly elliptical and so causing the anomaly while machining the substrates. At times this astigmatisic distortion could be worse. Laser instability, probably due to thermal instability in the cooling of the laser, could cause the features

to become even more elliptical and larger in diameter. Figure 3.12 shows a glass cover slip machined with the same parameters, indicating the effect of the laser instability.

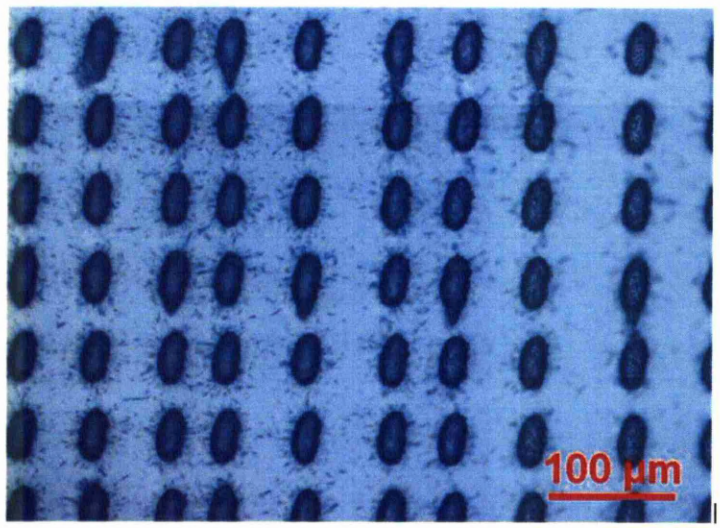

Figure 3.12 Microscope image showing a machined glass cover slip affected by laser instability

Debris can be observed on the machined samples, a result often observed when machining using a femto second laser [8]. It is not visible on the microscope images showing the HuES cells however. The cover slips were cleaned intensively before use due to the build up on the back of the samples. While effective, this is a time consuming extra step which seems un-avoidable with this method of production.

A third point to note about the process is the time taken to produce each sample. The low rep. rate of the laser, 1kHz, means that for the highest density of drill holes, (the 200x200 30µm sample) took 1000 second to produce each sample. A process time of over 15 minutes means a very slow production rate. When considering the need for many samples when conducting cell biology experiments, this can be a problem. The ability to mould from a master would possibly provide a solution to this.

3.4.2 HuES Cell Observations

From the observations made of figures 3.7 to3.11, the effect of increasing the spacing between wells appears to have a significant effect on the cells morphology and on culture formation, while all patterns appear to reduce cell attachment. How the individual cell focal adhesion attachment is affected, though, is unknown. This is due to the limited number of samples that were possible to be produced for the cell observations and so the number of tests that were possible. Further investigation by SEM would be desirable to prove that the cells only attached to the plain surface in-between the wells.

Comparing the effects observed here to others in the literature shows some corroboration in terms of orientation [10]. Few studies have looked at similar topography. Studies have looked at micro scale wells of a similar size to the ones presented here, [10][11]. These studies however look at increasing the size of the wells and keeping the pitch to the same ratio, so as the well increases in diameter so does the spacing between. One of the studies [10], using fibroblasts, reported no elongation in the cells on any of the samples. This is opposed to the observations made here, where cells on the 60 µm sample in particular, were observed to elongate into spindle shaped cells. It is not possible to determine if this is due to the cell type or the difference in topography, or even the underlying different material of the substrate. It does however highlight the difficulty in comparing the different studies conducted on the effect of cell-topography interactions. The studies that reported a similar reduction in cell adhesion, as indicated by the fewer number of cells on the machined samples compared with the control, were conducted using PMMA and nano scale pits [12]. The significance of comparing such different surfaces and topographies, however, is questionable, particularly when another study found increased cell adhesion on different polymers but with similar nano scale pits [13].

The machined samples produced here were designed to have as few variables as possible. The substrate, well diameter and depth, surface chemistry and substrate stiffness were all kept constant. A single cell type was used using standard cell culturing techniques. The only variable designed into the samples was the spacing between the machined wells. Even with this single variable a significant difference in cell morphology was observed. The extent of this change in morphology appears to be related to the spacing between the wells. A further factor is that of surface area. On average the processed area was ~10,000 x 10,000 μm (10 x 10 mm), the change in the available flat or non processed area (i.e. areas of the machined area that does not contain wells) was at most 12.6%. Table 3.3 details the area taken up by wells in a processed area. Figure 3.13 shows the variation of well total surface area against well spacing.

Spacing (μm)	Number of holes	Total area taken up by wells (mm^2)	Percentage area taken up by wells
30	40,000 (200x200)	12.57	12.6
40	22,500 (150x150)	7.07	7.0
60	10,000 (100x100)	3.14	3.1
90	4,900 (70x70)	1.54	1.5
120	3,025 (55x55)	0.95	1

Table 3.3. Percentage area taken up by micro machined wells on glass cover slips. Calculated assuming an average well diameter of 20μm

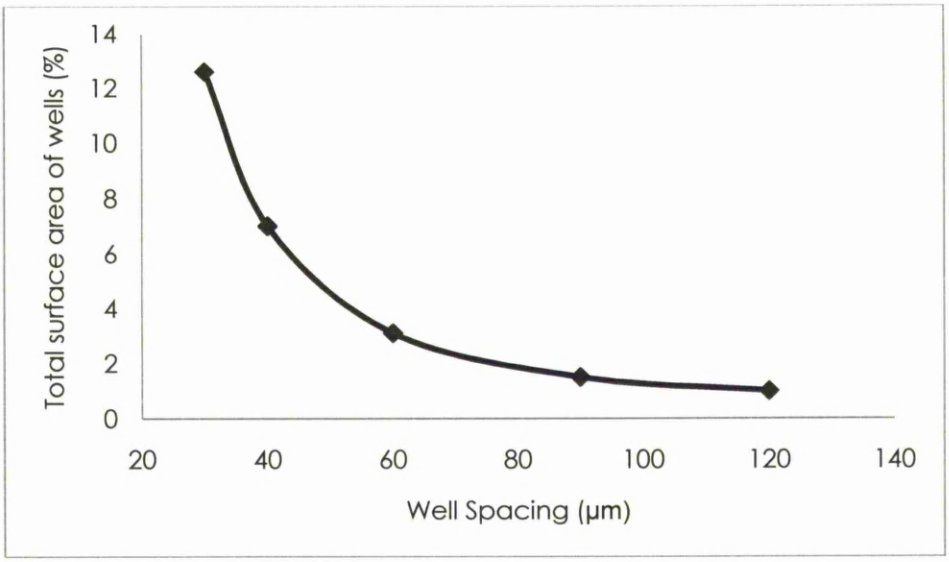

Figure 3.13 Variation of the percentage total surface area of the machined wells against the well spacing

It can be seen that even with a spacing of 30 µm (40,000 drilled wells) only a small amount of the processed area is that of wells. A useful further comparison would be to compare these data with cell proliferation and attachment observations. This however would require several more sets of machined samples.

The experiments performed were designed to establish if HuES cells could be affected by an artificial, laser micro machined topography. For all the samples surface chemistry, surface stiffness and method of production was kept constant. It appears from the results that the topography and the topography alone, was the contributing factor in the change of cell behaviour observed. Understanding the exact reasons and mechanisms behind this however, will require further study.

3.5 Conclusions

Laser micromachining of glass cover slips has been demonstrated. Features produced were roughly circular wells of ~20 μm in diameter and ~6 μm deep. These features were machined on a set of samples with a change in well spacing being the variable factor.

The laser was successful in producing a number of samples, enough to enable a limited set of observations involving HuES cells. Producing these samples however was very time consuming. A further issue was laser stability; day-to-day changes in temperature had an effect on the machined well dimensions and shape.

It was demonstrated that laser micro machined surfaces that varied in terms of the spacing between wells of a constant size, affected the HuES cell shape, size and colony. A reduction in cell attachment was also suggested when the HuES cells are grown on the sample topography. Only a limited assay was conducted however and further repeat experiments are needed to confirm the findings.

3.6 References

[1] E. Martıneza, E.Engelb, J.A.Plainllb, J.Samitiera. 2009. Effects of artificial micro-and nano-structured surfaces on cell behaviour. Ann Anat 191. 126—135

[2] Samira M. Azarina, Sean P. Paleceka. 2010. Development of scalable culture systems for human embryonic stem cells. Biochemical Engineering Journal 48. 378–384

[3] Frank A. Chervenak M.D.a and Laurence B. McCullough Ph.D. 2008. How physicians and scientists can respond responsibly and effectively to religiously based opposition to human embryonic stem cell research. Fertility and Sterility. 90, Issue 6, 2056-2059

[4] Brian E. Edwards B.A., John D. Gearhart Ph.D., Edward E. Wallach M.D. 2000. The human pluripotent stem cell: impact on medicine and society. Fertility and Sterility. 74, Issue 1, 1-7

[5] W. Perrie, M. Gill, G. Robinson, P. Fox, W. O'Neill. (2004). Femtosecond laser micro-structuring of aluminium under helium. Applied Surface Science 230, 50–59

[6] Lu, J., Hout, R., Booth, C.J., Shih-Hung, Y., Snyder, M. 2006. Defined culture conditions of human embryonic stem cells. PNAS. 103, 5688-5693

[7] Melissa A. Baxter, Maria V. Camarasa, Nicola Bates, Fiona Small, Patricia Murray , David Edgar, Susan J. Kimber. (2009). Analysis of the distinct functions of growth factors and tissue culture substrates necessary for the long-term self-renewal of human embryonic stem cell lines. Stem Cell Research 3, 28–38

[8] Semaltianos, N.G, Perrie, W., Vishnyakov, V., Murray, R., Williams, C.J., Edwardson, S.P., Dearden, G., French, P., Sharp, M., Logothetidis, S., Watkins, K.G. 2008. Nanoparticle formation by the debris produced by femtosecond laser ablation of silicon in ambient air. Materials Letters. 62, 2165–2170

[9] Bodnar, M., Meneses, J., Rodriguez, R. T., Firpo, M. T. 2004. Propagation and Maintenance of Undifferentiated Human Embryonic Stem Cells. Stem Cells and Development. 13, 243-253

[10] Hunt, J.A., Williams, R.L., Tavakoli, S.M. and Riches, S.T. 1995. Laser surface modification of polymers to improve biocompatibility. J. Mater. Sci. Mater. Med. 6, 813–817

[11] Green, A.M., Jansen, J, A., van der Waerden, J. P. C. M, Von Recum, A.F. 1994. Fibroblast response to microtextured silicone surfaces: Texture orientation into or out of the surface. Journal of Biomedical Materials Research. 28, 647–653.

[12]] Dalby, M.J, Gadegaard, N., Riehle, M.O., Wilkinson, C. D. W., Curtis, A. S. G. 2004. Investigating filopodia sensing using arrays of defined nano-pits down to 35 nm diameter in size. The International Journal of Biochemistry & Cell Biology. 36, 2005–2015

[13] Thapa, A., Webster, T.J., Haberstroh, K.M. 2003 Polymers with nano-dimensional surface features enhance bladder smooth muscle cell adhesion. Journal of Biomedical Materials Research Part A. 67A, 1374–1383

Chapter 4

Multi-scale Surface Topography

4.1 Introduction

In the previous Chapter, it was shown that a laser micromachined topography could have an effect on HuES cells, when they were cultured on the processed glass cover slips. The method of production, femtosecond laser machining, was however a slow process. One of the reasons for this was the stability of the laser. As it was operating at its limit, for machining resolution on glass and the inherent specification of the laser, the features were hard to reproduce for large scale production. The femtosecond laser has a pulse repetition rate of 1kHz, this means sample production was slow and the numbers produced were insufficient to allow for a wide range of cell observations and experiments. To further study HuES cells on artificially engineered surfaces a faster and more reliable solution was required.

The primary aim was to find a way to speed up the laser machining or find a way of producing more samples in the same amount of time. Using a master mould to cast against, to produce high numbers of samples from the one laser produced master would achieve this. A femto second laser could be used but the slow process speed of the laser would mean a significant time investment would be required to produce a master large enough to make

the moulding technique time saving. In the short term, this long processing time would mean that making lots of masters with different patterns would be as difficult as producing lots of smaller samples. A new laser system was therefore used, which not only has a faster process speed but it is capable of producing features on a significantly smaller scale. This was a picosecond laser process known as laser induced periodic surface structures (LIPSS).

The work in this Chapter involves the use of a picosecond pulsed laser to produce these LIPSS patterns on a substrate for moulding. The method of creating LIPSS patterns was to use a phenomenon called surface plasmon polaritons (SPP). The SPP causes a distinct sub-micron scale set of features to be produced on metal surfaces. This offers a fast and reliable method of producing large areas of patterned surfaces for use as a master mould.

4.1.1 Surface Plasmon Polaritons

Laser induced periodic surface structures have been shown to occur when an incoming laser beam is interfered with by a surface scattered wave [1]. For metals, where the laser radiation is very close to but not at the ablation threshold, this effect is thought to be caused by surface plasmon polaritons. Surface plasmon polaritons are non-radiative surface scattered waves. They are caused by the coupling of electrons and photons within a metal. This then causes resonant oscillations that result in the propagation of a surface wave [2]. The first work on SPP was done in the 1950's [3]. Since then several studies have investigated the mechanisms and theory behind SPP generation in metals [2][4][5][6].

In use the picosecond laser beam causes a LIPSS pattern. For this to occur, the laser beam incident on the metal surface must be below the ablation threshold of the metal. If the beam energy is below the ablation threshold, instead of removing material, the beam will melt a very shallow section of the metal surface. As well as this melting, surface waves are formed due to the surface plasmon polariton effect described above. These two effects combine to form a ripple in the liquid metal at the location of the laser

beam. Due to the short interaction time of the picosecond laser this ripple is left in the metal when the laser irradiation stops and the metal re-solidifies. Figure 4.1 shows how a LIPSS pattern is formed on a metal surface using a picosecond laser as the result of SPP effects. The features created by this process have a unique property for a laser technique. The ripple pattern in the metal has peaks and troughs that are above and below the surface of the metal. This feature is particularly beneficial for a moulding master. A mould will give the opposite topography from a master, so a pit will become a mound and a mound will become a pit in the moulded sample. The feature of the ripple pattern being both below and above the surface means that when a mould is taken, there will be no inversion of the pattern in the moulded sample.

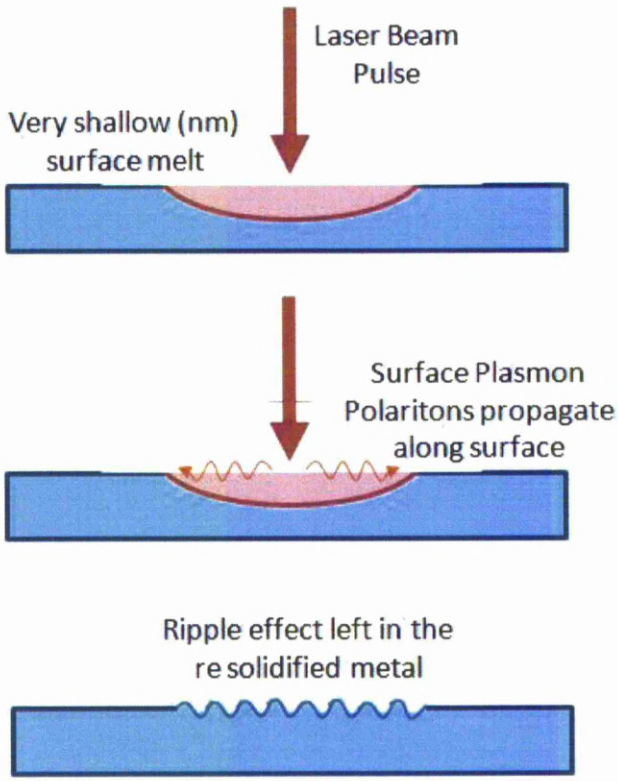

Figure 4.1 Diagram Showing how LIPSS patterns are formed on a surface of a metal, due to SPP, using an ultrashort pulsed laser beam.

4.2 Materials and Methods

4.2.1 Substrates

The metal used for the master substrate was Stainless Steel, AISI 316L (Fe/Cr18/Ni10/Mo 3). This was supplied in foil form, 2 mm thick, 100x100 mm square plates, from Goodfellow, UK. Also as 20 mm diameter tokens cut from bar. The tokens were provided by Biomer Technology Ltd. Runcorn, UK. The foil was supplied pre polished to a mirror finish. The tokens were un-polished. Some were then polished on an auto polisher. This grade of stainless steel is classed as medical grade. It was chosen to avoid any transfer contamination from the metal master to the polymer mould.

The polymer used to mould from the master samples was a BTL b_9 polyurethane solution (see appendix A). The polymer was provided by Biomer Technology Ltd. Runcorn, UK.

4.2.2 The Laser System

A Fianium FemtoPower1060-4J-pp picosecond fibre laser was used for the investigation. The system provided ~20ps pulses at 1064 ±5nm with an M^2 of <1.25. Two selectable repetition rates were available, 500 and 200kHz with maximum pulse energies of ~3 J & ~6 J respectively. Laser repetition rate and output power were set through computer controlled software via a HyperTerminal and USB connection.

For the optical setup, the beam was passed through a CVI dual wave Nd:YAG beam expander (DWBX-4.0-3x) anti reflection coated for ≥90% transmission at 1064/532nm. This corrected for spherical aberration, beam divergence, and coma. The beam then passed through a Newport 1/2 wave plate to allow for easy control over polarisation. A periscope then guided the beam into a scanning galvanometer with a 100 mm focal length f-theta lens (Nutfield Technology). Control over the scanner was given by WaveRunner advanced laser scanner control software (v.2.8.517.0). Samples were mounted on a 3-axis Aerotech ATS115 stage with a resolution of 0.5m

and repeatability of ±6μm [7] . Figure 4.2 shows a schematic diagram of the laser setup. Figure 4.3 shows a photograph of the laser and setup on site at the LLEC, Birkenhead, UK

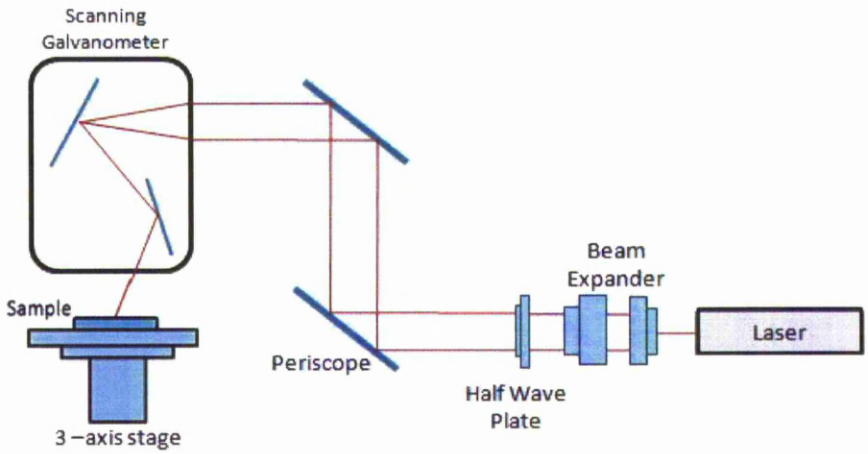

Figure 4.2 Schematic diagram of the laser setup

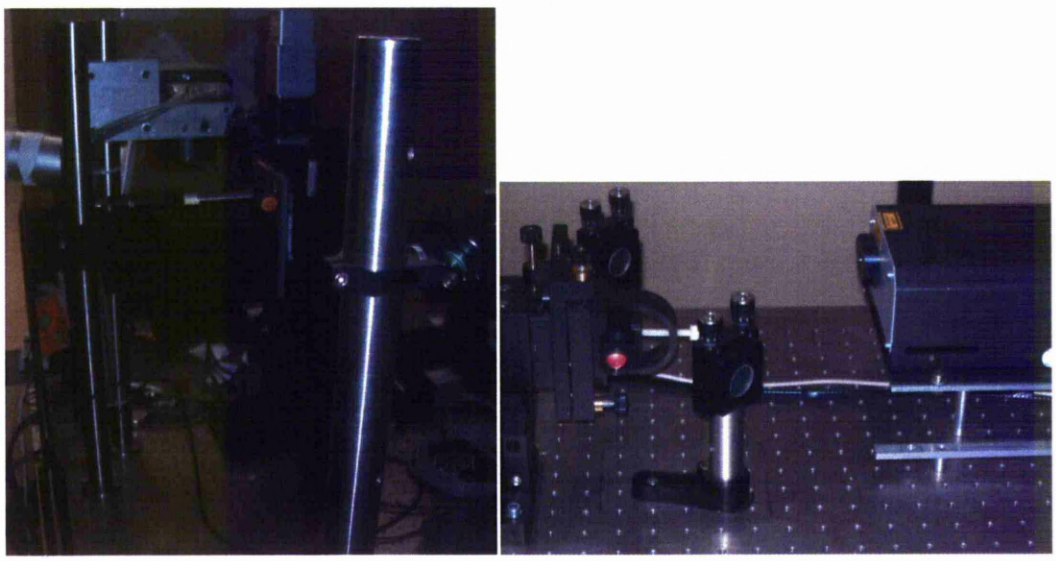

Figure 4.3 Photograph of the Fianium Laser and setup at the LLEC

4.2.3 Sample Production

Using the picosecond laser it was possible to produce two distinct types of LIPSS patterns, stripes and spots. Depending on how the laser was set up to process the substrate, stripe or spot patterns were produced, both taking advantage of the SPP effects caused by the laser.

4.2.3.1 Creating LIPSS Stripes.

The LIPSS stripe pattern was achieved by passing the laser over the stainless steel plates. The scanning galvanometer was set to pass the beam over the substrate leaving a preset distance between the lines. A set of 4 plates was produced that contained patterns with different spacings. Table 4.1 details the laser parameters used. The thickness of the lines was determined by the diameter of the laser beam spot. For thicker lines the scanning galvanometer was set to offset a second line by the thickness of the first and then leave a gap, before repeating the process. Figure 4.3 shows how the LIPSS stripes were hatched onto the stainless steel plates. Figure 4.4 shows a photograph of one of the processed stainless steel plates. The samples were imaged using a Veeco white light interferometer (WYCO).

Plate/Area	Laser Settings Laser traverse speed (mm/s)/ Laser Power (W)/ Laser Rep Rate (KHz)	Track Width (μm)	Track Spacing (μm)
1/A	1250, 1.5, 500	16	60
1/B	1250, 1, 500	16	60
1/C	1250, 0.75, 500	16	60
2/A	1250, 0.75, 500	16	10
2/B	1250, 0.75, 500	32	10
2/C	1250, 0.75, 500	16	5
3/A	1250, 0.75, 500	16	0 (5 overlap)
3/B	1250, 0.75, 500	16	0 (3 overlap
3/C	1250, 0.75, 500	16	0 (1 overlap)
4/A	1250, 0.75, 500	32	10
4/B	1250, 0.75, 500	16	45, 80 repeating
4/C	1250, 0.75, 500	16	21,18 ,8,6 repeating

Table 4.1 Laser and scanning galvanometer settings for patterning the Stainless Steel master plates.

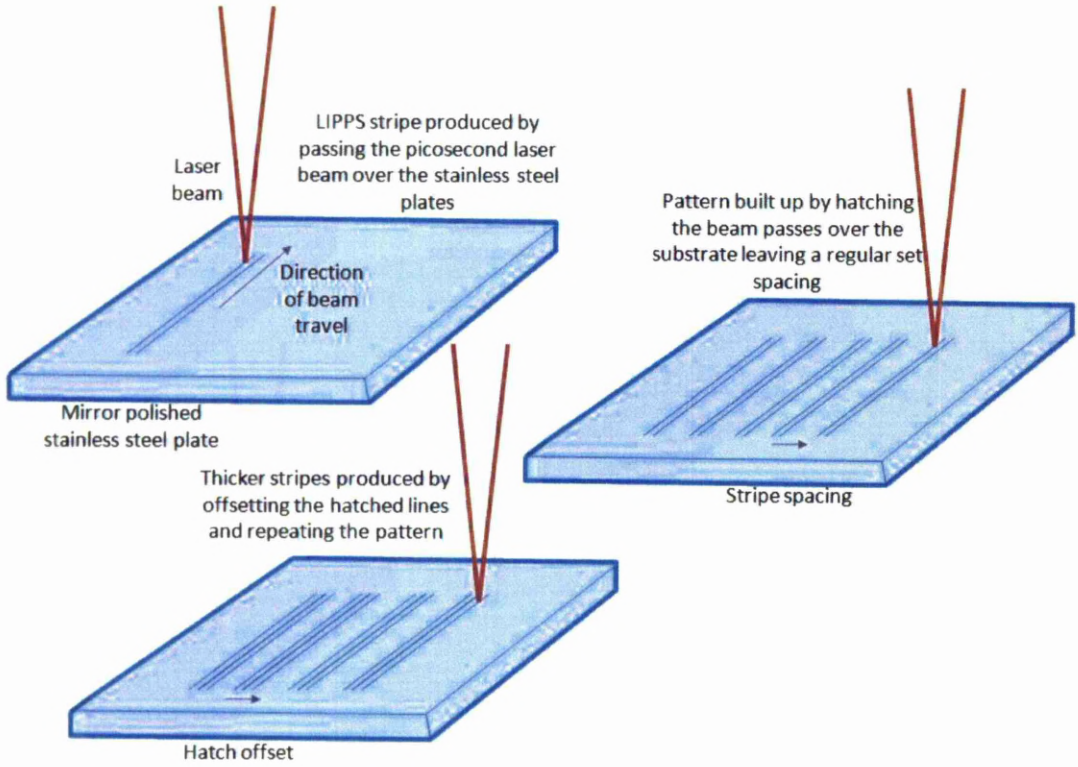

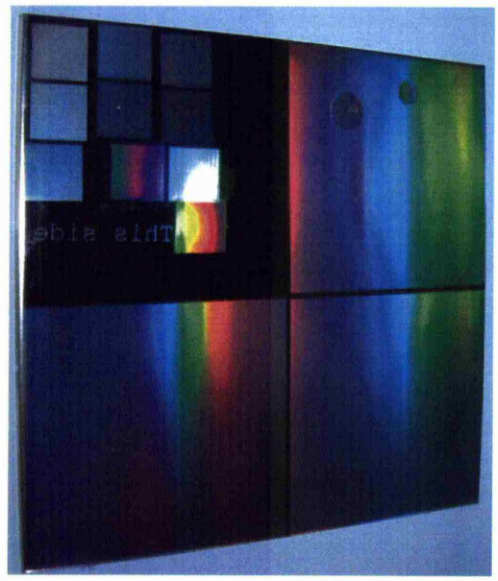

Figure 4.4 Schematic diagram of how the LIPSS patterns were produced on the Stainless Steel plates, (top) Photograph of Plate 3 (100mm x 100mm), showing the areas processed by the picosecond laser (bottom).

4.2.3.2 Creating LIPSS Spots.

The LIPSS spot pattern was created by using the laser in drill mode. The laser was set to produce drill events that would result in a spot. The spots were set to butt up against each other to produce areas of patterned surface. The spots were formed into a grid pattern, so leaving areas of unprocessed metal. This metal would act as a plain surface when a mould was taken. The master samples were produced on the stainless steel tokens, first on the un polished and then a polished master. Table 4.2 details the laser parameters used for the preliminary experiments and table 4.3 details the settings and samples produced for the main cell experiments. Figure 4.5 shows how the LIPSS spots were drilled onto the stainless steel tokens. Figure 4.6 shows a photograph of one of the processed stainless steel tokens.

Preliminary Sample	Laser Settings Rep rate (Hz) / Laser Power (W)	Hatch Spacing (µm)	Laser Dwell Time (ms)
A	200 / 680	40	1 and 10
B	200 / 680	30	1 and 10
C	200 / 680	20	1 and 10
D	200 / 680	15	1 and 10

Table 4.2 Table detailing the laser parameters used and the preliminary samples produced using the picosecond laser

Sample	Laser Settings. Rep rate (Hz) / Laser Power (W) / Dwell time (ms)	Hatch Spacing (μm)	Pattern
1	200 / 680 / 1	15	8x8 spot gap grid
2	200 / 680 / 1	15	12x12 spot gap grid
3	200 / 680 / 1	15	16x16 spot gap grid
4 (polished token)	200 / 680 / 1	15	12x12 spot gap grid

Table 4.3 Table detailing the laser parameters used and the samples produced using the picosecond laser.

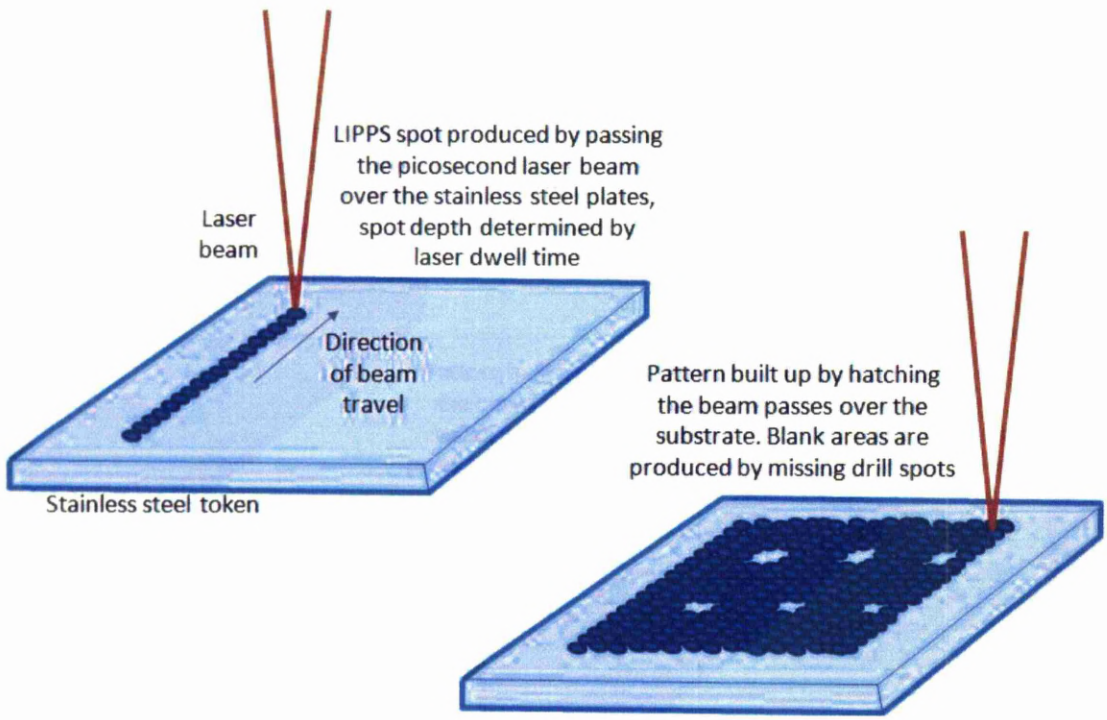

Figure 4.5 Schematic diagram of how the LIPSS patterns were produced on the stainless steel plates.

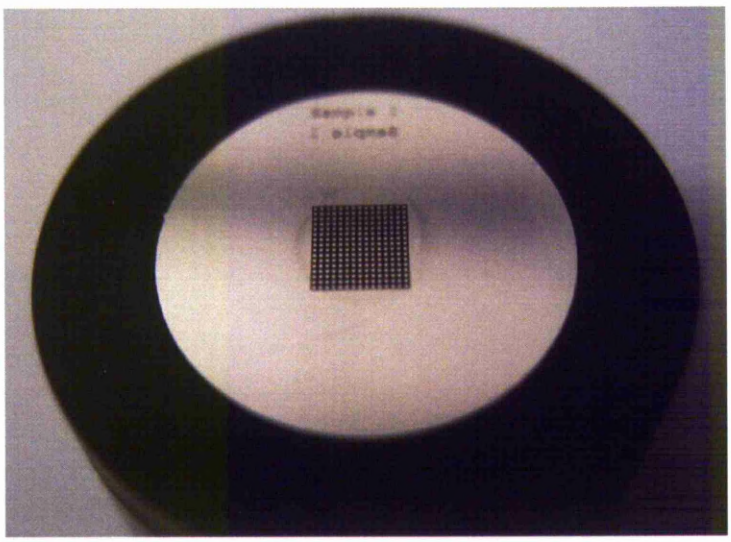

Figure 4.6 Photograph of a picosecond laser processed 2.5 cm diameter stainless steel token with the LIPSS spot pattern.

4.2.3.3 Casting from the Master Samples

The processed stainless steel plates and tokens were transported to Biomer Technology Ltd. Runcorn, for the polymer casting. This was to avoid contamination problems as was experienced with the spin coated glass cover slips, presented in the previous Chapter. The following details the method used to cast the polymer.

Biomer Technology b_9 Polymer Disc preparation

All substrate surfaces and the oven were cleaned with IPA (isopropyl alcohol) and dried prior to disc casting. Polymer solutions that have been stored for >1month or at temp < 5°C were required to be fully in solution. If not, they were rolled for ~ 2-3 hrs at room temperature.

Disc casting

Using a dropping pipette, 1-2 drops of polymer solution were carefully applied onto each of the substrate patterns to be cast, ensuring no air

entrapment. The disc was swirled as necessary to ensure even distribution of polymer across the patterned surface.

The disc was placed in oven at 50°C for 45 minutes. Once dry, it was removed from the oven and allowed to cool to room temperature.

A Petri dish was filled with clean, deionised water and the disc was immersed. After 15mins, forceps were used to gently prise up the edge of the film and transfer the disc to a clean microscope cover slip ensuring that the patterned surface was face (pattern side) up from the cover slip and allowed to dry. Dried cover slips were then placed in a 24 well plate and labelled (according to the pattern and repeat number) and the fully loaded plate irradiated under UV source for ~ 30 minutes prior to use.

4.2.4 Cell Experiments

4.2.4.1 Fibroblast Cell Culturing on the LIPSS Samples

The following is the protocol for the fibroblast cell culturing conducted at Biomer Technology Ltd.

Fibroblast culturing was performed at Biomer Ltd, Runcorn, by Fred Laws. The following is a brief outline of the fibroblast culturing procedure. The polyurethane test discs were supplied in 24 cell well arrays. The cell well array was then exposed for 15 minutes to a sterilizing UV light. The L929 fibroblst culture was trypsinized and the pellet of cells resuspended in C-MEM (Complete Minimum Essential Medium. A sample of this culture was taken and the cells counted in a haemocytometer. The count was then diluted with C-MEM to a concentration of 5 x104 cells per ml. Two ml. of this L929 cell dilution was added to each cell well containing a sample. The cell well array was then incubated in a CO_2 incubator at 5% CO_2 and 37°C. The cell well array with samples was examined microscopically at 24 hours and 48 hours. Photographs were taken of samples at appropriate magnifications between 100x and 400x. At 48 hours cell wells with samples were fixed with 1%

glutaraldehyde and then left in PBS or fixed in 1% glutaraldehyde and stained with methylene blue and left in PBS.

4.2.4.2 HuES Cell Culturing on the LIPSS Samples

The HuES cells were cultured on to LIPSS patterns in that same was as for the glass cover slips, described in Chapter 3, in the Department of Human Anatomy and Cell Biology by Dr J Downes.

4.2.4.3 Cell Staining

The HuES cells were stained using both dye and antibody staining. The protocols used for the staining are as follows;

Antibody Staining -

Materials

Vinculin - Indicates focal adhesions of the cell as red points in fluorescence microscopy.

Blocking buffer - 10% triton, 10% goat serum(Sigma-Aldrich) in PBS.

Mouse anti-vinculin (Sigma-Aldrich)- 1:200 in 1% goat serum in PBS.

Goat anti-mouse IgG (Invitrogen)- 1:1000 in 1% goat serum in PBS.

DAPI (Invitrogen) - 1:1000 in PBS.

DAPI - Indicates the cell nucleus as a blue colour in fluorescence microscopy

Blocking buffer - 10% triton, 10% goat serum in PBS.

Mouse anti-Oct4 (Santa Cruz)- 1:500 in 1% goat serum in PBS.

Goat anti-mouse IgG (Invitrogen)- 1:1000 in 1% goat serum in PBS.

Nanog - Used to indicate cell differentiation, a cell expressing nanog is still pluripotant. nanog is shown as green in fluorescence microscopy.

Blocking buffer - 10% triton, 10% rabbit serum (Sigma-Aldrich) in PBS.

Goat anti-nanog (R&D Systems)- 1:200 in 1% rabbit serum in PBS.

Rabbit anti-goat IgG (Invitrogen)- 1:1000 in 1% rabbit serum in PBS.

Procedure

The samples were fixed with 4% paraformeldehyde for 10 minutes. They were then washed x 3 in PBS before being incubated in blocking buffer for 5 minutes. After this they were washed x1 in PBS, before being Incubated again with 200µ off primary antibody overnight at 40°C. They are then washed x3 in PBS and incubated with 200µl of secondary antibody for 2 hours at room temperature. Finally they were washed x2 in PBS and incubated with DAPI for 5 minutes at room temperature before washing x1 in PBS and mounting onto slides using mounting media.

Actin dye, shows the cytoskeleton as green in fluorescence microscopy.

The samples were first fixed with 4% paraformeldehyde for 10 minutes. Then they were washed x3 in PBS before being Incubated in 1% BSA in PBS for 45 minutes at room temperature. Next they were washed x1 in PBS and i ncubated in 1:40 phalloidine dye (Invitrogen) for 30 minutes at 37°C. Finally they were washed x2 in PBS and Incubate with DAPI (1:1000 in PBS) for 5 minutes at room temperature, before being washed x1 in PBS and mounted onto slides using mounting media.

4.3 Results

As each plate was produced, it was used to create a set of moulds with for the cell (both fibroblasts and HuES cells) observations. The cells were observed and a new plate was produced to observe the effect of a different pattern. Both the spot and stripe LIPSS patterns were kept constant, the only variable was the spacing between spots or stripes. The pattern was changed in response to how the cells responded to the different spacings.

4.3.1 LIPSS Stripes

The LIPSS stripe patterns were very simple to produce with the picosecond laser system. Due to the inherent specification of the laser, the LIPSS features can be optimised with little effort. Using the laser in conjunction with a scanning galvanometer and control software meant that the laser could be used to produce different patterns of LIPSS stripes quickly and consistently. The stability of the laser system meant that once optimum settings for producing the LIPSS stripes were found, many samples could be produced as and when they were needed. These factors as well as the speed at which the laser could process large areas (50x50 mm^2 took ~ 1-2 minutes depending on the track spacing), meant the system performed very well as a rapid prototyping platform for the production of the master plate moulds.

The ease of producing the master plate moulds was enhanced by the ability to produce many polymer moulded samples from which to observe cell interaction with the surface. As well as the polymer moulds ability to replicate the LIPSS patterns, they were well suited for use in cell biology experiments. The process of moulding the polymer samples provided a clean (several mouldings were made and discarded to remove debris before the plate was used for actual samples) transparent substrate. As the polymer was not processed directly, the issue of a changed surface chemistry, due to heat, was not a issue. Problems such as surface debris (as with the femto system) were also avoided. A further benefit was that each batch of samples was taken from the same mould, meaning that each cell observation repeat was being done on exactly the same surface topography each time. This removed any error or uncertainty from producing slightly different samples for each batch of samples, so ensuring the repeatability of the experiment.

Using the picosecond laser system as a rapid prototyping tool meant that, depending on the outcome of the cell observations, different features could be produced quickly in response to the previous cell observations and cell behaviour to the features. This led to the ability to tailor the substrate features

to the cell response. The following details the changes in the processed surface topography with the observed cell responses.

The LIPSS stripe patterns were measured using an AFM. The laser beam passing over the substrate causes a ripple pattern on the surface perpendicular to the beam direction. The pitch of the features was determined to be ~1 µm and the height of the features ~300 nm. A 3D AFM image of the features is shown in figure 4.7.

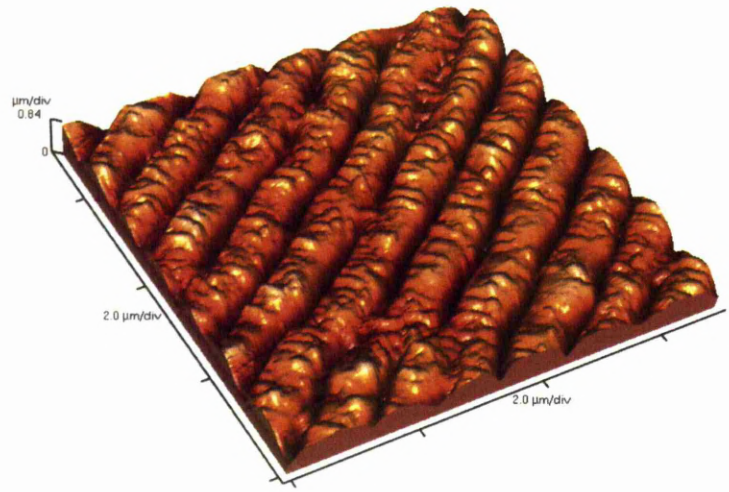

Figure 4.7 3D AFM image of the LIPSS features produced by the picosecond laser

Plate 1 - LIPSS production

Plate 1 was used as a preliminary test sample, using three different laser powers. The plates were examined using a Veeco WYCO white light interferometer. The aim was to determine which laser power produced the most consistent LIPSS features. Consistency in this case was defined as having the most uniform height profile of the ripples and containing the fewest blank areas, where no ripples were produced.

The three areas A, B and C were imaged and are shown in figure 4.8. The height profiles of each image is shown in figure 4.9.

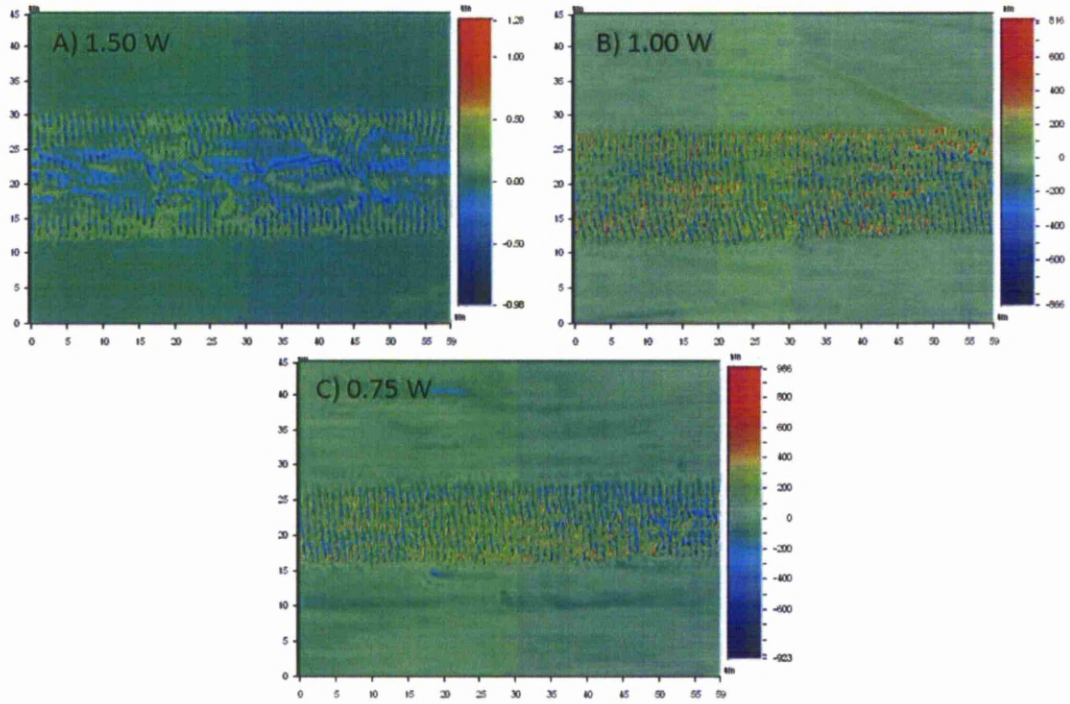

Figure 4.8 WYCO image of the LIPSS patterns produced on the stainless steel plates. The laser was set to 500 kHz rep rate, 1250 mm/s traverse speed and a power of A)1.5 W, B)1 W and C) 0.75 W

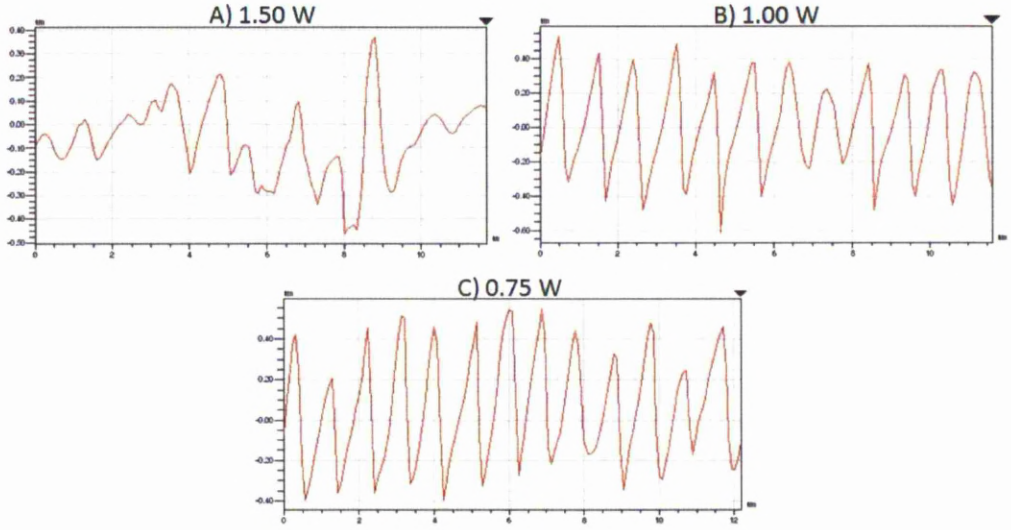

Figure 4.9 WYCO cross section of the LIPSS patterns produced on plate 1. Showing magnified typical sections, detailing the different consistency of the ripple patterns for a power of A)1.5 W, B)1 W and C) 0.75 W

The features appeared to be most consistent when using a laser power of 0.75 W. There is an artefact of production however, which involves the direction of the laser path. When the laser passes from left to right (as shown in figure 4.8) the features appear consistent. When the laser returns, right to left, the features appear different, particularly when using 0.75 W of laser power. For 1 W however there is little difference in the return laser pass (right to left). It is for this reason that 1 W of laser power was chosen as the default setting when producing the other sample plates. A WYCO image detailing an example of the difference between the 1 W and 0.75 W return laser passes is shown in figure 4.10.

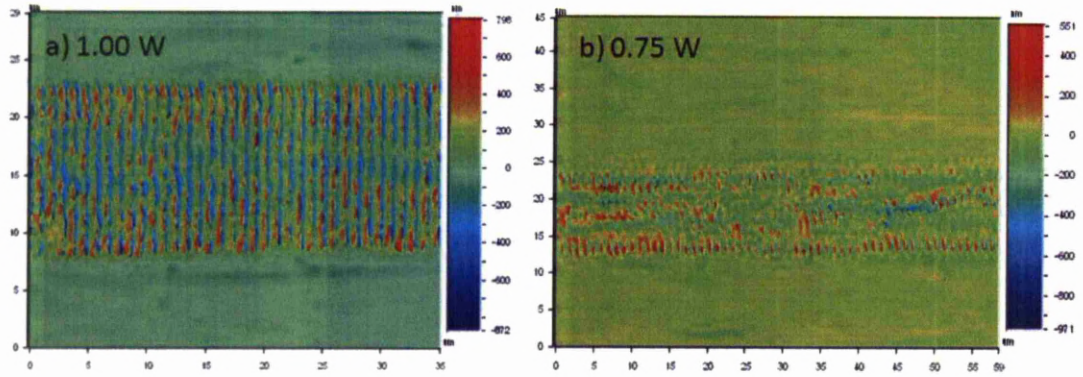

Figure 4.10 WYCO image of the return pass for the picosecond laser, showing the difference in the produced LIPSS stripe pattern.

Plate 1 - Cell Observations

Both fibroblasts and HuES cells were seeded onto the polymer moulds of area A (the LIPSS features produced at 1 W laser power). Figure 4.11 shows a microscope image of a typical area of fibroblast cells on the polymer moulds. It can be seen that some fibroblasts appear to bridge the LIPSS, however there are some that do not. Figure 4.12 shows the same but for HuES cells. The huES cells appear to grow normally and seem to be unaffected by the LIPSS stripe topography.

Initial observations revealed little reaction by the cells to the LIPSS stripes. Some fibroblasts seemed to bridge the stripes (figure 4.11) but this trend was difficult to quantify. The HuES cells did not appear to react in any way to the features, seeming to ignore the stripes and grow normally (figure 4.12). Taking these observations the stripe spacing was reduced and the track thickness was increased by butting together laser tracks to double the LIPSS strip width.

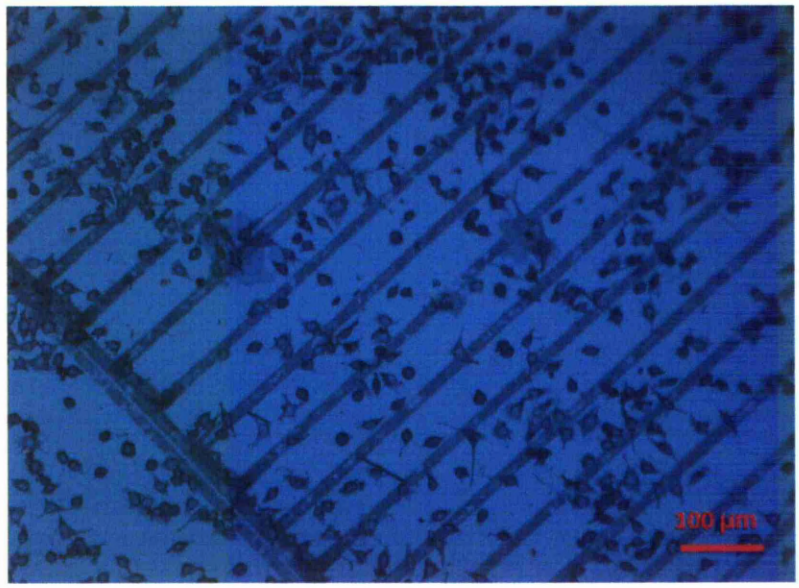

Figure 4.11 Microscope image of fibroblast cells on the polymer moulded LIPSS features after 24 hours (60µm track spacing).

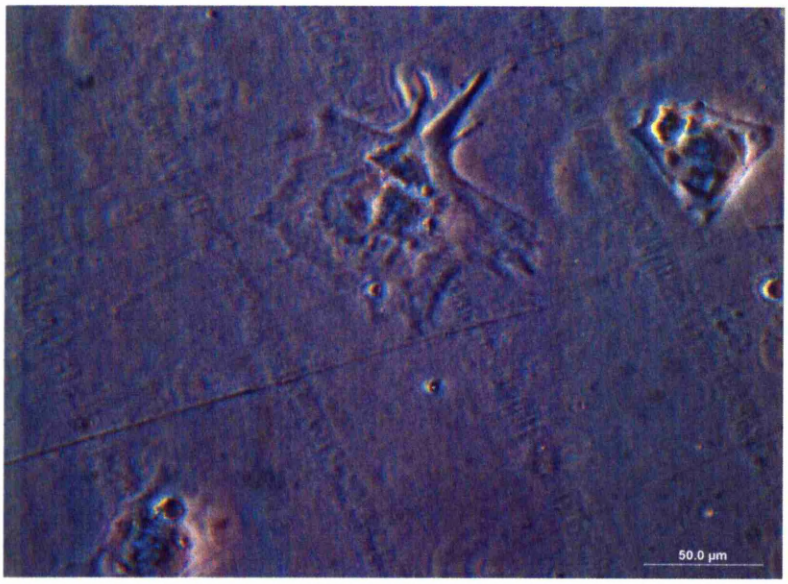

Figure 4.12 Microscope image of HuES on the polymer moulded LIPSS features after 24 hours (60µm track spacing).

Plate 2 - LIPSS production

Using the optimum settings that were ascertained from plate 1, the same LIPSS features were produced on plate 2 but with a different spacing between the stripes. The spacing was reduced from that used on plate 1. WYKO images of the produced features are shown in figure 4.13 showing false colour topography images of the LIPSS track (on the stainless steel plates). The images detail the different track spacing's used on plate 2.

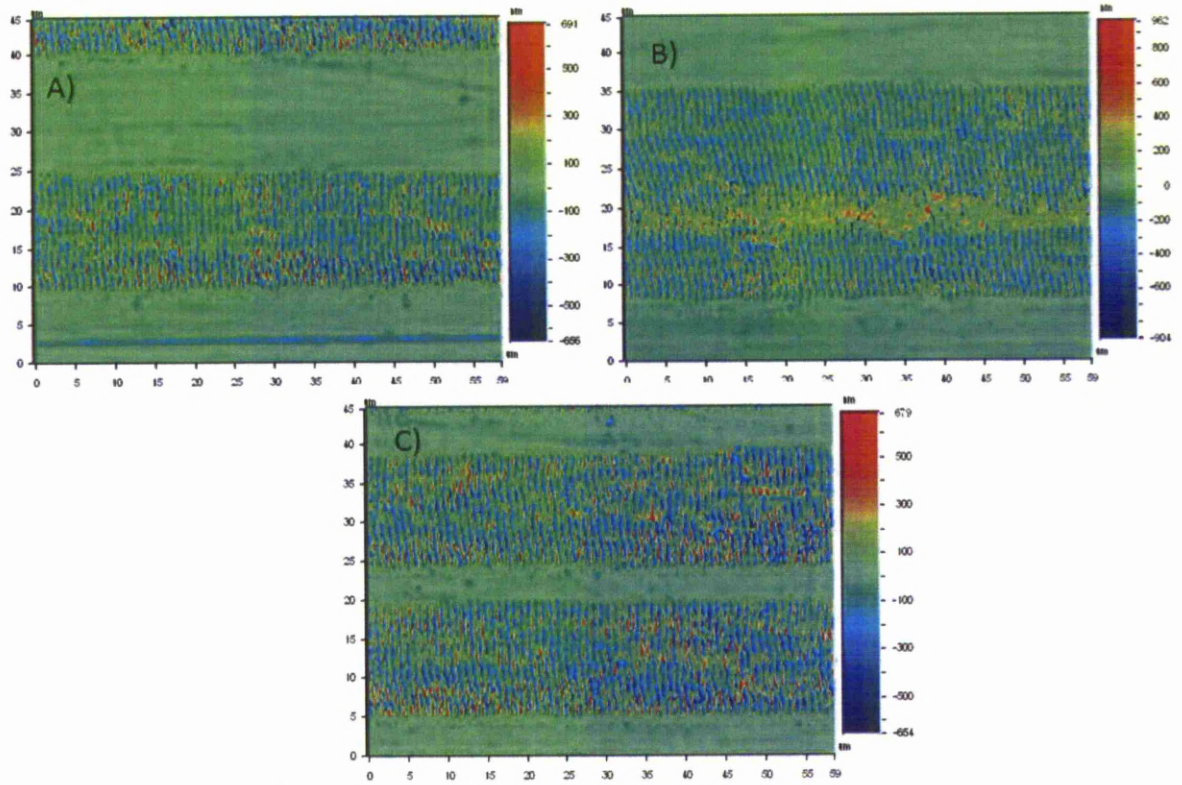

Figure 4.13 WYCO image of the LIPSS patterns produced on the stainless steel plates. The laser was set to 500 kHz rep rate, 1250 mm/s traverse speed and a power of 1 W A) single track, 10 µm spacing, B) double track, 10 µm spacing C) single track, 5 µm spacing

Plate 2 - Cell Observations

Initially, fibroblast cells were placed onto the polymer moulds, taken from plate 2. These are shown in figure 4.14. HuES cells were grown on the double track moulded polymer sample, a typical area is shown in figure 4.15.

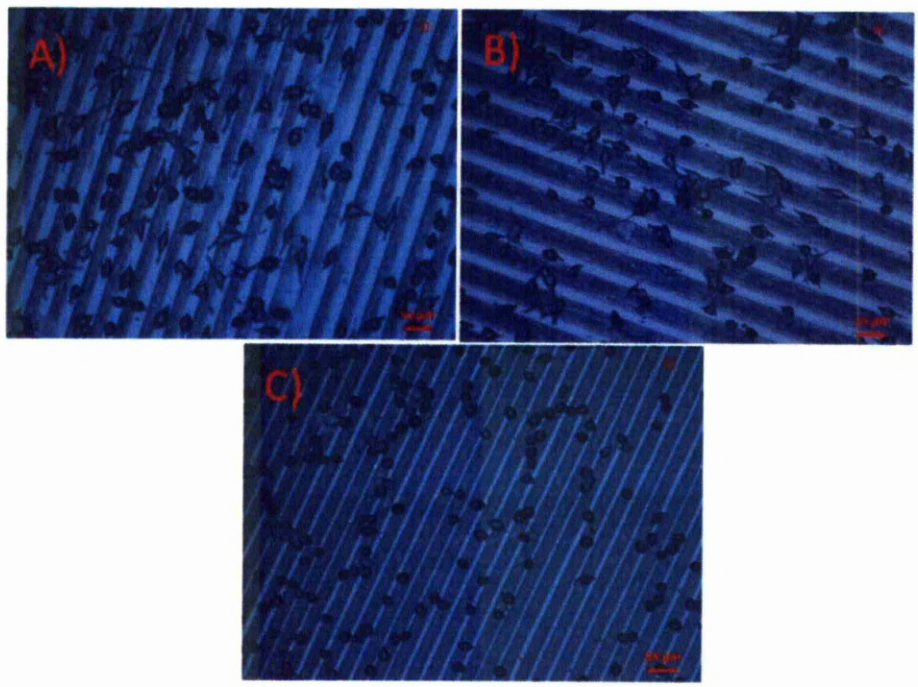

Figure 4.14 Fibroblast cells on polymer moulds taken from plate 2. A) 16 µm track, 10 µm spacing, B) 32 µm track, 10 µm spacing, C) 16 µm track, 5 µm spacing after 24 hours.

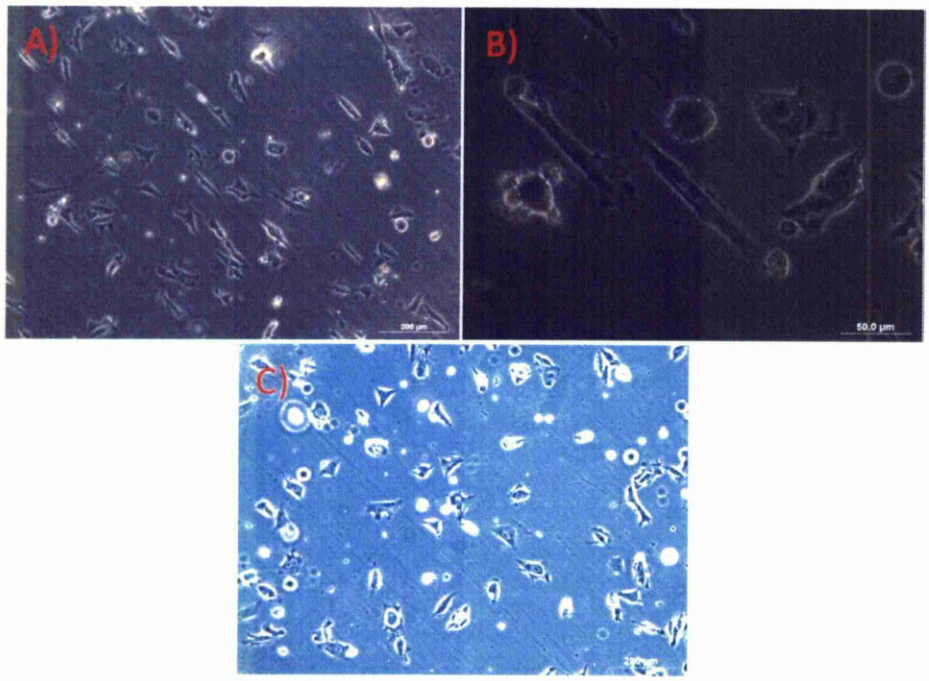

Figure 4.15 Microscope image of HuES cells grown on polymer moulds taken from plate 2 (32 µm track, 10 µm spacing) showing A) and B) spindle shaped cells growing in between the tracks, C) control, plain sample after 24 hours

It is again difficult to draw any conclusion from the fibroblasts, they do not appear to be displaying any significant change in behaviour. The huES cells on the multi-scale topography do however differ from huES cells on the control. It can be seen from figure 4.15 that several cell are elongated or spindle shaped. There appears to be a general trend for the huES cells to grow in between the LIPSS tracks. Figure 4.32 Shows a more detailed image of spindle shaped huES cells on area B.

More pronounced however was the alignment of the fibroblast cells on area C (16 µm track 10 µm spacing). The cells can be seen to grow in a slightly elongated manner, aligning with the stripes (figure 4.14). The cells also grow predominantly on the spacing's between stripes. Where they attach to the stripes they appear not to spread as much as those on the stripes. Area C (16 µm track 5 µm spacing) added evidence to this observation. The fibroblasts on area C are round and have not spread, an indication that they are not growing properly on this surface topography and stripe spacing.

Using this, the HuES cells were only seeded on area B. The observed cells appeared significantly different to the control (figure 4.15). The cells took on a spindle shape with many of the cells aligning with the stripes. Where the cells had spread sufficiently to come into contact with the stripes, the cell would bridge the stripe forming a fish tail like shape, an example of this is shown in figure 4.16

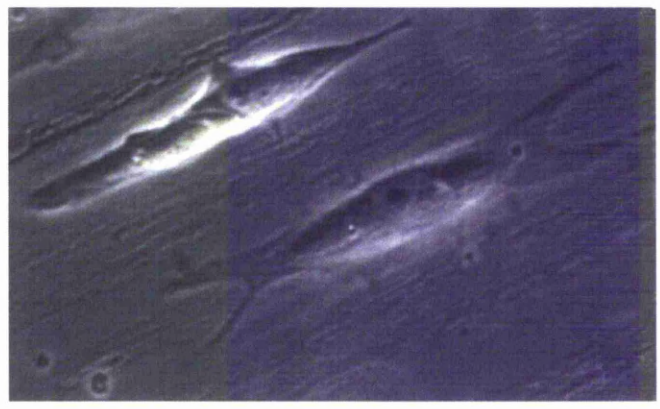

Figure 4.16 Example of a spindle (top) and fishtail (bottom) shaped HuES cell growing on a LIPSS stripe polymer moulded sample.

The HuES cells on area B were analysed and measured (using imageJ) for the average cell area, circularity and alignment to the LIPSS stripes. The results are shown in figures 4.17 to 4.19. The graphs show an example of how the huES cells are being affected by the LIPPS surface. Figure 4.17 show how the LIPSS surface affects huES cell size when attached to the surface by comparing average cell area for a sample image of huES cells. Figure 4.18 shows an example of how the huES cells shape is affected. The graph compares huES cells on plain and patterned polymer. Circularity is measured using the ratio of the major and minor axis of the cell, 1.0 being a perfect circle

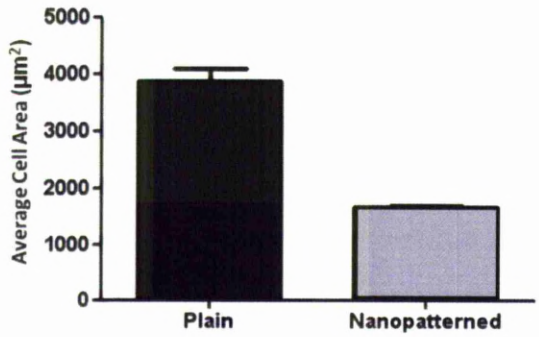

Figure 4.17 Average cell area of HuES cells seeded onto a polymer moulds of Area B of plate 2 and a polymer control sample.

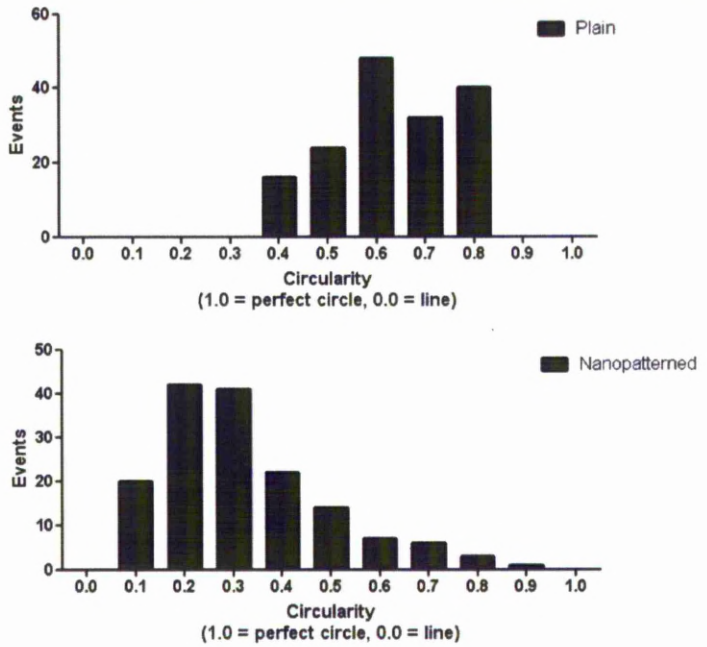

Figure 4.18 Circularity of HuES cells seeded onto a polymer mould of Area B of plate 2 and a polymer control sample, where a perfectly round cell is a 1.0 and a cell with no circularity is a 0.0

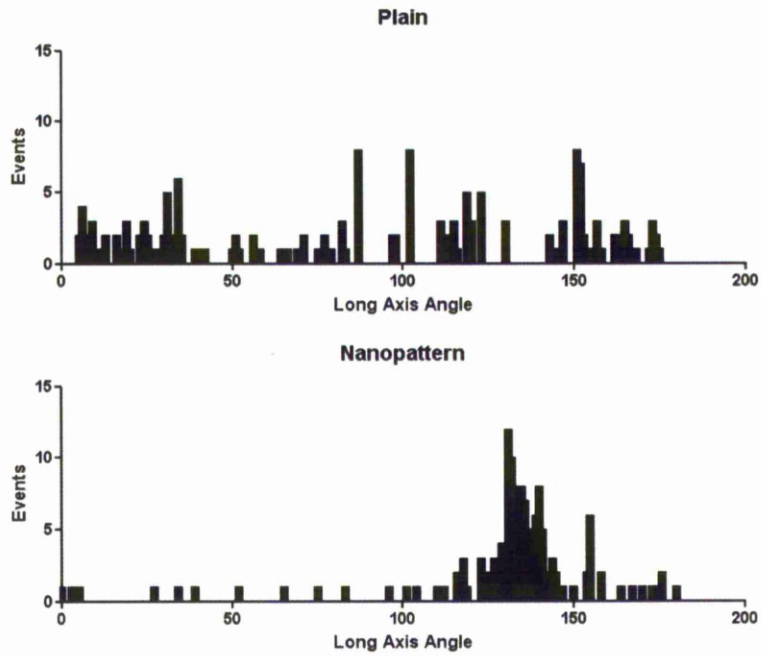

Figure 4.19 Angle of HuES cell long axis when seeded onto a polymer mould of Area B of plate 2 and a polymer control sample, indicating alignment with LIPSS stripes of the sample

Figure 4.19 was plotted using data from ImageJ, the long axis angle in this case is arbitrary and indicates the angle from the x-axis of the image. The nano patterns are at an angle of ~140° from the x-axis of the image, the spindle shaped cells are aligning with the stripes and are shown on the graph at similar angels from the x-axis of the image.

The above figures indicate that the LIPSS patterns have had a clear effect on the cell area, circularity and orientation when compared to a control sample. The cell area has been reduced and many cells have formed into an elongated shape. Many of these cells have also aligned themselves with the LIPSS stripes, confirming the visual observations of the samples.

A graph of how the huES cells appear to bridge the LIPSS stripes and meet other filaments, on the plane areas between the stripes, is shown in figure 4.20. The graph compares the number of actin filaments that meet on the plane surface of the mould to the number of actin filaments that meet on the nanopatterned areas or the mould. Areas where actin filaments meet are indications of focal adhesion sites.

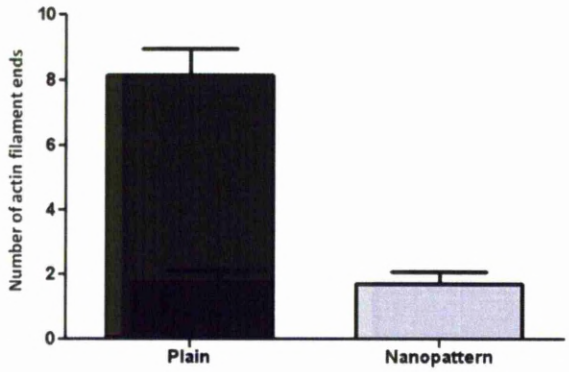

Figure 4.20 Number of HuES cell actin filament ends on polymer moulded samples of area C from plate 2.

Plate 3 - LIPSS Production

Plate 3 was designed to observe how cells would react to a surface totally covered by the LIPSS ripples. This was done by passing the laser over the steel plates without leaving a gap between the laser tracks. A degree of track overlap was incorporated into the processing to create 3 areas with slightly different topographies. The result of the laser processing is shown in figure 4.21.

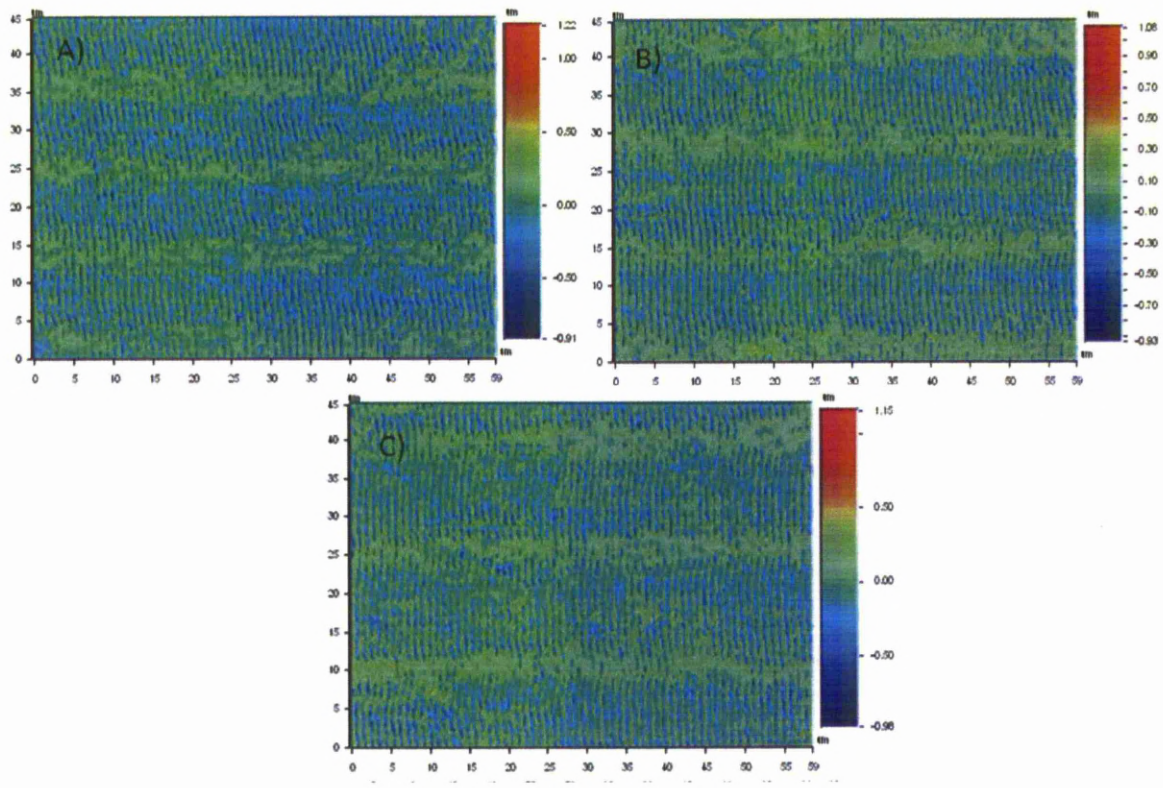

Figure 4.21 WYCO image of plate 3 showing overlapping laser tracks A) 1 µm, B) 3 µm and C) 5 µm track overlap.

Plate 3 - Cell Observations

Fibroblast and HuES cells were seeded onto the moulds taken from plate 3. After 24 hours no HuES cells could be found on the polymer moulds. Microscope images of the fibroblast cells on one of the polymer moulds are shown in figure 4.17 showing how the LIPSS pattern has affected fibroblast attachment when comparing to figure 4.11

Observations of moulds taken from plate 3 were conclusive, only fibroblast cells were observed attaching to the surface (figure 4.22). These cells however did not spread and were clumped together in patches. As with area C on plate 2, this is an indication that, they are not growing properly on the surface completely covered by the LIPSS stripes. Fibroblasts are hardy cells capable of attaching to most surfaces [8] but they appear to have difficulty growing on the LIPSS stripes.

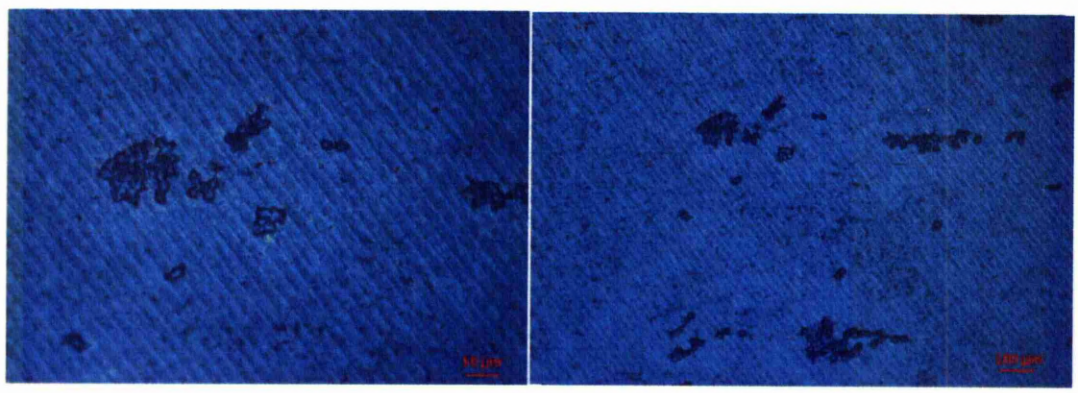

Figure 4.22 fibroblast cells on polymer mould of plate 2 after 24 hours

Plate 4 - LIPSS Production

Plate 4 was designed to test a wide range of track separations on the same sample and to observe the cells on samples with larger track spacings than on previous samples. The features produced are shown in figure 4.23. The dark lines are the LIPPS tracks.

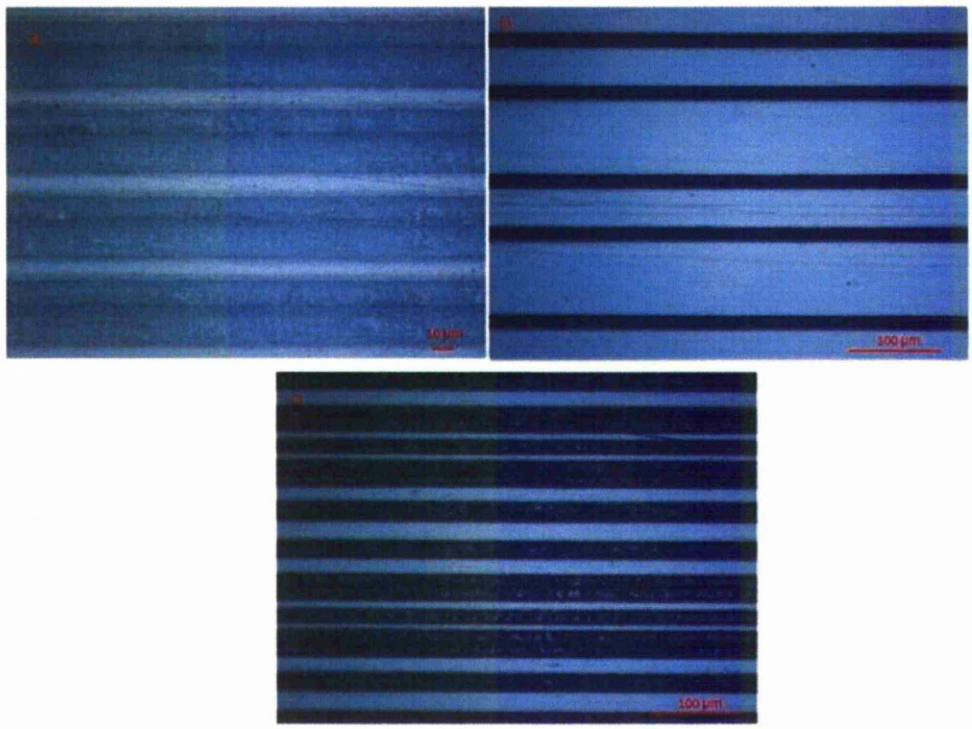

Figure 4.23 Microscope images of LIPSS features on plate 4, A) 32 µm track, 10 µm spacing, B) 16 µm track, 45 and 80 µm spacing repeating and C) 16 µm track, 21, 18, 8, 6, µm spacing repeating.

Plate 4 - Cell Observations

Plates 1, 2 and 3 had shown that the fibroblast cells and HuES cells behaved in similar ways to the moulded samples. Both cell types showed some alignment to the LIPSS stripes and formed elongated cells. Both cell types also seem to prefer the plane areas in between the LIPSS stripes, often bridging the stripes. Using this plate 4 was designed to test how HuES cells would react when the LIPSS stripes were even further apart than in previous samples and how they would react to a surface with changing stripe spacing's. Area B revealed no new results, the HuES cells would grow in-between the stripes. Where a cell encountered a track it seemed to ignore the feature as with a cell seeded on plate 1. The cells grown on polymer moulded samples of area C again formed into spindle or fishtailed shaped

cells, as they did for moulded samples from plate 2. These spindle and fishtailed shaped cells were found more predominately on the 8 µm spacings.

As the features on plate 4 were considered to be optimised for observing the cells, only HuES cells were cultured on the polymer moulds taken from plate 4. The preliminary observations of HuES cells on the moulds are shown in figure 4.24 showing the different shape of the huES cells depending on the LIPSS spacing.

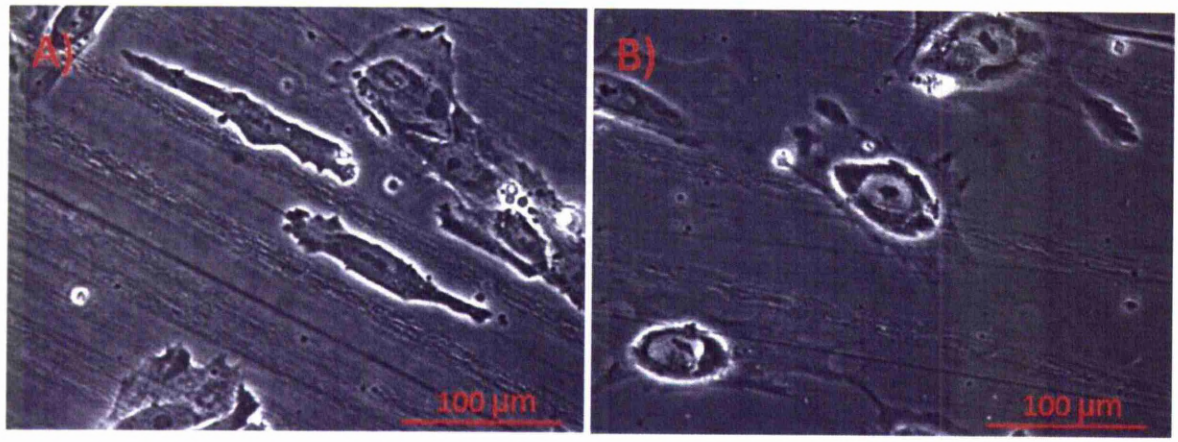

Figure 4.24 Microscope image of HuES cells on polymer moulds after 24 hours. A) 16 µm track, 21, 18, 8, 6, µm spacing repeating 16 µm track and B) 45 and 80 µm spacing repeating

The 16 µm track, 21, 18, 8, 6, µm spacing repeating sample consisted of the same width LIPSS stripe but with a repeating set of different stripe spacing's. This was used for more extensive HuES cell observations.

A more detailed observation of the cells grown on moulds of area C was undertaken. The cells were stained to observe the cytoskeleton, focal attachments and pluripotancy, The microscope images in figure 4.25 show some HuES cells stained for actin and the nucleus DAPI. This shows the

cytoskeleton, or actin filaments, as green and the nuclei as blue. It can be seen that actin filaments form as bright green lines around the edge of the cells. An illustration of how the huES cells appear to bridge the LIPSS stripes and meet other filaments, on the plane areas between the stripes,

This could be an indication that focal adhesions are predominantly being formed on the plain spaces in-between the LIPSS stripes. In an attempt to confirm this, the cells were vinculin stained. The staining was inconclusive. The vinculin was diffuse throughout the cell which, other than shape, appeared the same as the control cells grown on a control plain polymer mould. Further investigation is required to understand how the cells might be attaching to the surface. Figure 4.25 shows how the cytoskeleton appears to bridge the LIPSS tracks. Figure 4.26 shows vinculin stained huES cells. The vinculin will show the focal adhesion points of the huES cells.

Figure 4.27 shows huES cells stained for nanog. The nanog is visible clearly in the huES cells grown on plane control surface but is much less visible on the huES cells cultured on the LIPPS patterns. This can be compared with figure 4.28 which shows the shape of the huES cells after 1 hour and 7 days on both a plain and patterned sample.

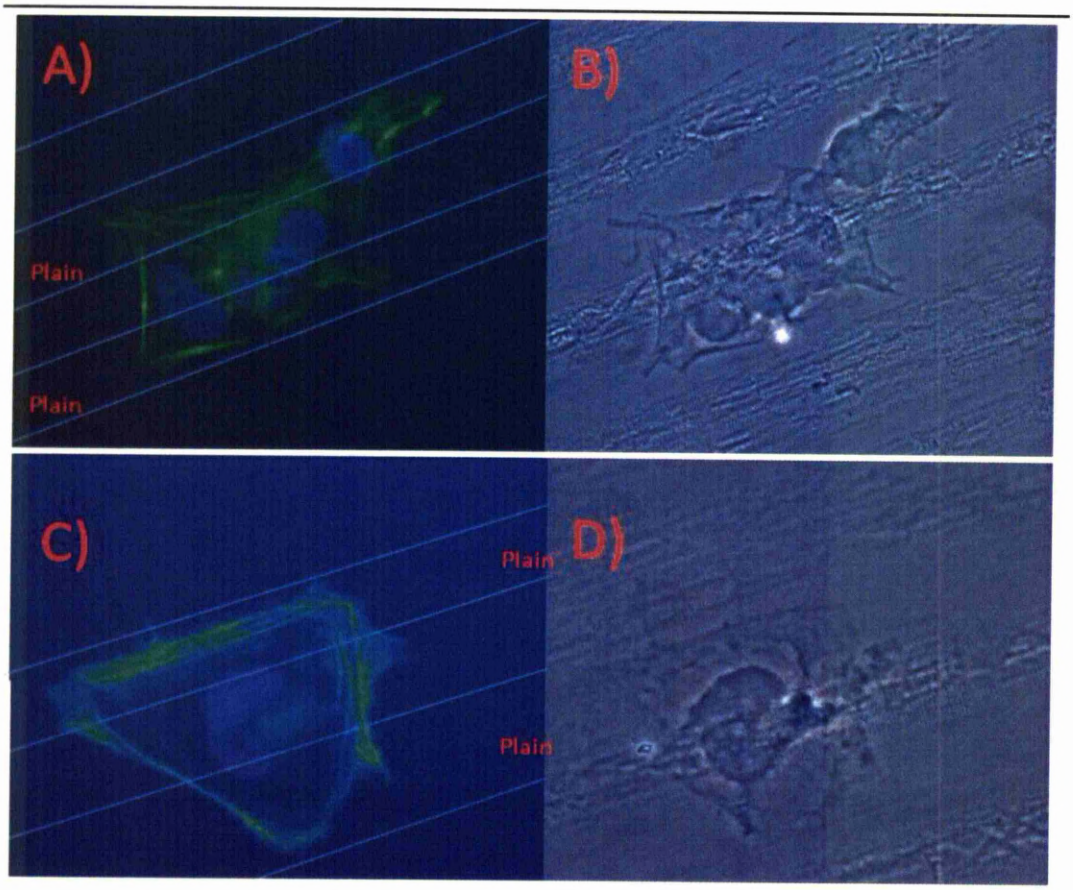

Figure 4.25 Microscope images of HuES cells on moulded polymer sample after 24 hours. (16 µm track, 21, 18, 8, 6, µm spacing repeating) A),B) fluorescent image of actin (cytoskeleton) and DAPI (cell nucleus) stained cell. B),D) phase contrast image for comparison to fluorescent image

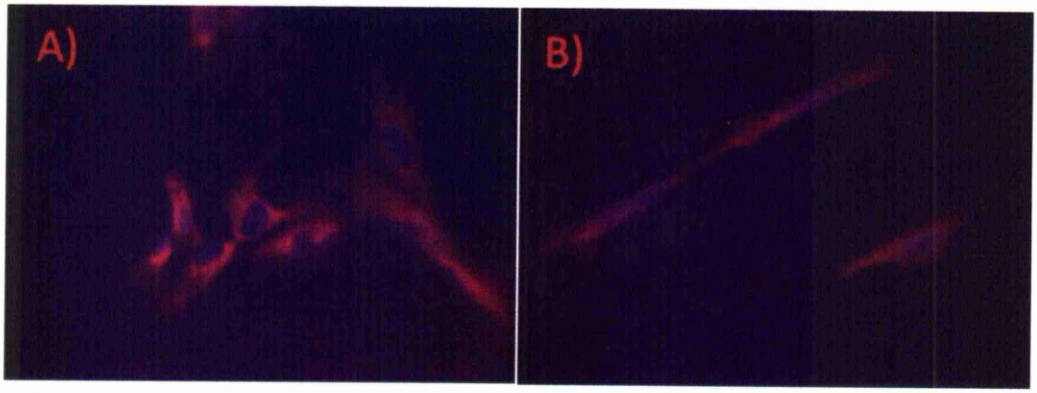

Figure 4.26 Microscope fluorescent image of vinculin stained HuES cells on moulded polymer sample after 24 hours A) plain control sample and B) cells on patterned (16 µm track, 21, 18, 8, 6, µm spacing repeating) sample.

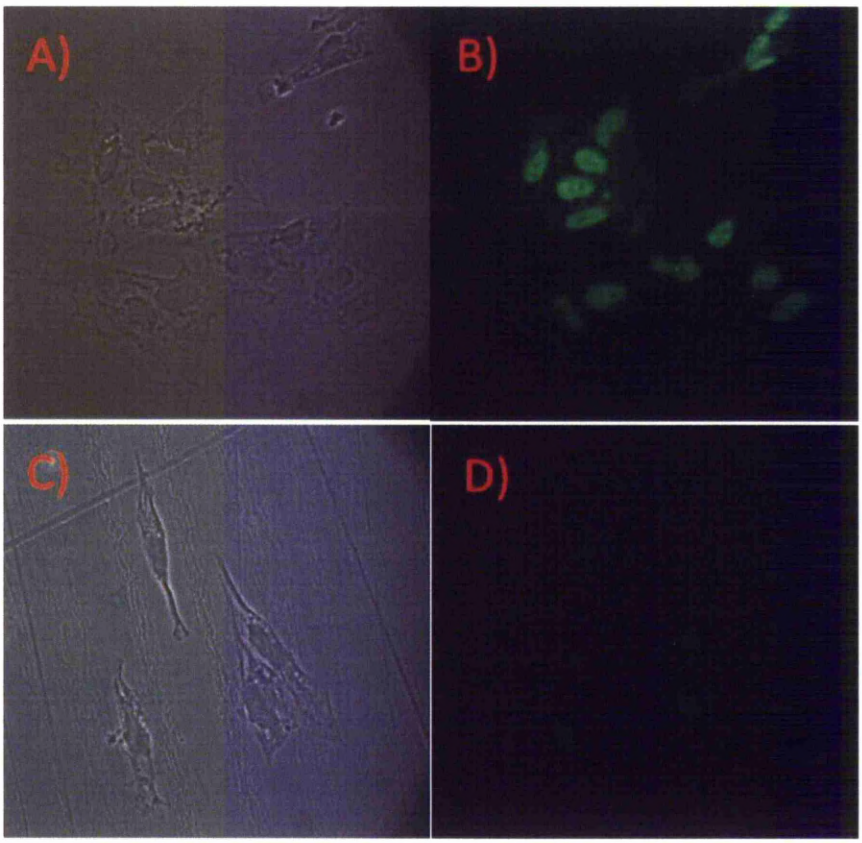

Figure 4.27 Microscope image of HuES cells on moulded polymer sample after 72 hours. A) Control unpatterned sample, B) fluorescent image showing cells stained for nanog expression on control sample, C) cells on patterned (16 µm track, 21, 18, 8, 6, µm spacing repeating) sample, D) fluorescent image showing cells stained for nanog expression on patterned sample

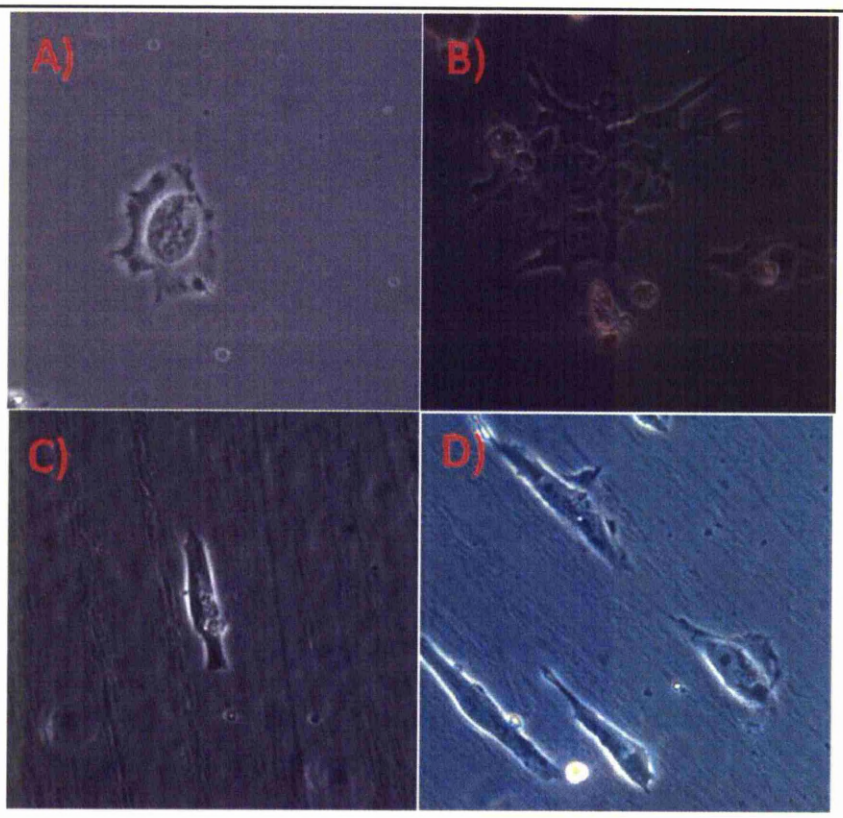

Figure 4.28 Microscope image of HuES cells on moulded polymer sample. A) control unpatented sample after 1 hour, B) control unpatented sample after 7 days. C) cells on patterned (16 µm track, 21, 18, 8, 6, µm spacing repeating) sample after 1 hour. D) cells on patterned (16 µm track, 21, 18, 8, 6, µm spacing repeating) sample after 7 days.

The HuES cells were then stained for nanog expressions. This is an indication of the pluripotancy of a HuES cell. The lack of nanog will indicate that a cell has differentiated and is no longer pluripotant. As can be seen in figure 4.23 after 72 hours, no nanog stain is visible in the HUES cells on the sample moulded from The LIPSS stripes but for the plain control sample nanog is still visible. Potentially this is a significant result. As the LIPSS patterns are moulded in a polymer an coated in fibronectin there is no difference in surface chemistry between the control and LIPSS patterned samples. Surface topography is the only difference. This is the clearest evidence that the cells can be made to differentiate by LIPSS stripe topography alone. The role of the LIPSS patterns is complex. Having just the LIPSS stripes is not enough to observe this differentiation effect. The spacing between the LIPSS stripes is an

important factor in how the HuES cells react to the overall surface topography. The LIPSS patterns appear to restrict cell spreading. If this is used with an optimised spacing, this can affect the behaviour of the HuES cells, which leads to the cells losing pluripotancy. This is an indication that the surface topography required to affect cell behaviour needs to have a multi-scale element to it. The LIPSS stripe patterns contain sub micro to nano scale patterns. When this is combined with the micro scale stripe spacings, a degree of control over the HuES cells is observed.

A final test was to observe the cells for a longer time period (greater than 72 hours). The HuES cells were seeded onto polymer moulds of area C from plate 4 and left in culture for 7 days. They were observed and compared to cells on a control plain polymer sample. The number of elongated cells was counted and is shown in figure 4.29. The graph shows that ~ 40% to 50% of the cells are elongated after 7 days. An interesting note is that the elongated spindle cells do not appear to proliferate as expected, i.e. the majority of cells were spindle shaped. The sample is covered in large areas by normal looking cell colonies with intermittently spaced lone spindle shaped cells. Again further study is needed to understand this observed cell behaviour. An example of this is shown in figure 4.30.

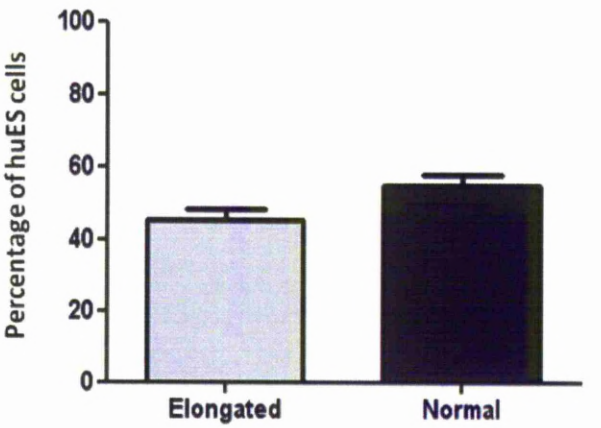

Figure 4.29 Percentage of elongated and normal cells when grown on a polymer moulded sample of area C on plate 4.

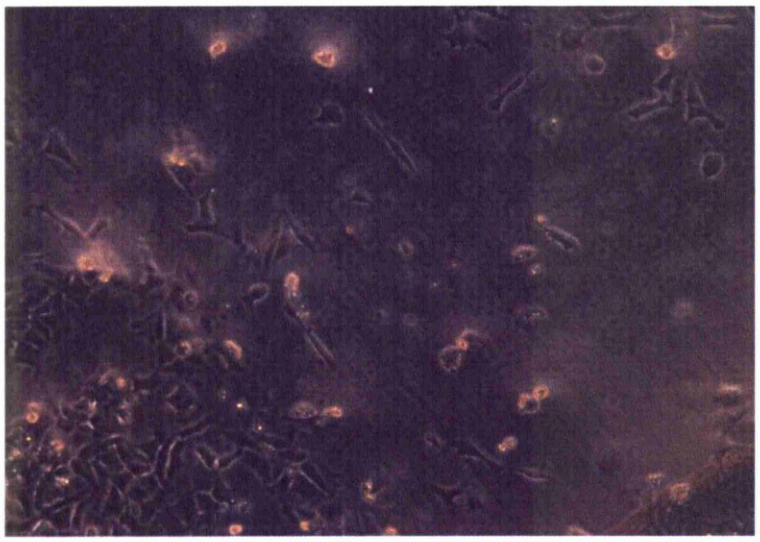

Figure 4.30 HuES cells grown on a polymer moulded sample of area C plate 4 after 7 days, showing how the spindle shaped cells appear not to be proliferating.

4.3.2 LIPSS Spots

Preliminary experiments involved setting the dwell time of the laser to produce two different depths to the laser spots. The laser dwell time was set to 1 ms and 10 ms. The spot patterns were then moulded in the Biomer polymer and fibroblasts were seeded onto the samples.

The preliminary experiments producing the LIPSS spot patterns produced two distinct types of surface feature. A long laser drill dwell time (10 ms) resulted in a relatively deep hole ~20-30 µm in depth. A short dwell time (1 ms) produced a more complex surface feature; a round moat like structure surrounding a ripple pattern like those observed in the LIPSS stripe features. When these features were moulded in the polymer, the 10 ms dwell time features produced a cone like structure. The 1 ms dwell time features were replicated in the same way the LIPSS stripes were with the exception that the moat like structure surrounding the ripples were inverted, into a wall like structure. When fibroblast cells were seeded onto the polymer moulded

sample, little affect was observed for the cones. When the cells were observed on the spots, more cells are seen on the surrounding space as compared to the spot features (figure 4.31) . Using these observations the 1 ms spot patterns were used to produce a more complex surface pattern.

Microscope images of the preliminary spot patterns and fibroblasts are shown in figure 4.31. The fibroblasts can be seen covering the some of the spots but around the cones.

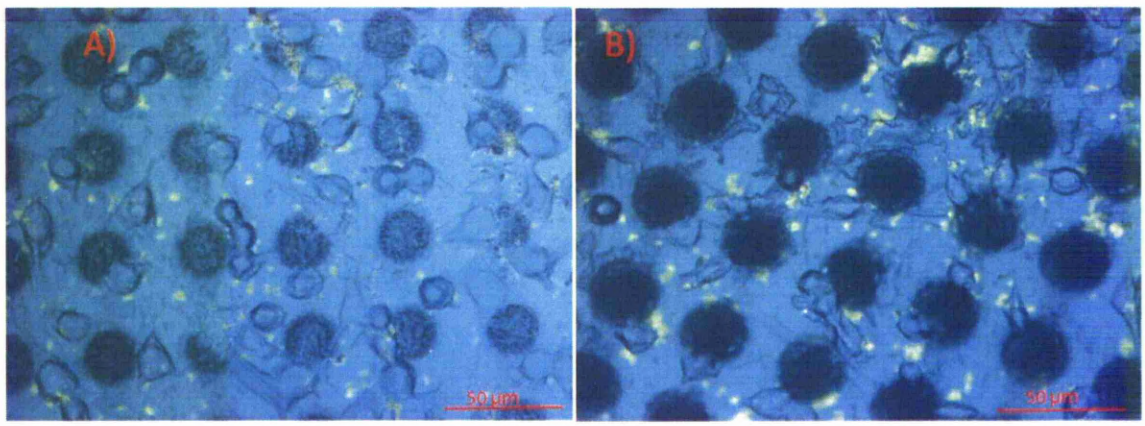

Figure 4.31 Microscope image of moulded preliminary LIPSS spot pattern A) 1 ms laser dwell time B) 10 ms laser dwell time after 24 hours

Using 10 ms dwell time (2500 pulses) produced deep pits, ~25-30 µm deep and about 20 µm in diameter. When these were cast this produced 25-30 µm cones with a separation of about 20 µm. Fibroblasts were placed on the moulded samples and grew around the cones. The 1ms dwell time (250 pulses) produced a more interesting feature, The LIPSS spot features produced a circular, 15 µm in diameter, crater like lip which surrounded the previously observed LIPSS stripe ripple pattern. When these were cast the features were replicated but with a moat type structure surrounding the ripples. Fibroblasts appeared to avoid these features.

To investigate the effect that the LIPSS spot patterns could have on cell behaviour further, the LIPSS spots were used to create cell pens. The laser was set to drill the holes so they would butt together. Areas of the sample

were then left free of the drill holes to create regular square pens of set sizes. These then formed a grid pattern. This was a relatively straight forward process of creating a script for the scanning galvanometer of a small area, then copying the script to build up a large area (~100mm^2) to be processed. At this point a small issue was encountered. Due to the large number of spots the scripting program had to produce, computer processing of the script was significantly slowed. This could be easily solved by upgrading the system with more physical memory but it could still prove an issue if even larger areas of coverage would be required. The LIPSS spot production is therefore much slower than the LIPSS stripe process, requiring more time to process smaller areas. It is however still faster than the femtosecond production due to the increased repetition rate of the picosecond laser system.

Three different sized grids were produced, 4x4, 8x8 and 12x12 holes missing from the pattern, the 4x4 pattern of missed drill sites was too small to leave a blank area. Microscope images of the LIPSS spots on the stainless steel tokens are shown in figure 4.32. The images show the LIPPS spots as the dark areas. The light areas are the underlying, unprocessed steel surface

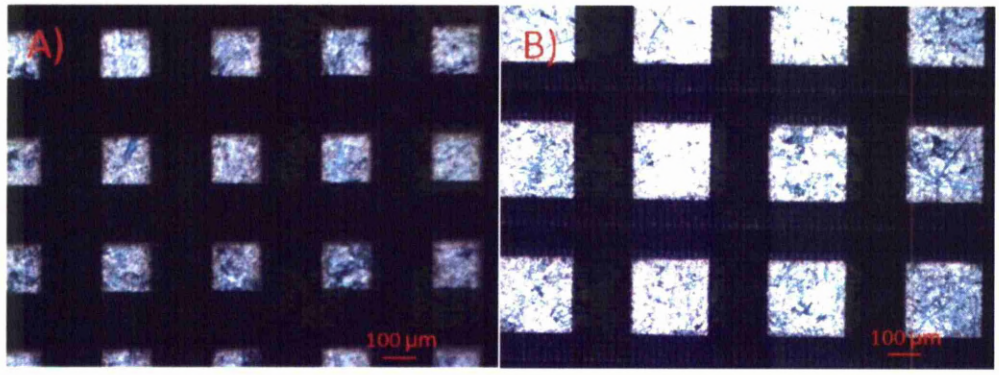

Figure 4.32 Microscope image of LIPSS spot patterns on stainless steel tokens, A) 8x8 grid pattern and B) 12x12 grid pattern.

Polymer moulds were taken of the two above master tokens and fibroblast cells were seeded onto them. Stained and fixed, as well as live images, were taken of the cells, these are shown in figure 4.33. Fibroblasts can be seen to be growing in the unprocessed areas but it is difficult to determine if any are on the LIPPS spot patterns.

Fibroblast cells were initially seeded on to polymer moulds of the LIPSS spot grid samples. The cells appeared to be confined to the pens created by the LIPSS spot grid pattern on both the stained and live cells when compared to the control sample (figure 4.33).

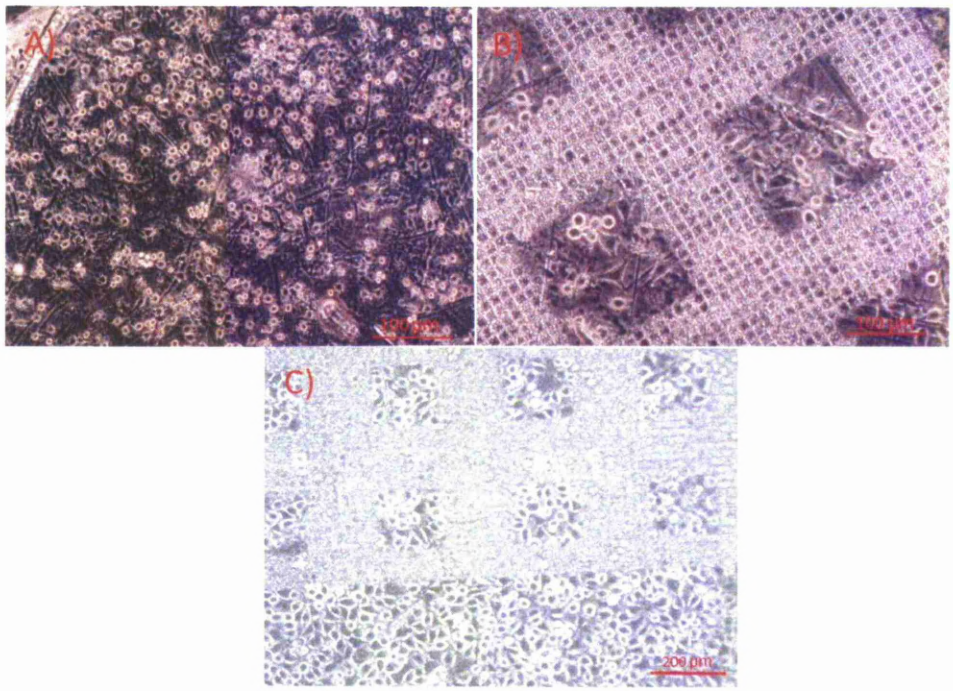

Figure 4.33 Microscope images showing fibroblast cells on polymer moulds of LIPSS stripes (12x12 grid pattern). A) Control unpatented sample, B) stained and fixed cells and C) live cells after 48 hours

The underlying unpolished metal of the stainless steel tokens meant that it was hard to distinguish the cells from the bare metal imprint in the polymer. This along with the rough features of the LIPSS spots meant a different sample and imaging technique was needed. A 12x12 grid pattern was produced on a polished steel token and seeded with fibroblasts. They were imaged using a scanning electron microscope and a microscope fitted with differential interference contrast (DIC) optics. Figure 4.34 shows the DIC images and the SEM images are shown in figure 4.35, figure 4.36 shows a microscope image of huES cells on a polished token. The images clearly

show fibroblasts and huES cells on the plain areas of the sample, with very few growing on the LIPSS pattern.

The images taken with the DIC optics (figure 4.27) also showed cells apparently confined within the pens created by the grid pattern. When the samples were observed under the SEM however several cells were observed on the LIPSS spots (figure 4.28), although these cells were less spread than the cells in the plain pens of the grid. The rough diffractive surface created by the LIPSS spots made it difficult to observe cells that are attached to them. Observations were made more difficult as the underlying metal is also rough, meaning observing the cells on the plain pen areas is also difficult. Before the HuES cells were tested, the steel tokens were polished and the 12x12 grid pattern reproduced on one of these polished surfaces.

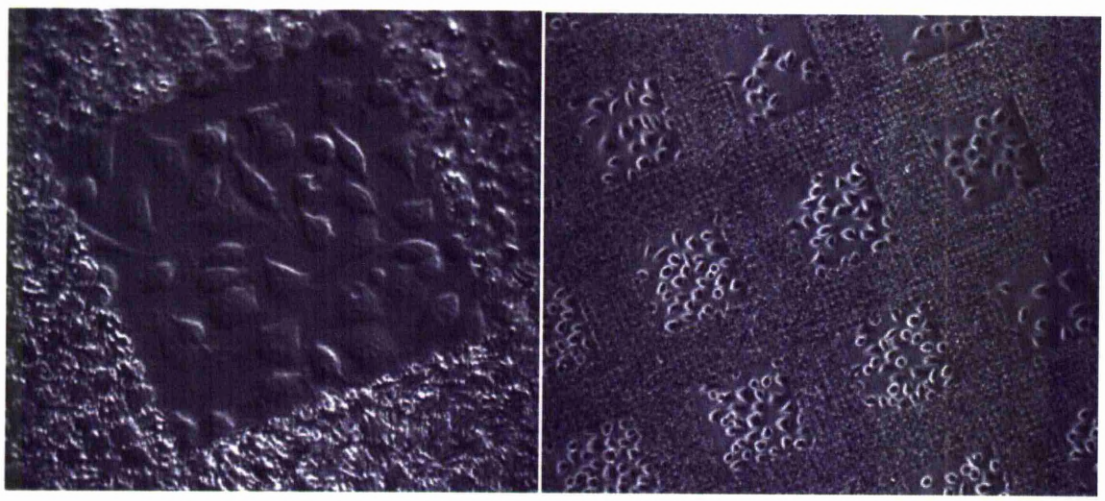

Figure 4.34 DIC image of polymer moulded LIPSS spot pattern (12x12 grid) seeded with fibroblasts after 24 hours

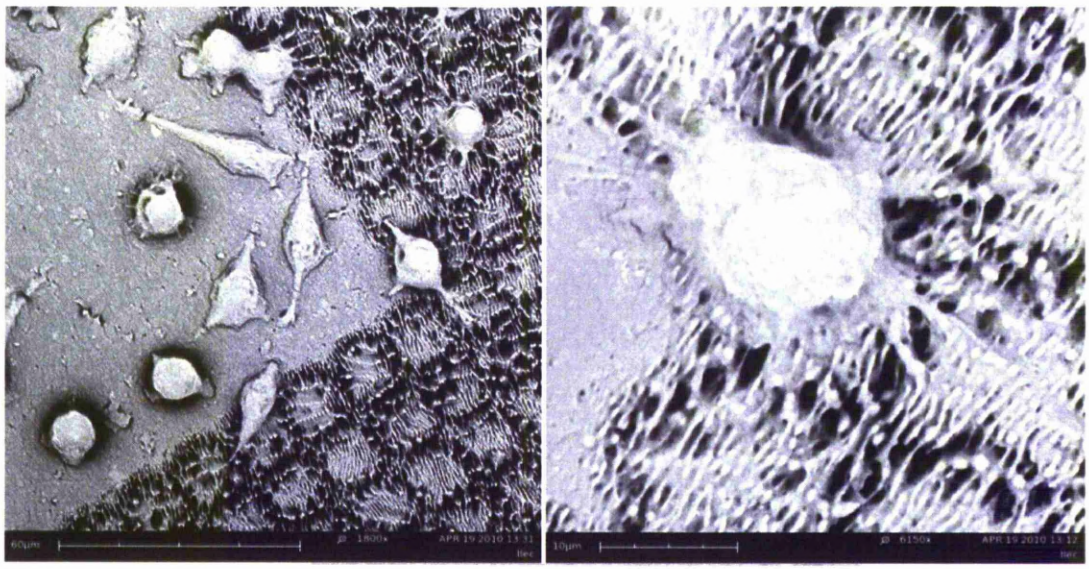

Figure 4.35 SEM image of polymer moulded LIPSS spot pattern (12x12 grid) seeded with fibroblasts. Sample was sputter coated with gold prior to imaging after 24 hours.

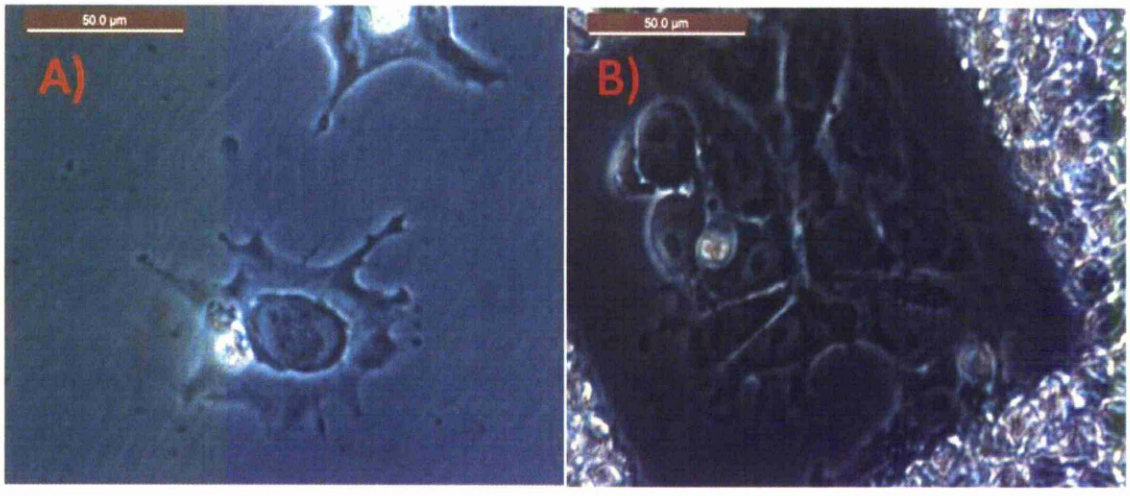

Figure 4.36 Microscope images of HuES cells on polymer moulded LIPSS spot features. A) control, B) 12x12 grid after 24 hours

Using the polished 12x12 grid master token, polymer moulds were produced and seeded with HuES cells. The cells were observed in phase contrast mode and fluorescently stained to show the cytoskeleton and cell nucleus.

Figure 4.37 shows the HuES cells on the polymer moulds. Figure 4.38 shows the HuES cells stained for nanog expression to indicate pluripotancy.

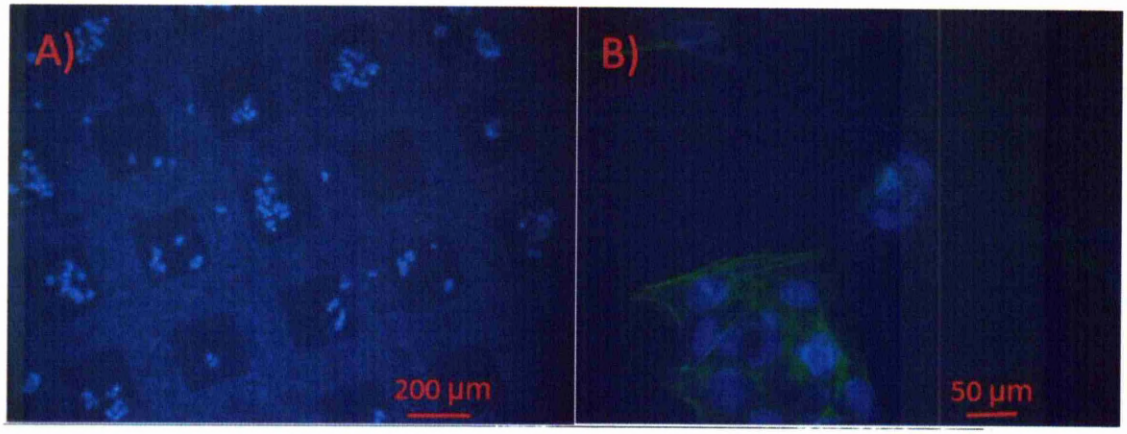

Figure 4.37 Fluorescent microscope images of HuES cells on polymer moulded LIPSS pattern. A) DAPI stained cells showing HuES cells B) actin (cytoskeleton) and dapi (cell neucleus) stained HuES cells, showing differences between cells on the LIPSS spots after 24 hours

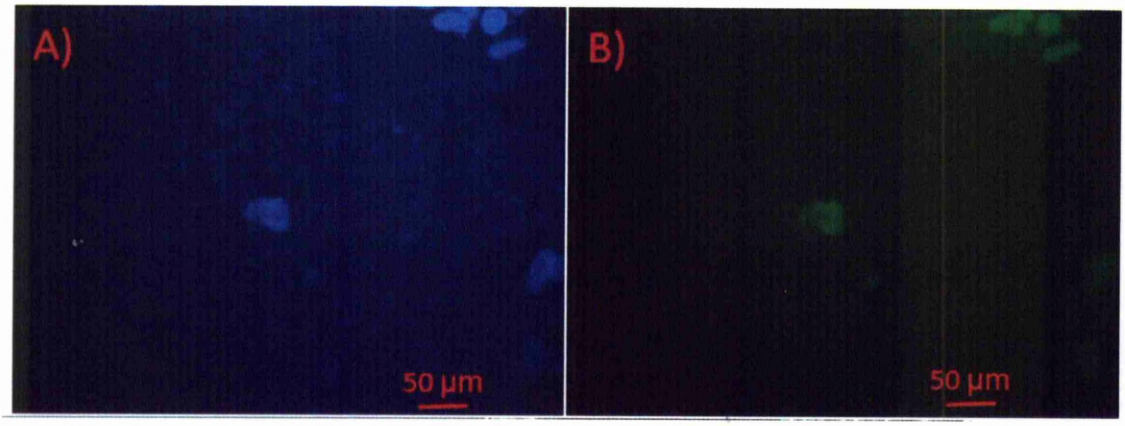

Figure 4.38 Fluorescent microscope images of HuES cells on polymer moulded LIPSS pattern. A) DAPI stained cells showing HuES cells B) nanog stained HuES cells, showing the cells are still pluripotant after 24 hours on the LIPSS spot patterns after 24 hours

Initial observations of the HuES cells show a similar result as for the fibroblasts. The cells appear to be confined to the pens formed by the LIPSS spot grids. The cells appear smaller and less spread than the cells of the control sample (figure 4.29). An interesting feature can be observed when the HuES cells contact the LIPSS spots surrounding the pen; where this occurs the cells elongate along the border of the LIPSS spots seemingly attempting to avoid contact with the LIPSS topography.

The HuES cells were again stained for actin and DAPI to observe the cytoskeleton and nucleus. This staining gave the clearest picture as to what was happening to the cells on the LIPSS spot samples. It can be seen from figure 4.37, that most of the cells are indeed, in the pens formed by the grid patterns. There are a small number of cells on the LIPSS spots. The cells sitting on the LIPSS spots appear balled up and not spread. They look significantly different to those on the plain polymer in the cell pens.

Finally, the HuES cells were stained for nanog expression, again to observe a change in the pluripotancy of the cells. The cells were only observed after 24 hours and the cells were still showing a nanog expression. As the HuES cells on the LIPSS stripe patterns did not stop expressing nanog until 72 hours after seeding, further investigation is required to determine if the LIPSS spot patterns can affect HuES cell differentiation.

Figure 4.37 gives the clearest indication of how the huES cells are growing on the LIPSS spot patterns, very few are directly on the spots. The huES cells are still pluripotant however after 24hours, as shown in figure 4.38.

Figure 4.39 Shows the percentage of cells observed on the LIPSS spot pattern compared with on the plain (cell pen) area of the moulded sample, again indicating most of the cells are growing on the plane parts of the sample

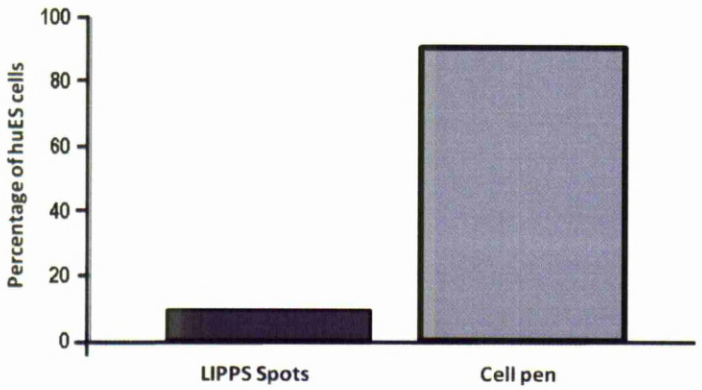

Figure 4.39 Percentage of HuES cells observed on the LIPSS spot pattern compared with those observed on the cell pen of the moulded polymer samples (n = 50).

4.4 Discussion

4.4.1 LIPSS Production

The LIPSS patterning demonstrated here takes advantage of an effect that is often considered a problematic consequence of laser ablation. Speckle (a similar phenomena to LIPSS which causes random distortions to be etched onto the processed surface, as opposed to LIPSS which are periodic structures) and LIPSS effects have been observed in and can cause problems in achieving desired machining patterns [9]. The exact mechanisms involved in producing the LIPSS effects are derived from, solutions of Maxwell's equations, the period of the structures being related to the laser wavelength and polarisation [10]. Other studies have observed however that of more importance is the material properties [11]. It was concluded that a given temperature range higher than the surface melting temperature but below the ablation threshold was needed for a stable surface rippling effect to take place. This is achieved by controlling the number of laser pulses and the laser fluence.

The picosecond laser system used this study allows for control of the laser power and pulse repartition rate making the production of the LIPSS patterns straightforward. Initial experiments found that modifying the laser traverse speed could have an effect on the LIPSS track width, increasing or decreasing the traverse speed would change the number of laser pulses a given area of sample would be subject to (slower traverse speed more pulses per given area, faster traverse speed fewer pulses per given area). This is supported by the conclusions drawn from [11] regarding controlling the laser pulse repetition rate.

The study of LIPSS patterning is still however primarily concerned with the understanding of the mechanisms involved and general observations when processing [12][13] with only a few recent studies showing an interest in patterning materials [14], in this case organic polymers. To the authors knowledge the use of LIPSS patterns for cell/topography interaction investigations are unique.

4.4.2 HuES Cell Observations

There have been many studies conducted on a wide range of topography scales [15] often with contradicting results depending on cell type. [16]. In this case 1µm deep grooves on silicon oxide 0.5µm in pitch were used with fibroblasts and keratinocytes . the fibroblasts aligned strongly with the groves but the keratinocytes showed no alignment. The wide range of cell types used in experiments looking at cell/topography interactions makes comparisons and trends difficult. Here it has been shown that huES cells align particularly well to the LIPPS stripes providing the stripe spacing is around 10µm or less. This is in agreement with several studies using different cell types and topography spacing of 0.5 to 12µm and a large range of feature heights/depths [16][17][18][19][20][21].

The huES cells when seeded onto the LIPPS striped samples with line pacing of 10µm or less appear to attach preferentially to the

unpatterned areas of the sample, i.e. the areas in-between the LIPPS stripes. The sample is seen with the LIPPS spot patterns, huES cells are observed almost entirely (greater than 90%) on the plane parts of the samples. It appears that there are two factors affecting the huES cell behaviour; the nanoscale surface pattern caused by the LIPPS processing and the microscale surface pattern caused by the spacing's left when processing the sample. For the LIPPS stripes, the track spacing will determine how the cells can develop. As the huES cells prefer to dislike the LIPPS nanoscale pattern increasing the LIPPS stripe spacing will mean larger areas of blank surface for the cells to attach and grow normally. As the spacing is decreased the huES cells are forced to grow in an elongated fashion as there is less plain sample for them to develop normally. The different affects micro and nanoscale topography has been noted in the literature [16], here both microscale and nanoscale surfaces were tested with a range of cells. The conclusions were that microscale groves could cause cells to align as the cytoskeleton was reformed. The same study also concluded that nanoscale surface topography resulted in significantly less cell adhesion, it was proposed that the nanoscale topography was preventing the formation of focal adhesions. It appears that the LIPPS stripes are acting in a similar way, the nanoscale topography in creating areas that the huES cells preferentially do not attach, leaving spaces which then result in a reformation of the cytoskeleton resulting in spindle shaped cells. It is proposed that this rearrangement of the cytoskeleton is causing the huES cells to lose pluripotancy.

The LIPPS spots have a slightly different affect, as the LIPPS spot patterns are effectively forming cell pens, the huES cells are growing normally inside them. It is possible that the pens will have an effect on colony formation, longer time length observations are required for any further analysis however,

4.5 Conclusions

Two methods of producing multi scale surface topographies with an ultrafast laser system have been demonstrated. To the authors knowledge, both methods provide a unique set of surface features with which to test the effect of surface topography on cell behaviour. The LIPSS stripe and spot methods are fast reliable and controllable.

Using the LIPSS submicron scale ripple features, in conjunction with micron scale patterns of the ripples, has been successful in controlling HuES cell shape by inhibiting cell spreading. By identifying the optimum feature spacing loss of HuES cell pluripotancy has been demonstrated where the surface topography was the only variable, offering evidence of control of cellular properties via surface topography.

4.6 References

[1] Nánai, L., Vajtai, R., Hevesi, I., Laiho, R., HeikkiläPeriodic, L. 1992. Nanostructures observed by STM on vanadium surface preilluminated with a cw Yag-laser. Superlattices and Microstructures.11, 435-438

[2] Ursu, I., Mihăilescu, I.N., Prokhorov, A.M., Tokarev, V.N., and Konov, V.I. 1987. High-intensity laser irradiation of metallic surfaces covered by periodic structures. J. Appl. Phys. 61, 2445-2457.

[3] Ritchie, R.H. 1957. Plasma Losses by Fast Electrons in Thin Films. Physical Review. 106, 874-881.

[4] Sipe, J.E., Young, J.F., Preston, J.S., and Van Driel, H.M. 1983. Laser-induced periodic surface structure. I. Theory. Physical Review B 27, 1141-1154.

[5] Young, J.F., Preston, J.S., Van Driel, H.M., Sipe, J.E. 1983. Laser-induced periodic surface structure. II. Experiments on Ge, Si, Al, and brass. Physical Review B 27, 1155-1172.

[6] Ursu, I., Apostol, I., Crăciun, D., Dinescu, M., Mihăilescu, L.N., Bakos, J.S., Foldes, I.B. 1985. Energy plasma-target coupling in the case a periodical structure is formed within the irradiation spot as an effect of powerful laser irradiation. Opt. Commun. 55, 409-412.

[7] Mellor, L., Edwardson, S.P., Perrie, W., Dearden, G., Watkins. K. 2010. Ultrashort Pulse Periodic Surface Structuring Of Metallic Surfaces. ICALEO 2010 proceedings, paper M103.

[8] Van Beurden, H.E., Snoek, P.A.M., Von Den Hoff, J.W., Torensma, R., Maltha, J.C., Kuijpers-Jagtman, A.M. 2006. In vitro migration and adhesion of fibroblasts from different phases of palatal wound healing. Wound Repair and Regeneration. 14, 66-71

[9] Jain, K. Excimer Laser Lithography. 1990. SPIE Bellingham.

[10] Ball, Z., Sauerbrey. R. Surface Modification with Lasers. 1997. Experimental Methods in the Physical Sciences, 30, 333-373.

[11] Dauscher, A., Feregotto, V., Cordier, P., Thorny, A.1996. Laser induced periodic surface structures on iron. Applied Surface Science. 96-98, 410-414.

[12] Clark, S,E., Emmony, D,C. 1989. Ultraviolet-laser-induced periodic surface structures. Phys. Rev. B 40, 2031–2041.

[13] Trtica, M,S., Gakovilmage, B,M., Petkovska, L,T., Tarasenko, Fedenev, A,V., Lipatov, E.I., Shulepov, M.A. 2004. Surface modifications of TiN coating by the pulsed TEA CO2 and KrCl laser. Applied Surface Science. 225, 362-371.

[14] Sendova, M., Hiraoka, H. 1993. Sub-Half-Micron Periodic Structures on Polymer Surfaces with Polarized Laser Irradiation. Jpn. J. Appl. Phys. 32, 6182-6184.

[15] Martınez, E., Engel, E., Planell, J,A., Samitier, J. 2009. Effects of artificial micro-and nano-structured surfaces on cell behaviour. Ann Anat. 191, 126—13.

[16] Wilkinson, C.D.W., Riehle, M., Wood,M., Gallagher, J. and Curtis A.S.G. 2002. The use of materials patterned on a nano and micro-metric scale in cellular engineering, Mater. Sci. Eng. C 19, 263–269.

[17] Clark, P. Connolly, P., Curtis, A.S.G., Dow, J.A.T. and Wilkinson, C.D.W. 1990. Topographical control of cell behavior: II. Multiple grooved substrata. Development. 108, 635–644.

[18] Baac, H., Lee J-H., Seo, J-M., Park, T.H., Chung, H., Lee, S-D., Kim, S.J. 2004. Submicron-scale topographical control of cell growth using holographic surface relief grating. Materials Science and Engineering. C. 24, 209–212.

[19] Charest, J.L., Bryant, L.E., Garcia, A.J., King, W.P. 2004. Hot embossing for micropatterned cell substrates. Biomaterials. 25, 4767–4775.

[20] Miller, C., Shanks, H., Witt, A., Rutkowski, G. and Mallapragada, S. 2001. Oriented Schwann cell growth on micropatterned biodegradable polymer substrates, Biomaterials. 22, 1263–1269.

[21] Recknor, J.B., Recknor, J.C., Sakaguchi, D.S. and Mallapragada, S.K. 2004. Oriented astroglial cell growth on micropatterned polystyrene substrates, Biomaterials. 25, 2753–2767.

Chapter 5

Scanning Probe Microscopy generated biomimetic nano structures

5.1 Introduction

The work presented in the previous chapters has involved the use of fibronectin (FN) to provide an extra cellular matrix (ECM) for the HuES cells. Without this ECM, provided by the FN, the HuES cells would be unable to survive on a surface in-vitro. The role of FN as an ECM is documented [reff] and has been adopted as a standard technique for working with HuES cells. However its more detailed workings are less understood, particularly how its topography may affect the HuES cells.

This chapter will investigate the 'natural' topographies produced as a result of fibronectin coatings adsorbed onto solid surfaces and its effect on cell behaviour. Previous work has looked at confining HuES cells using 3D scaffolds [1]. However, the 'natural' topography created by the adsorption of FN on solid surfaces is an important step in understanding how HuES cells respond to a true (<100nm) topography, in-vitro. These nature inspired topographies will give a useful tool to mimic the ideal nano environment of cells.

With this understanding of what the FN looks like at the nano scale, a synthetic nano topography that mimics the conditions of adsorbed FN will be produced using a nanolithography technique, involving an Atomic Force Microscope (AFM). The nanolithography or 'nano scratching' technique will allow for true nanometer scale features to be produced on a polymer.

The aim of the work presented in this chapter was to determine the physical state of FN molecules in terms of their diameter, spacing and distribution. This information would then be used to produce a 'synthetic' topography on bio-compatible polymer using the lithography capabilities of the AFM.

5.1.1 Fibronectin

Fibronectin (FN) is a high-molecular-weight glycoprotein. It is found in connective tissue, in the blood and other body fluids and at cell surfaces. Fibronectin has been demonstrated to interact with many other macromolecules including collagens, glycosaminoglycans, actin, fibrinogen and fibrin. Fibronectin is composed of two identical, or nearly identical, disulfide-linked polypeptides with a combined molecular weight close to 450000. FN exists in two forms, 'Soluble FN' (Plasma FN) is produced in the liver. And 'polymeric fibrillar network' (Cellular FN) is synthesised in tissues. FN has various adhesive bonding sites for fibrin, collagen, heparin and integrins at specific locations. FN has numerous functions that ensure the normal functioning of vertebrate organisms. It is involved in cell adhesion, growth, migration and differentiation [2][3].

5.2 Materials and Methods

The adsorbed fibronectin and cell culturing experiments were performed at the Department of Human Anatomy and Cell Biology at the University of Liverpool. The methods used are described in the following sections.

5.2.1 Substrates and Fibronectin

13 mm Borosilicate glass cover slips were obtained from VWR international (Lutterworth, UK). Human plasma fibronectin (1 mg/ml) was purchased from Millipore (Watford, UK). Phosphate Buffer Silane (PBS) and Fluo-Reporter Tetramethylrhodamine protein Labelling kit were obtained from Invitrogen (Paisley, UK).

5.2.2 Quantification of adsorbed Fibronectin on glass cover slips.

The fibronectin was fluorescently labelled using a Fluo-Reporter Tetramethylrhodamine protein Labelling kit (Molecular Probes, UK) as per the manufactures protocol. The mean degree of labelling was determined, as per kit protocol with spectrophotometry, to be 5 moles of dye per mol of FN. No difference in HuES cell behaviour was noted for the fluorescently labelled fibronectin as compared to the unlabelled fibronectin. Fibronectin adsorption on tissue culture polystyrene plastic was studied by using a range of coating concentrations of fluorescently labelled FN (Flu-FN) in PBS buffer solution. The samples were incubated at 37°C for 1 hour. The samples were washed 3 times with PBS without dewettling. Quantification of the adsorbed Flu-FN was carried out using a previously published procedure [4]. Adsorbed Flu-FN was digested using 400 µl of 10x trypsin solution (Sigma Aldrich, UK) for 24 hours at 37°C. The intensity of the adsorbed Flu-FN was measured with a CytoFluor Series 4000 Fluorescence Multi-Well Plate Reader, with the excitation and emission wavelength set at 555 nm and 580 nm respectively. The quantity of adsorbed FN was determined using a standard curve prepared under identical trypsinisation conditions with 0 -500 µg/ml Flu-FN solutions

5.2.3 Cell culture

HuES7 cells (obtained from Harvard University, HuES cells facility, Melton laboratory, MA, USA) were cultured in feeder/ serum free conditions on FN coated surfaces as described before [4]. Cell culture media used throughout this study was composed of 50:50 F12 :DMEM (Lonza) supplemented with

2mM L-glutamine, 1% NEAA, 0.1 mM β-marcatoethanol, 0.1% bovine serum albumin (BSA), serum free supplements N2 (1x), and B27 (1x), human recombinant growth factors i.e., activin A (10ng/ml), Neurotrophin-4 (4ng/ml) and FGF2 (40ng/ml). The cells were cultured on either 3.5 or 6 cm tissue culture dishes pre-coated with 50µg/ml of FN solution in PBS for 1 hour at 37°C. Cells were maintained in these conditions by subsequent passage after 3-4 days of culture using trypsin.

5.2.4 Cell adhesion and morphology assay

Borosilicate glass cover slips were coated with different concentrations of FN diluted in PBS for 1 hour at 37°C. The HuES cells grown on FN coated dishes were dissociated using 1x trypsin-EDTA diluted in PBS, and counted using a haemocytometer. Unless or otherwise stated 20,000 cells per sq. cm were seeded on pre-coated samples and incubated for a further 2 hours at 37°C. The unattached cells were removed by gently aspirating the media. The attached cells were later counted in 3 random fields of view, in triplicate, for each sample.

The mean cell area of a single cell was calculated to assess the extent of cell spreading on tissue culture plates coated with different concentrations of proteins. The cell area was measured using Image J analysis software with a drawing tablet and pen. The mean cell area was calculated from randomly captured cells (n=50).

5.2.5 Surface preparation

For characterisation with the Atomic Force Microscope (AFM), glass cover slips were coated with different concentrations of fibronectin in PBS for 1 hour at 37° C. The samples were later washed once with PBS, followed by two subsequent washing with distilled water and air dried in a laminar flow cabinet. The samples were kept in an enclosed 24 well plate until AFM analysis. Due to the very rough surface of tissue culture plates, imaging with AFM was made difficult and so only glass samples could be used for AFM analysis.

5.2.6 Atomic force microscopy measurement and image analysis

The atomic force microscope (AFM) used in the study was a Veeco CP-II SPM in conjunction with Budget Sensors TAP-300AL silicon probes. These have a typical radius of curvature of 10 nm. All imaging was done in 'tapping' or 'intermittent' contact mode. Images were analysed using Veeco Image Analysis software version 2.1. For optimum imaging, the AFM was fitted with a small area scanner, capable of scanning areas of 1-5μm^2

5.2.7 Characterisation of fibronectin coated glass cover slips

Glass cover slips coated with different concentrations of FN were analysed using the AFM to determine average molecular spacing and diameter. AFM imaging was performed in duplicate with 3 random scans per sample. The images were scanned in both topography and phase mode. The AFM image analysis was performed using Veeco image analysis software. Rv-p (average peak to trough spacing) values were used as a measure of molecular spacing. A population study of the FN coated cover slips was done to determine average molecule size. Lower coating concentrations of FN were used to identify individual molecules on the glass surface.

5.2.8 Nano-feature production using an AFM

For nano feature production, glass cover slips were first coated with acrylic based polymers. The polymer used was a complex multi-component acrylic based polymer whose composition can be discretely modified to alter surface properties. The polymer provided by Biomer Technology Ltd, Runcorn, UK. The polymer was used as supplied without further modification. The polymer was spin coated at 500 rpm for 45 min on the glass cover slips using a Single Wafer Spin Processor (WS-400B-6NPP-Lite) from Laurell Technologies Corporation. The glass cover slips were then placed on a hot plate at 100°C for 5 minutes and later cured in an oven at 100°C for 45 minutes.

It is possible to produce a variety of features using the Nanolithography software. To produce a topography that would mimic the size and spacing of the FN, a grid pattern was used in order to exploit the attributes of AFM machining. The resultant features produced by the AFM create a scratch into the surface of the substrate and form a subsequent build up of material surrounding the scratch. Using a grid it is possible to create a pattern where the build-up of material is formed into a series of mounds. By increasing the number of lines in the grid the resultant pattern can be formed to match the Rv-p and average molecule size of the FN. A grid pattern was produced on the polymer surface spin coated onto glass cover slips. The lithography was set for a 10x10 line grid with a relative z position of -0.07 µm, scratch speed 3µms^{-1}. This was then refined to a 60x60 line grid that covered an area of 4 µm, with the same scratch parameters.

5.2.9 Nano feature Characterisation

A set of lines was scratched onto the polymer to determine what size of features could be produced. The relative z position was set to -0.15, -0.1, -0.08, -0.05, -0.04 and -0.025 microns. The scratches were imaged and produced in 'tapping mode' and measured using Veeco Image Analysis 2.1.

5.3 Results

5.3.1 Quantification of surface adsorbed fibronectin on glass cover slips

The effect of FN adsorption with changing amounts of FN was studied by fluorescently labelling FN on glass cover slips.

The effect of the FN coating concentration on its adsorption on glass cover slips is shown in figure 5.1. From figure 5.1 it can be seen that when the glass cover slips were coated with FN, saturation is reached at about 350±50 ng/cm^2, meaning that the cover slip is effectively carpeted with the FN protein and no more of the protein can be adsorbed onto the surface.

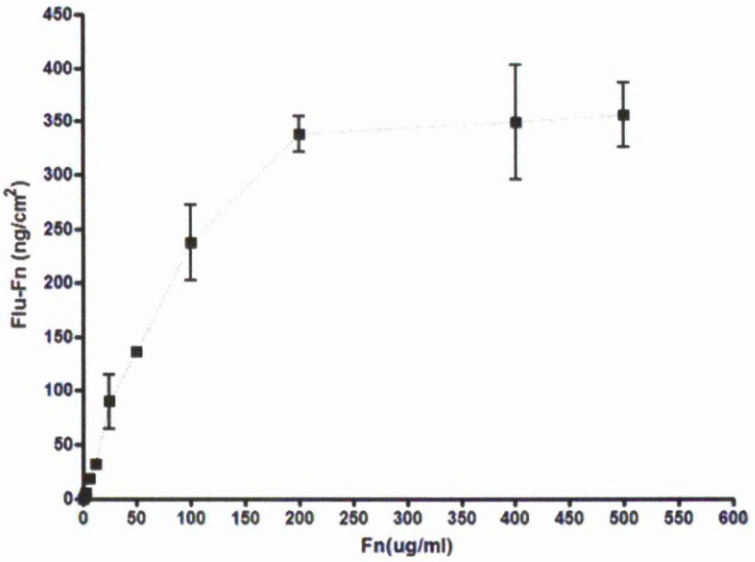

Figure 5.1 The amount of adsorbed fibronectin on glass cover slips as a function of fibronectin solution concentration

HuES cell attachment and spreading was measured as a function of FN coating concentrations. This was to study the optimum amount of adsorbed FN required for maximum cell attachment and spreading. The effect of FN coating concentration on cell attachment and spreading is as shown in figure 5.2.

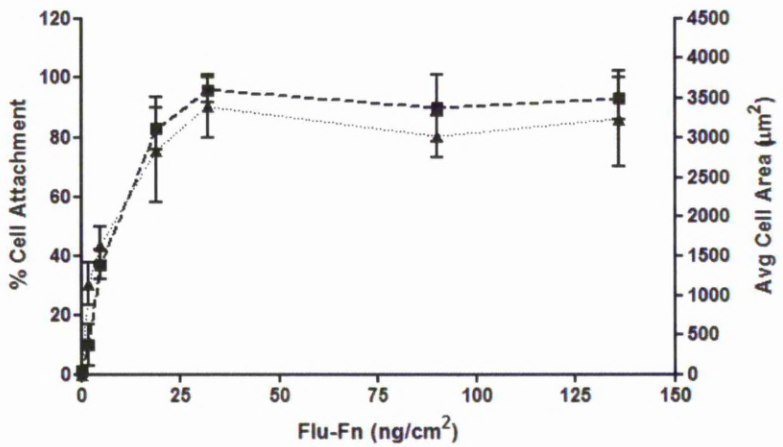

Figure 5.2 HuES cell attachment and spreading is effected by FN concentration

Figure 5.2 shows that maximum cell attachment and spreading is achieved with a very low (5% of saturated level) FN coating concentration. This indicates the absence of a direct correlation between the FN coating concentration and cell attachment and subsequent cell spreading.

5.3.2 Characterisation of fibronectin coated glass cover slips using AFM.

Preliminary experiments showed that at sub-saturated amounts of FN, patches of FN are formed on the glass substrates. The FN coated cover slips were imaged in both topography and phase mode, the phase images are shown in Figure 5.3. The patches can be seen in the images as roughly circular areas contrasting the background. In a) and c) the patches appear darker than the background, in b) they appear lighter. This is due to the effect of scanning in phase mode. The AFM was set to record data on both passes over the sample, i.e. when the tip moved from right to left and when moving back left to right. This causes an artefact, where the image contrast between the background and FN patch is inverted with the change in direction, right to left and left to right. Figure 5.4 shows how the average patch number, size and spacing changes with concentration. Eight images were taken for each concentration and the values for patch number, patch diameter and patch separation were averaged. The diameter was calculated along the major axis of the patch and the separation determined from the centre of each patch to the centre of all surrounding patches, taking the central patch in the field of view as a starting point. Above 50µg/ml FN concentration, no FN patches were observed as the concentration had become high enough to allow for a covering of the protein that resulted in the AFM being unable to distinguish individual FN molecules.

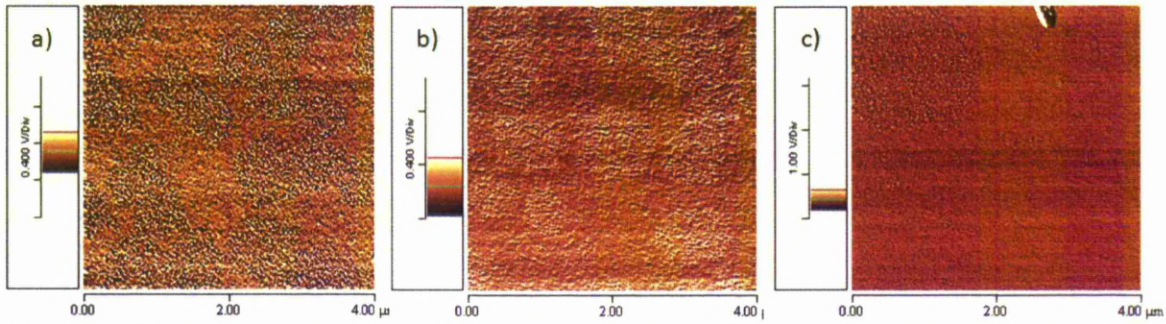

Figure 5.3 AFM phase image of FN on glass cover slips, showing patching for a) 32, b) 90 and c) 136 ng/cm^2

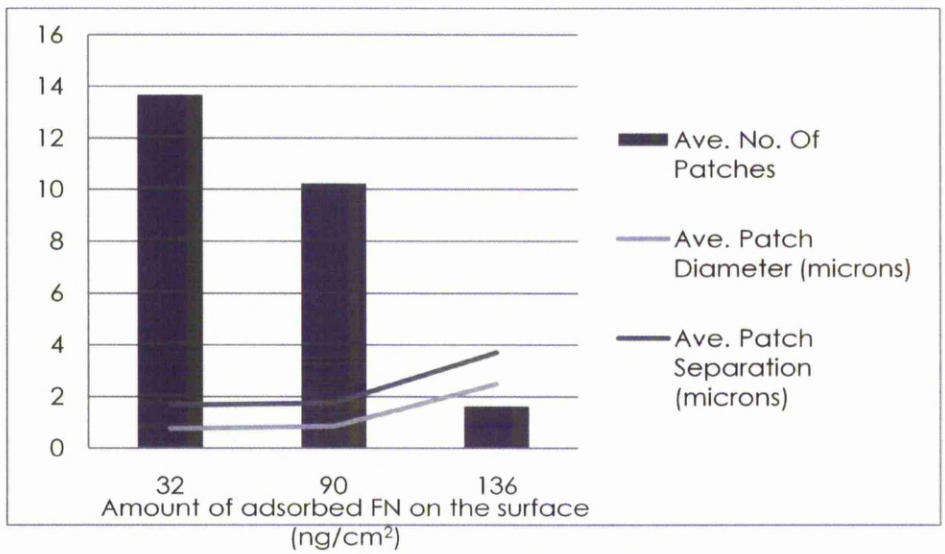

Figure 5.4 The effect of adsorbed FN concentration change on formed FN patch number, diameter and separation.

An area measurement was performed on each topography image of the FN coated cover slips. Figure 5.5 shows the images used to make the Rv-p measurements. The Rv-P was plotted against the FN amount adsorbed onto the surface of the glass. Figure 5.6 shows the graph for Rv-P against amount of FN. The zero amount of FN was taken from control images of the bare glass cover slips. As the amount of surface adsorbed FN was increased the spacing between molecules decreased. At saturated amounts of adsorbed FN molecules were closely packed with a minimum Rv-p of 5nm

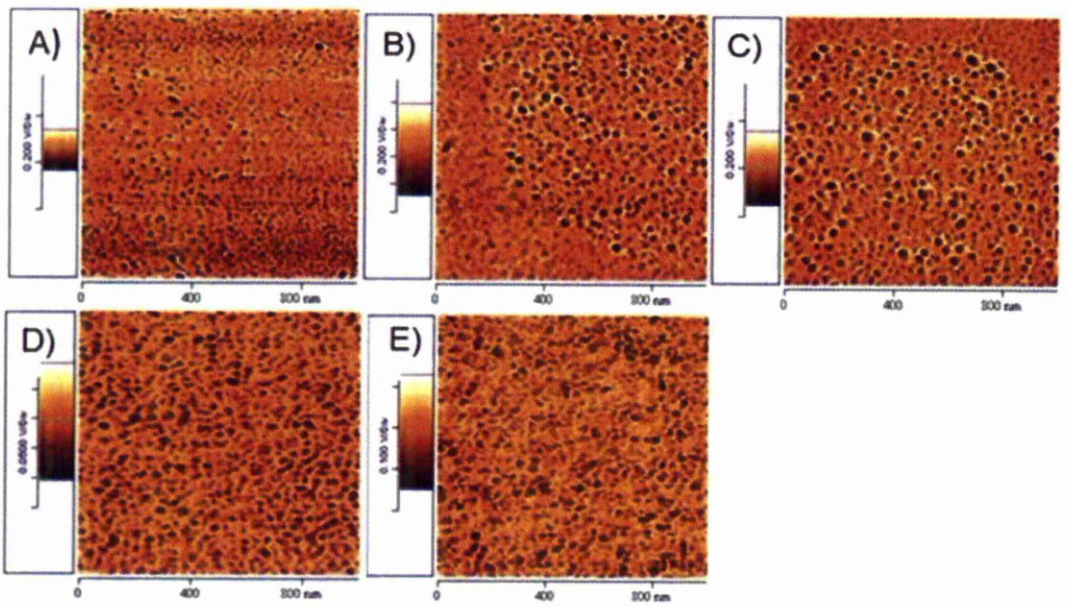

Figure 5.5 AFM topography images of FN coated cover slips at concentrations of A) 32, B) 90, C) 136, D) 237, E) 338ng/cm^2

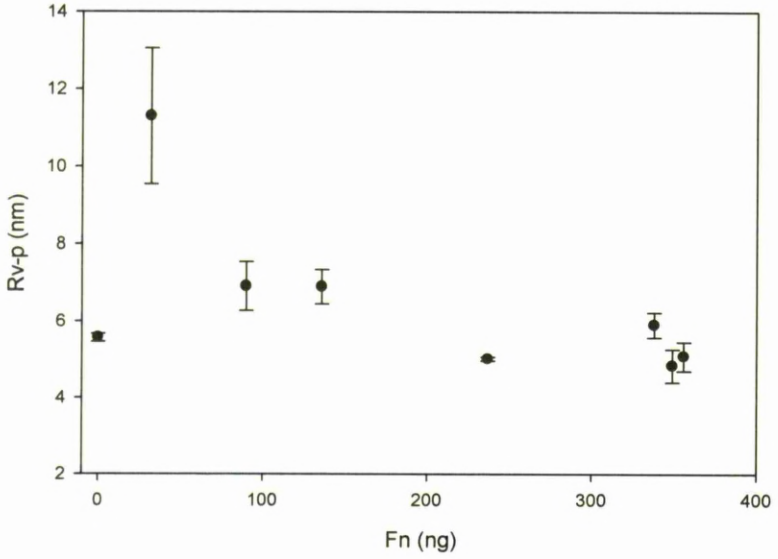

Figure 5.6 The change in FN molecule spacing (Rv-p) as the amount of adsorbed of fibronectin changes. The zero point represents the control sample with no adsorbed fibronectin

The average molecular diameter determined from AFM image analysis is shown in figure 5.7. This shows the population distribution of the width of the FN molecules when adsorbed onto the surface of the glass cover slips. The graph shows that for 32 and 90 ng/cm^2 samples the molecules range from 18-48nm, with the greatest number of molecules ranging between 27-36nm. Again only the lowest concentrations could be analysed as at higher concentrations the individual FN molecules were indistinguishable,

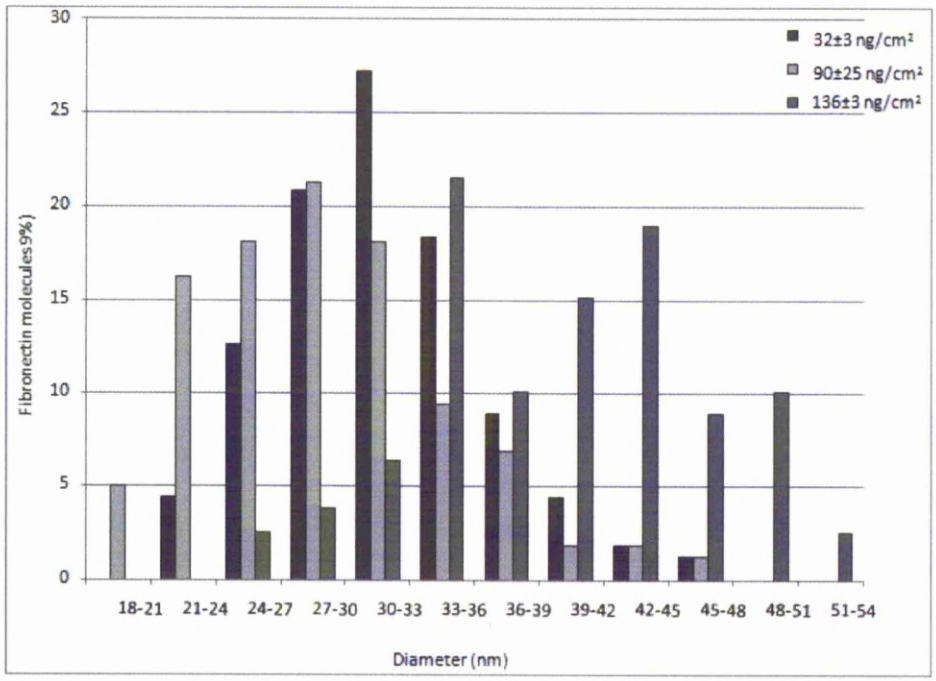

Figure 5.7 The population distribution for different diameters of adsorbed FN molecules on the surface of glass cover slips. Diameter measured of the major axis where the molecule was elliptical

5.3.3 Nano feature characterisation

An AFM topography image of the characterisation scratches, is shown in Figure 5.8. The relative z position was set (from top to bottom or right to left for the Y and X axis scratches respectively) to -0.15, -0.1, -0.08, -0.05, -0.04 and -0.025 microns. The final scratch at -0.025 microns is not visible. Figure 5.9 shows the effect of relative Z position on scratch size. Fig 5.10 shows the effect of scratching in the X or Y direction, on the cross section of a scratch.

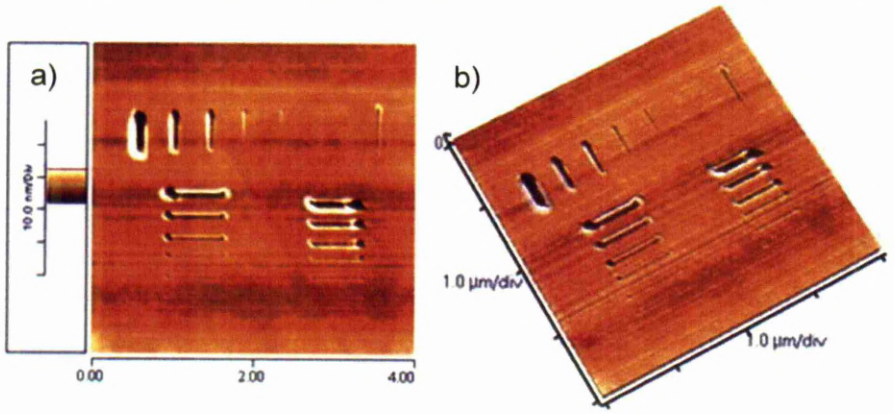

Figure 5.8 2D (a) and 3D (b) AFM images of scratches produced by force assisted nanolithography, in Relative Z mode.

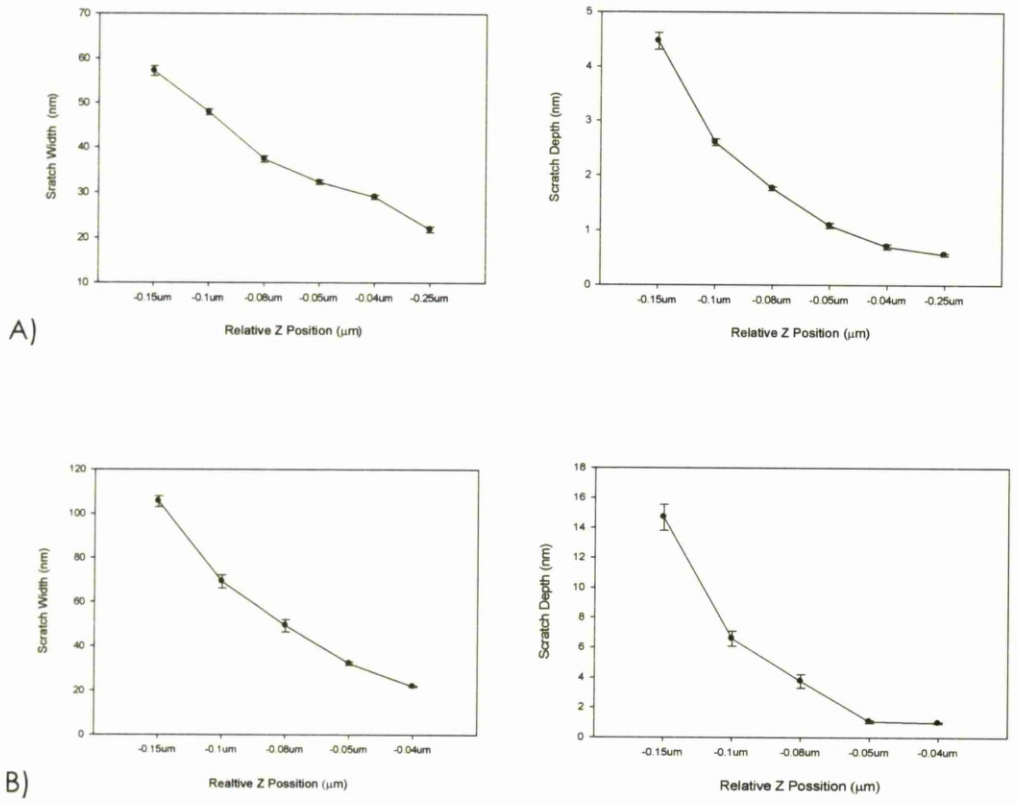

Figure 5.9 The effect of relative z position on scratch depth in a) x-axis and b) y-axis processing

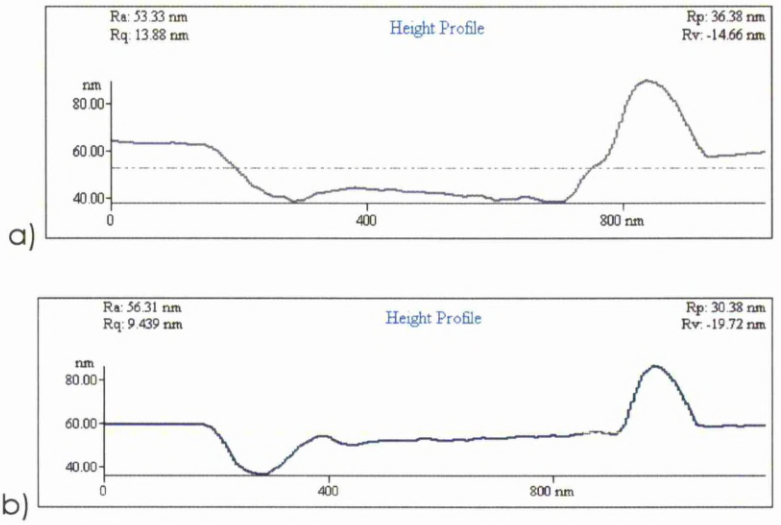

Figure 5.10 Cross section of a) Vertical nano scratch b) Horizontal nano scratch, relative z position -0.08microns and speed of 3microns/s. Scratch is processed from left to right

5.3.4 Creating a Bio-Mimetic Surface

As has been shown in the characterisation of the nano lithography process with the AFM, true nano scale features are possible. It is also possible to obtain features of similar size to that of the fibronectin. Using the Lithography software a grid pattern was set up and processed on to the polymer substrate. The AFM image is shown in figure 5.11. A population study, like that for the FN, was done to measure the produced features, this is shown in Figure 5.12. The cross section, taken by the AFM, is shown in Fig 5.13

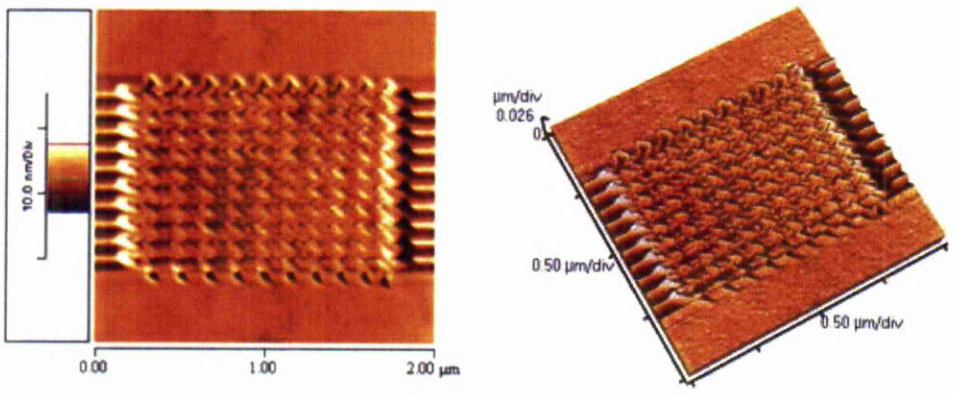

Figure 5.11 AFM image of Nanolithography pattern designed to mimic FN Rv-p and molecule size. The lithography was set for a 10x10 line grid with a relative z position of -0.07µm, scratch speed 3µm/s.

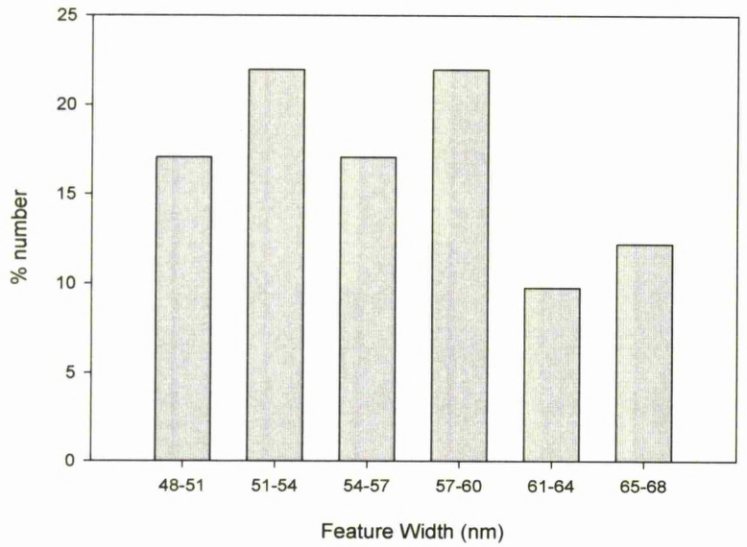

Figure 5.12 Population study into the diameter produced using the nanolithography nano-scratching

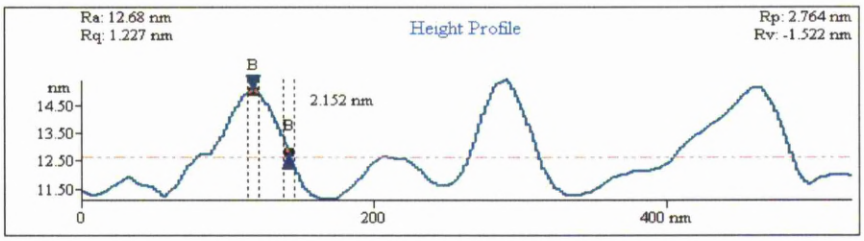

Figure 5.13 Population study into the diameter produced using the nanolithography nano-scratching

The Lithography script was refined and extended to cover a larger area. Using the same relative z point (-0.07µm) and speed (3µms^{-1}) an area of about 4.5 x 4.5 µm was covered. An AFM image is shown in Figure 5.14

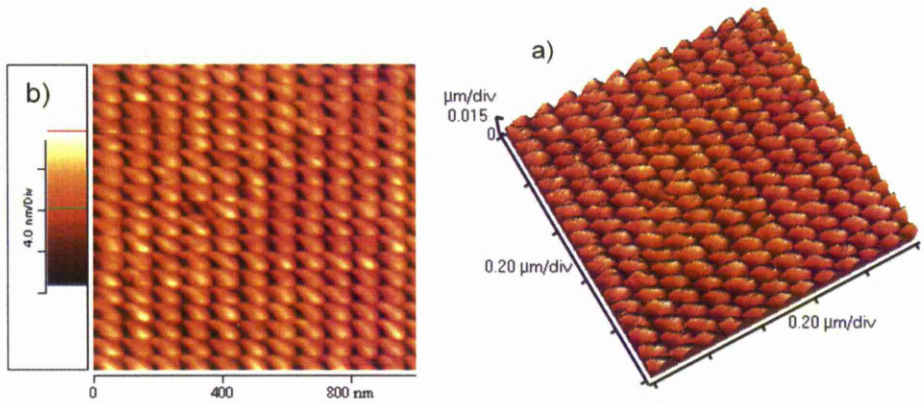

Figure 5.14 3D (a) and 2D (b) AFM images of refined nano lithography biomimetic topography on a polyacrylamine surface

Using the same analysis program as for the FN, the Rv-p of the AFM nanolithography was measured to be 15.48 nm. This matches very closely to the result from the FN. Figure 5.15 shows the cross section of the pattern with the height of the features; approximately 2 nm.

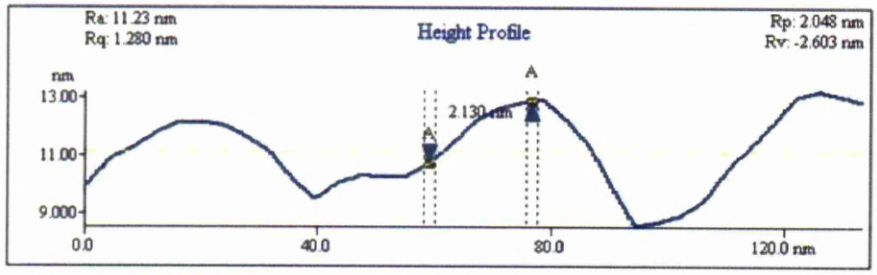

Figure 5.15 AFM Cross Section of the refined nano Lithography showing the height of the machined features

Again as with the FN, a population study was carried out on the nano features, shown in figure 5.16. The refined feature sizes closely match those of the FN.

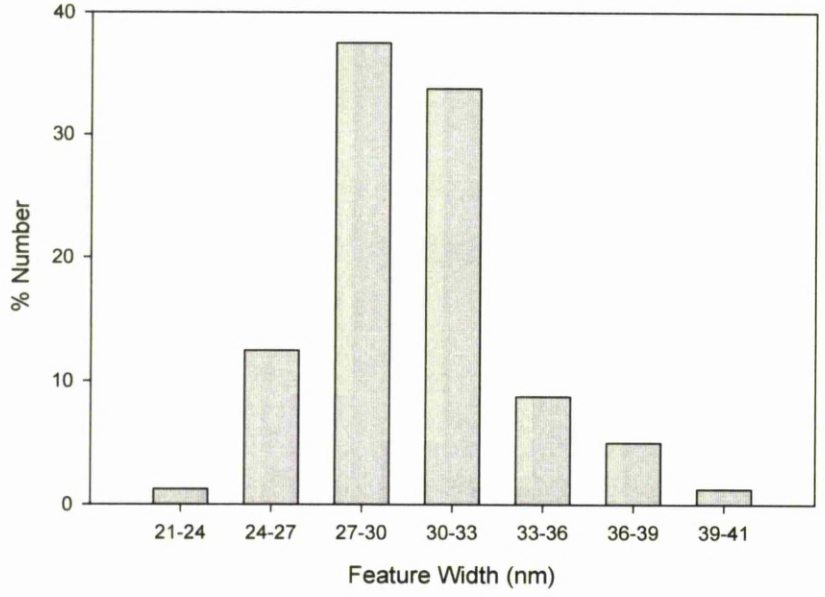

Figure 5.16 Population study of the refined nano lithography designed to mimic the natural topography of fibronectin.

5.4 Discussion

5.4.1 Fibronectin and Stem Cell Observations

The quantification of FN adsorption on tissue culture well plates showed that FN forms a saturated layer at about 345 ±3 ng/cm^2. This value for saturated level of adsorbed FN is in agreement with previous studies on tissue culture polystyrene and silica surfaces [5][6][7]. Fibronectin exists in a soluble form in blood plasma and forms insoluble fibrous structure after integration with ECM [8]. The shape of the FN molecule however, depends on the solution pH and salt concentration [9][10]. For physiological conditions of salt concentration, pH and ionic strength, the FN molecule adopts a more compact form [9][10]. When the FN is adsorbed onto solid surfaces however, it undergoes a conformation change and adopts a more elongated structure [11]. Electron microscopy and atomic force microscopy studies of adsorbed FN on mica and silica surfaces suggest that the FN molecule is 120 nm long and has 2 nm diameter [12][13] Using these dimensions, the theoretical maximum quantity of adsorbed FN required is 365 ng/cm^2. This assumes a side on conformation [6]. This value is close to the experimental value of 345±3 ng/cm^2 calculated from adsorption curve for FN as shown in figure 5.1. The FN adsorbed onto the tissue culture well plates can therefore be assumed to be adsorbed in the side on conformation. This is in agreement with a previous study on surface adsorbed FN on polystyrene and silica surfaces [6].

From the study, it is indicated that optimum conditions for cell attachment and spreading of HuES cells can be achieved using very low amounts of surface adsorbed FN (5% of saturation value). This implies that there is no direct correlation between cell response and the FN adsorption isotherm on tissue culture surface as seen from figure 5.2. The surface adsorbed FN, as low as 32 ng/cm^2, was found to be enough to achieve these conditions. Based on the FN adsorption isotherm, when the theoretical spacing (centre to centre distance) between molecules was estimated (for surface adsorbed FN of 32 ng/cm^2, assuming that molecules are of the same size and have uniform surface distribution), it was found to be 15 ±1 nm.

According to FN adsorption and cell response studies, FN at 32 ng/cm^2 and with a theoretical spacing of 15±1 nm provides optimum conditions for HuES culture. This was taken to be the model for producing a synthetic mimetic surface with which to simulate the natural, nano scale topography of the FN when adsorbed onto a substrate. A surface with this configuration could feasibly be used to test the effect of the natural FN topography but with a different surface chemistry.

5.4.2 Nanolithography scratching effects

The nanolithography scratching used here is also commonly referred to as dynamic ploughing [14]. It is operated in tapping mode as opposed to contact mode and it has been reported to give a faster and more practical method of machining with an AFM [14]. The distinctive build up of material along the track is attributed to the breaking of polymer chains in the bulk material [15]. This was shown, in the literature, to increase the volume of the wall material, also providing an explanation for why the volume of the built up walls was greater than that of the volume of the ploughed scratch.

A noticeable feature is the low aspect ratio of the nano features; typically wide shallow features are produced. In this case it makes the technique very suited to producing a topography that will match the FN which is itself of low aspect ratio. A further feature is the build-up of material around the scratch. The scratched features also differ depending on the direction they are processed and differ in shape with a change in relative z position. This could be the result of two main factors; first the geometry of the cantilever/tip and the way it is mounted onto the AFM and second, that the tip is asymmetric. The AFM tip is mounted on a long cantilever, relative to the tip length (tens of microns depending on the type). This is then mounted to the AFM so that the cantilever is perpendicular to the x-axis of the scanner. This means that when the AFM is set up to scratch a surface, the cantilever will experience a different force depending on whether the scratch is vertical or horizontal [16] [17]. A horizontal (x-axis) scratch will result in a lateral force, relative to the cantilever, which creates a torsion force around the major axis of the

cantilever. This twists the tip away from the direction of the scratch. When a vertical (y-axis) scratch is produced, the cantilever will experience a longitudinal force, along the major axis of the cantilever, with no resultant twisting of the tip. Looking at the cross sections, scratches have the distinctive build up of material at the end of the scratch and an initial pit as the tip is first forced into the substrate. The main difference is the middle section of the scratch. As the vertical scratch does not result in twisting of the tip, a deeper section is scratched.

A second factor which can affect the shape of the lithography objects is the tip asymmetry and tip wear [15]. The Budget Sensors TAP-300AL probes do not have symmetrical tips; the tip is the shape of a rough pyramid with an elongated front and narrower sides towards the bottom of the tip. As the tip wears down it will become increasingly more asymmetric and the effect on the shape of the features will become more apparent. The same is true for the deeper scratches. As the tip is forced further into the sample the more the asymmetric part of the tip is used to scratch. This is a possible explanation for the difference in the appearance of the dross, which surrounds the scratched features. The horizontal (X-axis) dross is even on both sides. This could be down to a combination of better tip symmetry and that the tip is not being pressed into the substrate as deeply due to the torsion effects of scratching horizontally. The vertical (y-axis) scratches, however, show a distinct unevenness in dross build up, seeming to build up significantly more on one side. Again a combination of a less symmetric tip geometry and increased depth to which the tip is driven into the substrate could lead to an asymmetric build up of dross material. Both the horizontal and vertical scratches have improved scratch and dross symmetry at lower relative z positions (and hence lower scratch depth and width) indicating that the very tip of the AFM probe is more symmetric and/or the effect of twisting is significantly reduced at lower applied forces.

5.4.3 Producing a Bio Mimetic Surface

The results obtained by imaging and analysing FN were used to base a possible 'Bio Mimetic' surface. Using the spacing and dimension results from the FN, a similar surface topography was produced. This was achieved by exploiting the resultant build up of material formed when processing using the AFM. Often this has been seen as an un wanted effect in the production of nano features with the AFM, the use of the technique for creating nano-channels for example, where the dross build up would prevent a second surface from being used to create an enclosed channel.

Using a grid of intersecting scratches and reducing the scratch pitch sufficiently to achieve the desired feature size, without overwriting the previous scratch; it was possible to create an approximation of adsorbed FN in terms of molecule size and spacing. The problem however is that of production scale. It is, with the current AFM, only possible to produce the nano features over an area of ~4.5 x 4.5 µm. This can take between 5 and 10 minutes to process. Considering the typical HuES cell is ~20µm in diameter, it would take many production steps to produce an area large enough to grow even a few cells. This coupled with the need to produce many samples for accurate and repeatable cell experiments, make the production of these surfaces a very time consuming task. This draws concerns on the feasibility of this method for the production of samples for cell biology experiments. There are, however, factors that could mean that production would be faster. The FN study showed that at sub saturated amounts of adsorbed FN, the FN formed patches these patches were a few microns across and an average of ~10 to 15µm apart. Using this the machined features could be spaced out, removing the need to completely cover an area with the features.

The major problem, when using this system, however, was the lack of automation. Each area of scratches needed to be set up manually, which can be very time consuming. The system did not have an accurate way of translating the head meaning that producing an area of scratches, a specific distance apart was not possible. More sophisticated AFM systems are available and steps have been made to automate the AFM nano lithography process [18]. This will allow accurate translation and automated machining. If an automated system could be used, production time would be low enough to consider the AFM nano lithography method a viable technique to produce enough samples for use in the cell biology experiments. Thus it is for the above reasons, that no samples were used for testing the AFM nano features with the HuES cells.

5.5 Conclusions

A series of fibronectin coated glass cover slips were imaged with an atomic force microscope to determine how the topography (molecule size and spacing) of the fibronectin coating changed with different coating amounts. These coated cover slips were also used to investigate the effect the change in adsorbed fibronectin had on the attachment and spreading of human embryonic stem cells. The saturation amount of FN was determined to be 350 ±50 ng/cm^2. HuES cells were observed to attach and spread on adsorbed amounts of FN down to 32 ±3 ng/cm^2. At 19 ±4 ng/cm^2, HuES cell would not survive. AFM analysis showed that for the three samples that were possible to image (32, 90 and 136 ng/cm^2) the average height of the FN molecule was ~2nm. 32 and 90 ng/cm^2 samples had an average molecule size of between 27 and 36 nm. The average molecule size for the 136 ng/cm^2 was slightly larger, between 39 and 48 nm in diameter. The average molecule spacing, Rv-p, for the three samples (32, 90 and 136 ng/cm^2) was measured to be 11 nm, 7 nm and 7 nm respectively. This was compared to an Rv-p of 5 nm for a saturated sample (350 ng/cm^2) and 5.5 nm for the control uncoated sample. The Rv-p and average FN molecule size for the 32

ng/cm^2 sample were taken as optimum parameters and were the aim for the nano machining with the AFM.

A method for producing true (>100nm) nano features has been demonstrated. Using the AFM as a machining tool a surface topography has been created that mimics the surface topography of FN adsorbed onto a substrate. The resultant pattern had an average feature height of ~2nm, an average feature diameter of 27-33 nm and an Rv-p of 15.48 nm. This very closely matches the optimum FN amount of 32 ng/cm^2.

5.6 References

[1] Sharon Gerecht, Seth A. Townsend, Heather Pressler, Han Zhu, Christiaan L.E. Nijst, Joost P. Bruggeman, Jason W. Nichola, and Robert Langer. 2007. A porous photocurable elastomer for cell encapsulation and culture. Biomaterials. 28, 4826–4835.

[2] Price, T.M., Rudee, M.L., Pierschbacher, M., Ruoslahti, E. 1982. Structure of Fibronectin and Its Fragments in Electron Microscopy. Eur. J. Biochem. 129, 359-363

[3] Elodie Velzenberger a, Karim El Kirat a, Gilbert Legeayb, Marie-Danielle Nagel a, Isabelle Pezronc. 2009. Characterization of biomaterials polar interactions in physiological conditions using liquid–liquid contact angle measurements Relation to fibronectin adsorption. Colloids and Surfaces B: Biointerfaces. 68, 238–244

[4] Baxter, Melissa A., Camarasa, Maria, Bates, Nicola, Small, Fiona, Murray, Patricia, Edgar, David, Kimber, Susan J.2009. Analysis of the distinct functions of growth factors and tissue culture substrates necessary for the long term self-renewal of human embryonic stem cell lines. Stem Cell Research.10.1016/j.scr.2009.03.002

[5] Frederick Grinnell, Marian Feld and Dianne Minter. 1980. Fibroblast adhesion to fibrinogen and fibrin substrata: Requirement for cold-insoluble globulin (plasma fibronectin). Cell. 19, 517—525

[6] Garcı, A.J., Vega, M.D., Boettiger, D. 1999. Modulation of Cell Proliferation and Differentiation through Substrate-dependent Changes in Fibronectin Conformation. Molecular Biology of the Cell. 10, 785–798

[7] L. Baujard-Lamotte, S. Noinvillenext, F. Goubardd, P. Marque and E. Pauthe. 2008 Kinetics of conformational changes of fibronectin adsorbed onto model surfaces. Colloids and Surfaces B: Biointerfaces. 63, 129-137

[8] Jennifer R. Potts and Iain D. Campbell. 1996. Structure and function of fibronectin modules. Matrix Biology. 15, 313-320

[9] Harold P. Erickson and Nadia A. Carrel. 1983. Fibronectin in Extended and Compact Conformations. Journal of Biological Chemistry. 258, 14539-14544

[10] David L. Amrania, Gene A. Homandberga, Nancy M. Tooney , Carlota Wolfenstein-Todel and Michael W. Mosesson, 1983. Biochimica et Biophysica Acta (BBA) - Protein Structure and Molecular Enzymology. 748, 308-320

[11] Hanna M. Kowalczynska, Małgorzata Nowak-Wyrzykowska, Robert Kołos, Jacek Dobkowski, Jarosław Kaminski. 2008. Semiquantitative evaluation of fibronectin adsorption on unmodified and sulfonated polystyrene, as related to cell adhesion. J Biomed Mater Res A. 15, 944-56.

[12] Magnus Bergkvist, Jan Carlsson, Sven Oscarsson. 2002. Surface-dependent conformations of human plasma fibronectin adsorbed to silica, mica, and hydrophobic surfaces, studied with use of Atomic Force Microscopy. J Biomed Mater Res Pt A. 64, 349-356.

[13] Eliot C. Williams, Paul A . Janmey, John D. Ferry, and Deane F Masher. 1982. Conformational States of Fibronectin. Journal of Biological Chemistry. 257, 14973-14978

[14] Ulrich Kunze. 2002. Nanoscale devices fabricated by dynamic ploughing with an atomic force microscope. Superlattices and Microstructures. 31.

[15] B. Cappella, H. Sturm and S. M. Weidner. (2002). Breaking polymer chains by dynamic plowing lithography. Polymer. 43, 4461–4466

[16] Y.D. Yan, T. Suna and S. Dong. 2007. Study on effects of tip geometry on AFM nano scratching tests. Wear. 3-4, 477-483

[17] Y.D. Yan, T. Suna, Y.C. Lianga and S. Dong. 2009. Effects of scratching directions on AFM based abrasive abrasion process. Tribology International. 42, 66-70.

[18] S. Cruchon-Dupeyrat, S. Porthun and G. Y. Liu. 2001. Nanofabrication using computer-assisted design and automated vector-scanning probe lithography. Applied Surface Science. 175-176, 636-642

Chapter 6

Conclusions and Future Work

6.1 Conclusions

The study has considered three different methods of producing unique surface topographies. These different methods have all produced very different surface features.

A micro scale topography has been demonstrated using a femtosecond laser system to produce wells on glass cover slips. The wells were measured to be ~20 µm in diameter and ~6 µm deep. These wells were then used to produce a set of samples where the only variable was the well spacing. The change in well spacing was shown to affect cell growth and spreading. Issues were encountered, however, due to the laser system stability and sample production speed.

A novel and multiscale surface topography has been designed and produced using a laser micromachining technique employing a picosecond fibre laser. The patterns produced consisted of submicron scale surface ripples which were then used to create a micro scale pattern of stripes on

the surface of stainless stell master moulds. This topography was then moulded using a polymer and used for experiments where human embryonic stem cells were observed and the behaviour of the cells, in reaction to the surface features, recorded. The HuES cells have been shown to differentiate when cultured on the samples for 72 hours. The cause of the differentiation of the cells can be attributed to the topography. The multiscale features appear to control cell spreading which in turn controls the cell behaviour and so the cell differentiation, as a reaction to the surface features. The method of producing the master moulds was fast and reliable. The system was flexible, allowing for the production a range of different surface patterns. The ability to mould samples for HuES cell experiments meant a wide range of samples could be produced quickly and with reproducible patterns time after time.

Using the same laser method, different surface patterns were possible. Using the laser to produce spots containing sub micron features, these were then used to form a grid pattern. Effectively this pattern created cell pens. The pattern also demonstrated an ability to control HuES cell behaviour by corralling the HuES cells into the cell pens, thus reducing cell spreading. Where a HuES cell attached to a laser spot pattern, the cell did not spread. Fewer HuES cell observations were made however and the extent to which these patterns are of use is still unknown at this point.

The final topography to be demonstrated was on the nano scale. Fibronectin coated glass cover slips were measured using an atomic force microscope (AFM). The fibronectin molecule average size and spacing was recorded and used as a model for a biomimetic topography. Using an AFM nanolithography technique, a pattern that very closely matched the fibronectin was machined into polymer samples. The AFM lithography technique is slow and can only cover areas up to 4.5 x 4.5 µm. This meant that sample production was unable to provide enough cells for use with the HuES cell observations.

The aim of the investigation was to produce a surface topography that could affect HuES cell behaviour. For the experiments conducted, it has been demonstrated that the surface topography has directly affected the cell and caused changes in cell spreading shape and differentiation.

6.2 Further and Future Work

Although the study has demonstrated HuES cells being affected by surface topography, it is not yet understood as to how the topography is causing this.

Further work is needed to further observe how the HuES cell attach to the surface and the machined surface features. Another aspect that would warrant future research is how the underlying fibronectin and ECM are affected by the surface topography.

Each different surface topography could be investigated further. The micro scale wells could be produced by a different more reliable laser system of more practical use produced on a steel master mould and moulded in polymer. This is a simple change to the experiment and would allow for more detailed observations of HuES cells on the micro scale well samples.

The multiscale surface features, both spots and strip patterns, could be investigated further by producing more complex spot and strip spacing. This could lead to different cell reactions. Currently the polymer used to mould from the master plates has been polyurethane. Biomer Technology produce a wide range of polymers designed to promote cell growth. Using different polymers to mould the master plates would give an insight as to how dominant an effect topography is when compared to different and changing surface chemistries.

Finally, producing true nano scale features is still a difficult task. Producing such small features in a rapid prototype setting is even more so. The AFM lithography technique allows for a wide range of surface features to be produced without the need for costly masks, expensive photolithography

equipment or complex electron and ion beam machining vacuum systems. The main drawback is process area and throughput. New AFM systems are available that can produce larger areas in an automated fashion, increasing throughput. If the features demonstrated in the study could be produced with one of these systems, it would provide a very suitable test sample to observe HuES cells on controlled nano scale topographies.